frontiers | Research Topics

Multimodality imaging techniques in PD and atypical Parkinsonism

Edited by
Zachory Wei, Binbin Nie and Lihong Bu

Coordinator by
Tianbin Song

Published in
Frontiers in Neurology
Frontiers in Aging Neuroscience

ISSN 1664-8714
ISBN 978-2-8325-4517-1
DOI 10.3389/978-2-8325-4517-1

About Frontiers

Frontiers is more than just an open access publisher of scholarly articles: it is a pioneering approach to the world of academia, radically improving the way scholarly research is managed. The grand vision of Frontiers is a world where all people have an equal opportunity to seek, share and generate knowledge. Frontiers provides immediate and permanent online open access to all its publications, but this alone is not enough to realize our grand goals.

Frontiers journal series

The Frontiers journal series is a multi-tier and interdisciplinary set of open-access, online journals, promising a paradigm shift from the current review, selection and dissemination processes in academic publishing. All Frontiers journals are driven by researchers for researchers; therefore, they constitute a service to the scholarly community. At the same time, the *Frontiers journal series* operates on a revolutionary invention, the tiered publishing system, initially addressing specific communities of scholars, and gradually climbing up to broader public understanding, thus serving the interests of the lay society, too.

Dedication to quality

Each Frontiers article is a landmark of the highest quality, thanks to genuinely collaborative interactions between authors and review editors, who include some of the world's best academicians. Research must be certified by peers before entering a stream of knowledge that may eventually reach the public - and shape society; therefore, Frontiers only applies the most rigorous and unbiased reviews. Frontiers revolutionizes research publishing by freely delivering the most outstanding research, evaluated with no bias from both the academic and social point of view. By applying the most advanced information technologies, Frontiers is catapulting scholarly publishing into a new generation.

What are Frontiers Research Topics?

Frontiers Research Topics are very popular trademarks of the *Frontiers journals series*: they are collections of at least ten articles, all centered on a particular subject. With their unique mix of varied contributions from Original Research to Review Articles, Frontiers Research Topics unify the most influential researchers, the latest key findings and historical advances in a hot research area.

Find out more on how to host your own Frontiers Research Topic or contribute to one as an author by contacting the Frontiers editorial office: frontiersin.org/about/contact

Multimodality imaging techniques in PD and atypical Parkinsonism

Topic editors

Zachory Wei – Emory University, United States

Binbin Nie – Institute of High Energy Physics, Chinese Academy of Sciences (CAS), China

Lihong Bu – Renmin Hospital of Wuhan University, China

Topic Coordinator

Tianbin Song – Capital Medical University, China

Citation

Wei, Z., Nie, B., Bu, L., Song, T., eds. (2024). *Multimodality imaging techniques in PD and atypical Parkinsonism*. Lausanne: Frontiers Media SA. doi: 10.3389/978-2-8325-4517-1

Table of contents

frontiers | Frontiers in Neurology

TYPE Editorial
PUBLISHED 13 February 2024
DOI 10.3389/fneur.2024.1370437

OPEN ACCESS

EDITED AND REVIEWED BY
Volker Rasche,
University of Ulm, Germany

*CORRESPONDENCE
Tianbin Song
✉ Songtb_1984@163.com

RECEIVED 14 January 2024
ACCEPTED 30 January 2024
PUBLISHED 13 February 2024

CITATION
Song T and Nie B (2024) Editorial: Multimodality imaging techniques in PD and atypical Parkinsonism.
Front. Neurol. 15:1370437.
doi: 10.3389/fneur.2024.1370437

Editorial: Multimodality imaging techniques in PD and atypical Parkinsonism

Tianbin Song[1,2]* and Binbin Nie[3]

[1]Department of Radiology and Nuclear Medicine, Xuanwu Hospital, Capital Medical University, Beijing, China, [2]Beijing Key Laboratory of Magnetic Resonance Imaging and Brain Informatics, Beijing, China, [3]Beijing Engineering Research Center of Radiographic Techniques and Equipment, Institute of High Energy Physics, Chinese Academy of Sciences, Beijing, China

KEYWORDS

PD, Parkinsonism, PET, MRI, neuromelanin, DAT-PET, ^{18}F-FDG

Editorial on the Research Topic
Multimodality imaging techniques in PD and atypical Parkinsonism

In this editorial, we provide a summary of the articles that have contributed to the Research Topic "*Multimodality imaging techniques in PD and atypical Parkinsonism*" in the journal Frontiers in Neurology.

Parkinson's disease (PD) is the second most common neurodegenerative disorder, known for its variety of motor and non-motor symptoms (1). Molecular imaging technologies like PET/CT and PET/MR have seen significant advancements in recent years, making them the most valuable tools for diagnosing PD today and in the near future. In this Research Topic on "*Multimodality imaging techniques in PD and atypical Parkinsonism*," researchers have provided distinct perspectives and innovative solutions for this challenge.

Diagnosing prodromal PD in clinical settings poses significant challenges. Over the past decade, several studies have concentrated on the prodromal stage of PD and have identified potential biomarkers for its diagnosis. Jackson et al. utilized the PD progression markers initiative (PPMI) to compare the prevalence of clinical markers of PD with prodromal PD. Their findings indicated that symptoms such as constipation and speech difficulty could potentially serve as predictors of prodromal PD and PD, respectively. This suggests that clinical markers could be valuable tools in identifying individuals at higher risk of developing PD.

Neuromelanin-sensitive MRI is capable of accurately measuring nigral damage and distinguishing PD from healthy subjects. In the substantia nigra, iron deposition is typically concentrated in the reticular zone, while neuromelanin is predominantly concentrated in the dense zone. In PD patients, the content of neuromelanin in the dense zone of the substantia nigra decreases and iron deposition increases, reflecting the degeneration process of dopamine neurons (2). Cao et al. discovered that the amplitude, phase value, and R2* value of upper, middle, and low segments of right substantia nigra compact zones in PD patients differed significantly from those in the control groups. The R2* value of the substantia nigra dense zone was correlated with the H-Y grade, indicating that quantitative iron deposition in the substantia nigra dense zone could be a sensitive imaging biomarker for early diagnosis, assessment of severity, and follow-up evaluation of PD. Quantitative iron–neuromelanin parameters can enhance the clinical evaluation of Parkinsonism. Additionally, Hartono et al. found that quantitative neuromelanin–iron MRI is associated with PD motor severity and has the potential to enhance diagnostic confidence in clinical settings and monitor PD progression.

In addition to the abnormal alterations in iron deposition and neuromelanin of substantia nigra of PD patients, dynamic functional connectivity has emerged as a valuable biomarker for evaluating the progression of PD (3). Excessive daytime sleepiness (EDS) is a common non-motor symptom in PD patients. Tan et al. discovered that the strong dynamic functional connectivity within and between the SMN and VIS served as an imaging biomarker of EDS in PD patients, potentially reflecting the pathophysiological features of EDS in PD patients.

Brain glucose metabolism was found to be reduced in PD patients with cognitive dysfunction. Sun et al. found decreased glucose metabolism in the frontal and posterior cortex in newly diagnosed and untreated PD patients, indicating that changes in glucose metabolism in specific brain regions can indirectly reflect the level of cognitive function.

Cognitive impairment and autonomic impairment such as orthostatic hypotension (OH) are the most common non-motor symptoms in PD patients (4). Even though the relationship between OH and cognitive dysfunction has been reported, it remains unclear if they are frequently observed simultaneously. Xue et al. used ^{18}F-FDG-PET to investigate the relationship between OH and cerebral glucose metabolism in PD patients. Their findings revealed a negative correlation between glucose metabolism in the right medial temporal lobe and delayed recall verbal memory ability. PD patients with OH exhibited poor delayed recall verbal memory function, suggesting that impaired memory function in PD with OH may be attributed to the decreased metabolic function in the medial temporal lobe due to OH.

DAT-PET imaging utilizes ^{11}C-methyl-N-2β-carbomethoxy-3β-(4-ffuorophenyl)-tropanel (^{11}C-CFT) tracers to evaluate the function of presynaptic dopaminergic neurons in the striatum, providing insight into the severity of dopaminergic neuronal degeneration. This method is valuable for distinguishing PD from essential tremor, dystonia, drug-induced Parkinsonism, and vascular Parkinsonism (5). Fan et al. observed that ^{11}C-CFT uptake in the caudate nucleus was higher in the early-onset PD (EOPD) group compared to the late-onset PD (LOPD) group. Furthermore, they found that ^{11}C-CFT uptake in the caudate nucleus, as well as the anterior and posterior part of the putamen, was negatively correlated with the age of onset, H&Y stage, disease duration, UPDRS score, UPDRS III score, rigidity score, and bradykinesia score. These findings demonstrate that ^{11}C-CFT PET can be used as an important objective biomarker to evaluate disease severity and monitor disease progression.

Total-body PET/CT scanner has the advantage of accurately observing PET tracer biodistribution throughout the entire human body. Xin et al. first utilized the total body PET/CT to study DAT PET biodistribution in a real-time and dynamic mode in major organs, which include kidneys, lungs, spleen, thyroid, heart wall, liver, whole brain, muscle, striatum, and bone. They found that different organs had several unique types of ^{11}C-CFT distribution pattern types. ^{11}C-CFT was also calculated to be an extremely low radiation dose according to the study result, which is ∼2.83E-03 mSv/MBq. It only accounts for one-third of the previous literature that has published radiation dose values, which makes it much more suitable for PD patients to do multiple follow-up examinations.

Multimodality imaging techniques hold significant promise for advancing our comprehension of PD and atypical Parkinsonism. Future research should prioritize investigating the interplay between structural, functional, metabolic, and molecular changes in these conditions to achieve a more comprehensive understanding of the pathological mechanism of PD. Furthermore, larger prospective studies are essential to confirm the diagnostic precision and therapeutic effectiveness of multimodal imaging techniques in PD and atypical Parkinsonism.

Author contributions

TS: Conceptualization, Supervision, Writing—original draft, Writing—review & editing. BN: Writing—original draft.

Funding

The author(s) declare that no financial support was received for the research, authorship, and/or publication of this article.

Conflict of interest

The authors declare that the research was conducted in the absence of any commercial or financial relationships that could be construed as a potential conflict of interest.

Publisher's note

References

1. Grover S, Kumar Sreelatha AA, Pihlstrom L, Domenighetti C, Schulte C, Sugier PE, et al. Genome-wide association and meta-analysis of age at onset in Parkinson disease: evidence from the COURAGE-PD consortium. *Neurology*. (2022) 99:e698–710. doi: 10.1212/wnl.0000000000200699

2. Sulzer D, Surmeier DJ. Neuronal vulnerability, pathogenesis, and Parkinson's disease. *Mov Disord*. (2013) 28:715–24. doi: 10.1002/mds.25187

3. Li Z, Chen W, Zeng X, Ni J, Guo Y, Zhang H, et al. Dynamic functional connectivity assesses the progression of Parkinson's disease. *Innov Med*. (2023) 1:100027. doi: 10.59717/j.xinn-med.2023.100027

4. Oka H, Umehara T, Nakahara A, Matsuno H. Comparisons of cardiovascular dysautonomia and cognitive impairment between

de novo Parkinson's disease and *de novo* dementia with Lewy bodies. *BMC Neurol.* (2020) 20:350. doi: 10.1186/s12883-020-01928-5

5. Massa J, Chahine LM. Revision of diagnosis in early Parkinsonism with abnormal dopamine transporter imaging. *J Parkinsons Dis.* (2019) 9:327–34. doi: 10.3233/jpd-181517

frontiers | Frontiers in Neurology

TYPE Original Research
PUBLISHED 04 January 2023
DOI 10.3389/fneur.2022.1096966

OPEN ACCESS

EDITED BY
Binbin Nie,
Institute of High Energy Physics, Chinese Academy of Sciences (CAS), China

REVIEWED BY
Yuto Uchida,
Johns Hopkins Medicine, United States
Luo Song,
Nanjing General Hospital of Nanjing Military Command, China

*CORRESPONDENCE
Yaowei Li
✉ weiweihao168@sina.com
Jiangong Zhang
✉ jiangongzh@126.com

†These authors have contributed equally to this work

SPECIALTY SECTION
This article was submitted to Applied Neuroimaging, a section of the journal Frontiers in Neurology

RECEIVED 13 November 2022
ACCEPTED 13 December 2022
PUBLISHED 04 January 2023

CITATION
Cao Q, Huang J, Tang D, Qian H, Yan K, Shi X, Li Y and Zhang J (2023) Application value of multiparametric MRI for evaluating iron deposition in the substantia nigra in Parkinson's disease. *Front. Neurol.* 13:1096966. doi: 10.3389/fneur.2022.1096966

Application value of multiparametric MRI for evaluating iron deposition in the substantia nigra in Parkinson's disease

Qing Cao[1†], Jinjin Huang[2†], Dongping Tang[3], Hao Qian[4], Kun Yan[4], Xun Shi[5], Yaowei Li[1*†] and Jiangong Zhang[5*†]

[1]Department of Radiology, Guangzhou Xinhai Hospital, Guangzhou, Guangdong, China, [2]Department of Neurosurgery, The PLA 74th Group Army Hospital of Chinese, Guangzhou, Guangdong, China, [3]Department of Science and Education Department, Guangzhou Xinhai Hospital, Guangzhou, Guangdong, China, [4]Department of Neurology, Guangzhou Xinhai Hospital, Guangzhou, Guangdong, China, [5]Department of Nuclear Medicine, The First People's Hospital of Yancheng, The Fourth Affiliated Hospital of Nantong University, Yancheng, Jiangsu, China

Objective: This study aimed to investigate the application value of multi-parametric magnetic resonance imaging (MRI) in the diagnosis of iron deposition in the substantia nigra dense zone in Parkinson's disease (PD) and to evaluate the diagnostic value of the correlation among multi-parametric imaging indicators, clinical stage, and disease duration.

Materials and methods: Thirty-six patients with clinically confirmed PD and 36 healthy controls were enrolled. The disease course was recorded, and PD severity was graded using the Hoehn–Yahr (H–Y) scale. All subjects underwent magnetic sensitivity weighted imaging (SWI), neuromelanin magnetic resonance imaging (NM-MRI), and a T2*mapping sequence. Based on the fusion of the NM-MRI and SWI amplitude maps, phase maps, and T2*MAPPING value maps, NM-MRI was used to delineate the dense zone of the substantia nigra, which was divided into three sub-regions: upper, middle, and lower. In this way, the amplitude, phase, and R2* values of each sub-region and the average value of the sum of the three sub-regions were obtained simultaneously in the SWI amplitude, phase, and T2*MAPPING maps. The multi-parameter imaging indices were compared between the two groups, and the correlation between them and clinical indices was evaluated in the PD group.

Results: The upper (amplitude, phase value, R2* value), middle, and lower (amplitude) right substantia nigra compact zones were significantly different between the PD and control groups. The upper (phase value, R2* value) and middle (amplitude) areas of the left substantia nigra compact zone were also significantly different between the two groups (all $P < 0.05$). The mean values (amplitude, phase value, R2* value) of the right substantia nigra densification zone and the mean values (phase value) of the left substantia nigra densification zone were also significantly different (all $P < 0.05$). Amplitudes in the middle and lower parts of the right substantia nigra dense zone were negatively correlated with the H–Y grade (middle: $r = -0.475$, $P = 0.003$;

lower: $r = -0.331$, $P = 0.049$). Amplitudes of the middle and lower parts of the dense zone of the left substantia nigra were negatively correlated with the H–Y grade (middle: $r = -0.342$, $P = 0.041$; lower: $r = -0.399$, $P = 0.016$). The average amplitude of the right substantia nigra compact zone was negatively correlated with the H–Y grade ($r = -0.367$, $P = 0.027$). The average R2* value of the compact zone of the left substantia nigra was positively correlated with the H–Y grade ($r = 0.345$, $P = 0.040$).

Conclusion: Multiparametric MRI sequence examination has application value in the evaluation of iron deposition in the dense zone of the substantia nigra in PD. Combined with NM-MRI, fusion analysis is beneficial for accurately locating the substantia nigra compact zone and quantitatively analyzing the iron deposition in different sub-regions. Quantitative iron deposition in the middle and lower parts of the substantia nigra dense zone may become an imaging biological indicator for early diagnosis, severity evaluation, and follow-up evaluation of PD and is thus conducive for clinical diagnosis and treatment evaluation.

KEYWORDS

Parkinson's disease, magnetic sensitivity weighted imaging, T2*mapping, image fusion, MR

1. Introduction

Parkinson's disease (PD) is a common condition associated with neurological degeneration, and clinical symptoms are aggravated with an increase in neuronal degeneration (1). Imaging modalities, especially using magnetic resonance imaging (MRI), and new sequences have been used to explore more sensitive imaging biological and clinical indicators for correlation analysis. The main neuropathological changes in patients with PD are damage to the substantia nigra neurons and the related dopamine receptor pathway; an increase in abnormal iron deposition in the substantia nigra area; and an increase in the content of neuromelanin iron complex, which induces glial cell aggregation, thus leading to neuronal damage and accelerated cell death (2, 3). Previous studies have indicated that iron deposition in the substantia nigra is normally concentrated in the reticular zone, while neuromelanin is mainly concentrated in the dense zone of the substantia nigra. In PD patients, the neuromelanin content in the dense zone of the substantia nigra decreases and iron deposition increases, reflecting the degeneration process of dopamine neurons (4). To better understand the association between iron deposition in the substantia nigra compacta and the degeneration of dopamine neurons (5), it is necessary to accurately locate iron deposition in the substantia nigra compacta and evaluate the changes in iron deposition in the substantia nigra compacta (6).

Thus, this study aimed to analyze the differences in iron deposition in the substantia nigra compact zones and the correlation between iron deposition and PD onset, to find more sensitive biological imaging indicators, and to provide new approaches for the imaging diagnosis of PD. This study was based on magnetic sensitivity-weighted imaging (SWI), which has highly sensitive for detecting iron deposition area and its scope (7). Neuromelanin magnetic resonance imaging (NM-MRI) can better show the distribution of neuromelanin in the substantia nigra (8, 9), and T2*mapping can be used to quantify iron deposition (10). In this study, these three sequences were fused in pairs, and the substantia nigra was divided into the upper, middle, and lower regions for analysis and comparison.

2. Materials and methods

2.1. Study design and participants

This prospective study enrolled 36 patients with PD from the Department of Neurology of Guangzhou Xinhai Hospital between March 2020 and August 2022. The inclusion criteria were as follows: (1) PD diagnosis according to the Chinese diagnostic standard (2020 version), that is, the patient has motion retardation and at least static tremor or myotonia; (2) ability to cooperate with MRI examination and no contraindications to MRI scanning; and (3) the image quality meets the evaluation criteria. The exclusion criteria were as follows: (1) secondary Parkinson-like syndrome caused by other organic diseases of the nervous system or drugs and (2) other neurological and psychiatric diseases, trauma, and developmental malformations affecting the image evaluator. The clinical data, medical history, and Hoehn–Yahr (H–Y) grade of

TABLE 1 Scan each sequence parameter value.

Sequence	TR (ms)	TE (ms)	Voxel size (mm)	Number of layers	Layer spacing (mm)	Roll back angle	Average times	Interpolation	IR (ms)
T2WI_TRA	5,103	119.9	0.67∗0.60∗5.00	23	1	150	2	–	–
T1WI_TRA	2,267	10.2	0.69∗0.63∗5.00	23	1	135	1	–	920
FLAIR_TRA	8,000	118.6	0.95∗0.76∗5.00	23	1	120	2	–	2,500
DWI_TRA	2,087	107.1	1.44∗1.44∗5.00	23	1	–	–	–	–
T2WI_SAG	5,683	121.8	0.77∗0.65∗5.00	23	1	145	1.2	–	–
FLAIR_COR	8,000	112.9	0.90∗0.72∗5.00	25	1	150	1.5	–	2,500
SWI_TRA	30.3	20	0.51∗0.51∗2.00	56	–	–	1	2	–
NM-MRI_TRA	738	10.54	0.62∗0.44∗3.00	22	0	130	5	–	–
T2∗MAPPING_TRA	436.7	2.24/4.48/ 6.72/8.96/11.2	0.48∗0.48∗3.00	11	0.3	–	1	–	–

the PD patients were collected, and multiparameter MRI images were obtained.

In addition, 36 healthy control subjects were recruited from Guangzhou Xinhai Hospital staff and society. The inclusion criteria were as follows: (1) no PD-related exercise or non-exercise symptoms; (2) no family history of PD and idiopathic tremor; (3) ability to cooperate with magnetic resonance examination and no contraindication to magnetic resonance scanning; and (4) the image quality met the evaluation criteria. The exclusion criteria were: (1) other neurological and psychiatric diseases and taking central medicine; (2) trauma, developmental malformation, and other conditions affecting image evaluation.

This study was approved by the ethics committee of Guangzhou Xinhai Hospital (Approval No.: GZXH-20200147) and was conducted according to the tenets of the Declaration of Helsinki. All subjects and their family members were informed of the purpose of the study, the duration of the scan, no radiation risk, and precautions for examination in detail. Informed consent was obtained from all participants. The general brain conditions were interpreted by him and his family afterwards.

2.2. Instrument and imaging

A 3.0T MRI system (United-Imaging Medical, uMR780) and a 24-channel coil for the head and neck were used. Conventional MRI sequence acquisition included transverse axial [T1 weighted imaging (T1WI), T2 weighted imaging (T2WI), fluid attenuated inversion recovery (FLAIR), diffusion-weighted imaging], sagittal (T2WI), coronal (FLAIR), SWI, NM-MRI, and T2*mapping sequences. All parameters are listed in Table 1. The total scanning time of the MRI was 28 min 36 s.

2.3. Image preprocessing analysis

All multiparameter image data were processed in a 3.0 T post-processing workstation (model: uWS-MR-R004). Two diagnostic imaging physicians with 12 and 20 years of experience independently evaluated the images in a blinded manner before meeting for consensus. They measured the relevant image indicators and considered the average value of the two. NM-MRI was fused with the SWI amplitude, phase, and T2*MAPPING maps. Using NM-MRI, the melanin distribution of neurons in the bilateral substantia nigra was delineated layer-by-layer, and the upper, middle, and lower sub-regions were equally divided. The upper layer included the red nucleus and the substantia nigra reticulata with a maximum low signal (Figure 1A), and the middle layer included the area of the substantia nigra compact zone with a high signal. This layer indicated the boundary between the red nucleus and the substantia nigra reticulata and the substantia nigra compact zone and was delineated based on the high NM-MRI signal (Figure 1B). The central layer was located at the largest level of the substantia nigra compact zone based on the high NM-MRI signal at the time of delineation and indicated the boundary between the red nucleus and the substantia nigra reticularis and the substantia nigra compact zone (Figure 2A). The lower layer was located at the caudal level of the substantia nigra, which was also delineated with a NM-MRI hyperintensity (Figure 3A).

The SWI amplitude (Figure 1A), phase value (Figure 2B), and T2* value of the T2*maps (R2* value = 1/T2* value, Figure 3B) of the delineated area at each level were converted to radians using the following formula: $f(x) = x^*\pi/1{,}800$, where x is the actual measured value, and the phase value range is between $-\pi$ and$+\pi$. The measurement and data processing methods were performed under the guidance of the Joint Photographic Engineer. All images were automatically fused using the image fusion function of the post-processing

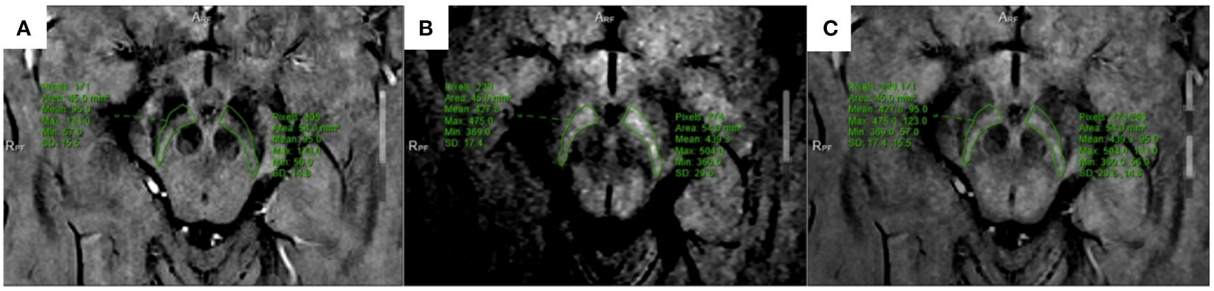

FIGURE 1
Located in the upper part of SNc. **(A)** SWI-amplitude diagram; **(B)** NM-MRI map; **(C)** The two images are fused, and the corresponding region amplitude is obtained.

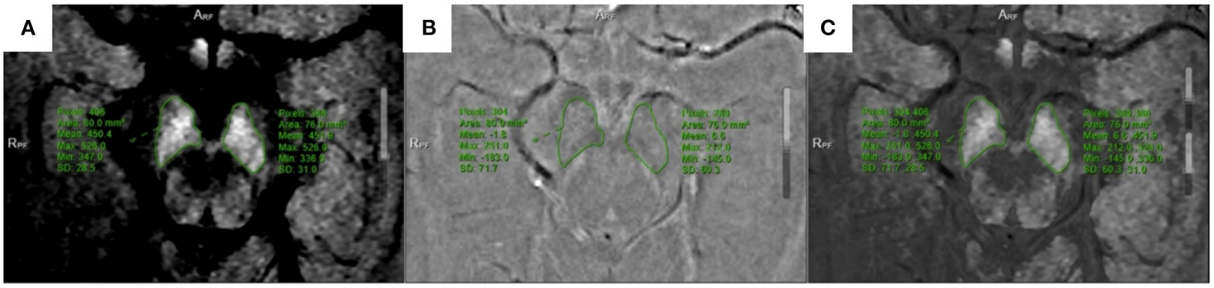

FIGURE 2
Located in the middle of SNc. **(A)** NM-MRI map; **(B)** SWI-phase diagram; **(C)** The two images are fused, and the phase value is obtained.

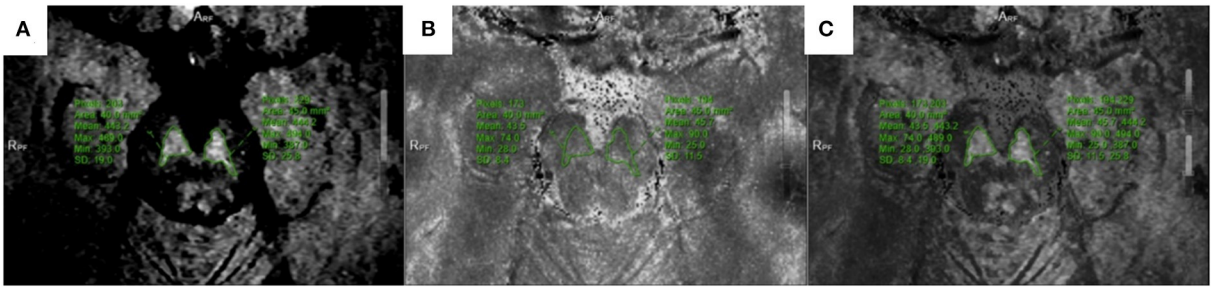

FIGURE 3
Located in the lower of SNc. **(A)** NM-MRI map; **(B)** T2*mapping; **(C)** Combine the two maps and obtain T2* value.

workstation (Figures 1C, 2C, 3C), and the image fusion effect, including the edges of anatomical structures, blood vessels, and 3D MPR reconstruction layers, was evaluated by the two physicians to ensure that the image fusion met the diagnostic requirements. Before sketching, the window width and position were adjusted to be consistent to reduce the difference between the vision and signal.

The boundary of the melanin high-signal area was clear and easily sketched, while the attenuation area was not sketched (11). The region of interest corresponding to the anatomical region of SWI and T2*mapping was used to measure its value. The two physicians easily reached a consensus on the boundary of the region of interest with high operability and repeatability. Images were collected without space. Based on the voxel, the dense zone regions of the upper, middle, and lower parts of the substantia nigra were delineated to measure the signal changes of the corresponding regions to achieve a quantitative analysis of iron deposition in the dense zone of the substantia nigra. In the image processing, six cases in the PD group had partial plane motion, resulting in angle deviation, which could not be

corrected for fusion measurement. Thus, 36/42 patients in the PD group were included.

After the data of all sub-regions are counted, the amplitude, phase value and R2* value of the three sub-regions of the substation nigra compact zone on both sides are added respectively, and then the average value is calculated as the signal representation of the overall substation nigra compact zone compact zone on both sides, and the energy analysis is made for each average value parameter to help understand the impact of iron deposition on the overall substation nigra compact zone.

2.4. Statistical analysis

An independent sample *t*-test or chi-square test was used for comparisons between the two groups. Pearson's correlation analysis was used to evaluate the correlation between each sequence of imaging indicators and clinical indicators in PD. All statistical analyses were performed using SPSS Statistics software (version 22.0). Statistical significance was set at $P < 0.05$.

3. Results

3.1. Subject characteristics

Among the MR images of 42 patients, images could not be fused for quantitative analysis due to poor image quality in 6 patients. Therefore, 36 patients (16 males and 20 females) in the PD group were included in the final analysis. The average patient age was 70.28 ± 13.14 years, the average disease duration was 6.48 ± 6.09 years, and the average H–Y grade was 2.76 ± 1.07. Meanwhile, the control group ($n = 36$) included 17 males and 19 females, and the average patient age was 63.83 ± 14.41 years. There was no significant between-group difference in age ($P = 0.051$).

3.2. Multi-parameter MRI fusion image analysis

3.2.1. Comparison of iron deposition in the upper, middle, and lower parts of the substantia nigra compacta zone and average values between the two groups based on fusion images

There were significant between-group differences in the amplitude (amplitude: $t = -2.138$, $P < 0.05$), phase value ($t = -2.802$, $P < 0.05$), and R2* value ($t = 2.424$, $P < 0.05$) in the upper part of the right substantia nigra compact zone. Meanwhile, only the amplitude ($t = -2.711$, $P < 0.05$) but not the phase value ($t = -1.680$, $P > 0.05$) and R2* value ($t = 1.992$, $P = 0.05$) in the middle of the right substantia nigra dense zone was significantly different between the two groups. Similarly, there were significant between-group differences in the amplitude ($t = -2.019$, $P < 0.05$) but not in the phase value ($t = -0.808$, $P > 0.05$) and R2* value ($t = 0.642$, $P > 0.05$) in the lower part of the right substantia nigra dense zone.

In contrast, in the upper part of the left substantia nigra compacta, the phase value ($t = -2.242$, $P < 0.05$) and R2* value ($t = 2.018$, $P < 0.05$), but not the amplitude ($t = -1.248$, $P > 0.05$), were significantly different between the two groups. For the middle of the left substantia nigra dense zone, there was a significant between-group difference in amplitude ($t = -2.039$, $P < 0.05$) but not in phase value ($t = -0.760$, $P > 0.05$) and R2* value ($t = 1.336$, $P > 0.05$). For the lower part of the left substantia nigra compacta zone, there were no significant between-group differences in amplitude ($t = -1.670$, $P > 0.05$), phase value ($t = -1.266$, $P > 0.05$) and R2* value ($t = 0.472$, $P > 0.05$).

Meanwhile, the average values in the right substantia nigra compacta (amplitude: $t = -2.747$, $P < 0.05$, phase value: $t = -2.338$, $P < 0.05$, R2* value: $t = 2.334$, $P < 0.05$) was significantly different among the three sub-regions. For the overall average values in the left substantia nigra compact zone, only phase was significantly different between the two groups (amplitude: $t = -1.892$, $P > 0.05$; phase value: $t = -2.197$, $P < 0.05$; and R2* value: $t = 1.200$, $P > 0.05$) (Table 2). In addition, the ROC curve was used to analyze these average values, and it was found that the R2* value on the right side (AUC = 0.678) has a high diagnostic efficiency for the detection of iron deposition in the substation nigra compact zone of PD, and the calculation of threshold value of each index (Figure 4 and Table 3).

3.2.2. Correlation analysis of PD patients

In the PD group, the correlation of the amplitude, phase, and R2* values of each sub-region in the substantia nigra compact zone with disease onset time and H–Y grade was analyzed using Pearson correlation analysis. The results showed that the amplitudes of the middle and lower parts of the right side of the substantia nigra compacta zone were negatively correlated with the H–Y grade (middle: $r = -0.475$, $P = 0.003$; lower: $r = -0.331$, $P = 0.049$, Figure 5A), while those in the left side of the substantia nigra compacta zone were negatively correlated with the H–Y grade (middle: $r = -0.342$, $P = 0.041$, lower: $r = -0.399$, $P = 0.016$, Figure 5B). In addition, Pearson correlation analysis was performed for the correlation between the average value of amplitude, phase value, and R2* value of the three sub-regions of the substantia nigra dense with disease onset time and H–Y grade. The results showed that the average amplitude on the right side of the substantia nigra compacta zone was negatively correlated with the H–Y grade ($r = -0.367$, $P = 0.027$, Figure 5C), while the average R2* value on the left side of the substantia nigra compacta zone was positively correlated with the H–Y grade ($r = 0.345$, $P = 0.040$, Figure 5D). In

TABLE 2 Based on the comparison between the upper, middle and lower three sub regions and the average iron deposition groups of SNc.

	Group (mean ± standard deviation)		*t*	*P*
	PD ($n = 36$)	Healthy control group ($n = 36$)		
Amplitude of upper R-SNc	90.17 ± 12.04	95.76 ± 10.07	−2.138	0.036
Phase value of upper R-SNc	−0.0463 ± 0.0580	−0.0135 ± 0.0396	−2.802	0.007
R2* value of upper R-SNc	31.73 ± 3.89	29.63 ± 3.46	2.424	0.018
Amplitude of middle R-SNc	85.73 ± 11.29	92.13 ± 8.56	−2.711	0.008
Phase value of middle R-SNc	−0.0326 ± 0.0772	−0.0081 ± 0.0407	−1.680	0.097
R2* value of middle R-SNc	31.40 ± 4.25	29.65 ± 3.15	1.992	0.050
Amplitude of lower R-SNc	96.44 ± 11.61	101.65 ± 10.26	−2.019	0.047
Phase value of lower R-SNc	−0.0353 ± 0.1007	−0.0190 ± 0.0682	−0.808	0.422
R2* value of lower R-SNc	27.61 ± 4.79	26.92 ± 4.21	0.642	0.523
Amplitude of upper L-SNc	92.24 ± 9.19	94.78 ± 8.05	−1.248	0.216
Phase value of upper L-SNc	−0.0399 ± 0.0459	−0.0186 ± 0.0337	−2.242	0.028
R2* value of upper L-SNc	30.39 ± 4.19	28.67 ± 2.93	2.018	0.047
Amplitude of middle L-SNc	86.96 ± 10.04	91.55 ± 9.06	−2.039	0.045
Phase value of middle L-SNc	−0.0170 ± 0.0576	−0.0079 ± 0.0420	−0.760	0.450
R2* value of middle L-SNc	29.86 ± 4.01	28.78 ± 2.74	1.336	0.186
Amplitude of lower L-SNc	94.54 ± 12.53	99.12 ± 10.67	−1.670	0.099
Phase value of lower L-SNc	−0.0677 ± 0.0804	−0.0463 ± 0.0613	−1.266	0.210
R2* value of lower L-SNc	26.22 ± 4.65	26.67 ± 3.43	−0.472	0.639
Average amplitude of R-SNc	90.50 ± 10.24	96.51 ± 8.23	−2.747	0.008
Average phase value of R-SNc	−0.0381 ± 0.0548	−0.0135 ± 0.0311	−2.338	0.022
Average R2* value of R-SNc	30.25 ± 2.87	28.73 ± 2.63	2.334	0.022
Average amplitude of L-SNc	91.24 ± 9.33	95.15 ± 8.14	−1.892	0.063
Average phase value of L-SNc	−0.0415 ± 0.0358	−0.0243 ± 0.0305	−2.197	0.031
Average R2* value of L-SNc	28.82 ± 3.40	28.03 ± 1.93	1.200	0.234

Independent-sample t-test; R, right; L, left.

addition, the onset time of PD was positively correlated with the H–Y scale grade ($r = 0.396$, $P = 0.017$).

4. Discussion

Histologically, neurons in the dense zone of the substantia nigra have rich melanin and poor iron content. In contrast, the cells in the reticular zone of the substantia nigra are rich in iron but not in melanin. Previous physiological, pathological, and anatomical studies have confirmed that the neuronal degeneration in the substantia nigra compacta in patients with PD is closely related to an abnormal increase in iron content. Therefore, quantitative analysis of iron deposition in the substantia nigra compact zone is particularly important for understanding the pathophysiological changes of neuronal degeneration in PD patients (12–15).

There are currently many quantitative analysis studies for iron deposition in the substantia nigra using magnetic resonance methods, such as SWI, QSM, and T2*mapping (14–16). However, these single sequences cannot distinguish the dense zone of the substantia nigra from the reticular zone during measurement, especially when the iron deposition in the dense zone of patients with PD increases abnormally. In addition, these sequences are sensitive to iron deposition but cannot distinguish their boundaries well. Therefore, the dense and reticular zones of the substantia nigra are mostly used to analyze the iron deposition content to judge the degree of neuronal degeneration (17, 18).

To better understand iron deposition and distribution in the substantia nigra compact zone, as well as their correlation with the course and severity of the disease, this study used NM-MRI to better display the distribution of melanin neurons in the substantia nigra, so as to better locate the substantia nigra compact zone. NM-MRI of the same case was fused with SWI and T2*mapping sequences, which can accurately delineate iron deposition by SWI and T2*mapping sequences in the distribution area of melanin neurons, to achieve a quantitative analysis of iron deposition in the dense zone of the substantia nigra (19). To better understand the distribution of iron deposition in the substantia nigra compact zone, the area of the substantia nigra compact zone was equally divided into three regions, and iron deposition in each region was analyzed.

The results showed that iron deposition in the upper part of the right substantia nigra compact zone was significantly higher in the PD group than in the control group, and the amplitude, phase value, and R2* values were also significantly different. In contrast, in the middle and lower parts of the right substantia nigra compact zone, only the amplitude was significantly different between the two groups, and the phase value and R2* value was not. This may be because the amplitude is more sensitive to the iron deposition measurement than is the phase value and R2* value in the middle and lower parts of the substantia nigra compact zone. Another reason is because the difference between the phase value and R2* value cannot be observed when the iron deposition content in the substantia nigra compact zone is smaller than that in the reticular zone.

Compared with the normal control group, the PD group showed significantly higher iron deposition in the upper part of the left substantia nigra compact zone, and the phase and R2* values were also significantly different. Meanwhile, for the middle of the left substantia nigra compact zone, only the amplitude value, but not the phase value and R2* value, showed significant differences. The lower part of the left substantia nigra compact zone did not show significant changes in iron deposition, and the amplitude, phase, and R2* values were not significantly different between the two groups. Collectively, these results indicated more significant neuronal degeneration in the substantia nigra of PD patients or a top-down degeneration process of PD. The research of Du Guangwei et al. is based on the analysis of the whole substantia nigra dense zone and reticular zone. It is mentioned that R2* and quantitative susceptibility map are higher in the substantia nigra dense zone and reticular zone of all PD patients (20). Arribarat et al. (21) divided the substation nigra into anterior and posterior parts for analysis, showing that the relaxometry T2* values were greater for PD patients than HCs in the anterior SN, but not in relation with the iron deposition in the posterior SN with the relaxometry T2*. This also shows that the results of comparison between various parameters and the sensitivity to iron deposition are different in the overall analysis of substation nigra compact and the analysis of sub regions. This study will compare and analyze different parameters and indicators in different sub regions, observe the parameters in each sub region of substation nigra compact zone. Through the study of iron deposition in each sub-region, the influence of iron deposition in the substantia nigra compact zone on melanin neurons and whether the change of iron deposition in each sub-region is related to the occurrence

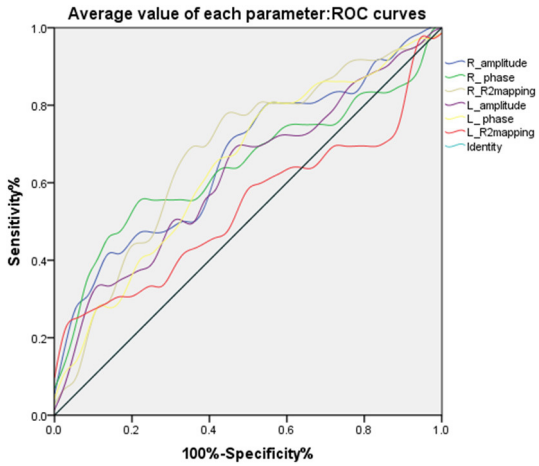

FIGURE 4
ROC curves of the average values of different parameters in bilateral substantia nigra compact zone.

TABLE 3 Analysis of ROC curves for average value of each parameter.

Parameter average	Sensitivity	Specificity	AUC	*P*	Threshold	95%CI
R_amplitude	41.7%	88.9%	0.664	0.011	87.23333	0.543∼0.771
R_phase	55.6	80.6	0.645	0.032	−0.0339	0.523∼0.754
R_R2*mapping	77.8	58.33	0.678	0.006	28.37	0.557∼0.783
L_amplitude	33.3	91.7	0.621	0.070	85.8667	0.499∼0.733
L_phase	77.8	50.0	0.644	0.028	−0.0187	0.523∼0.754
L_R2*mapping	25.0	97.2	0.538	0.592	30.8733	0.416∼0.656

R, right; L, left.

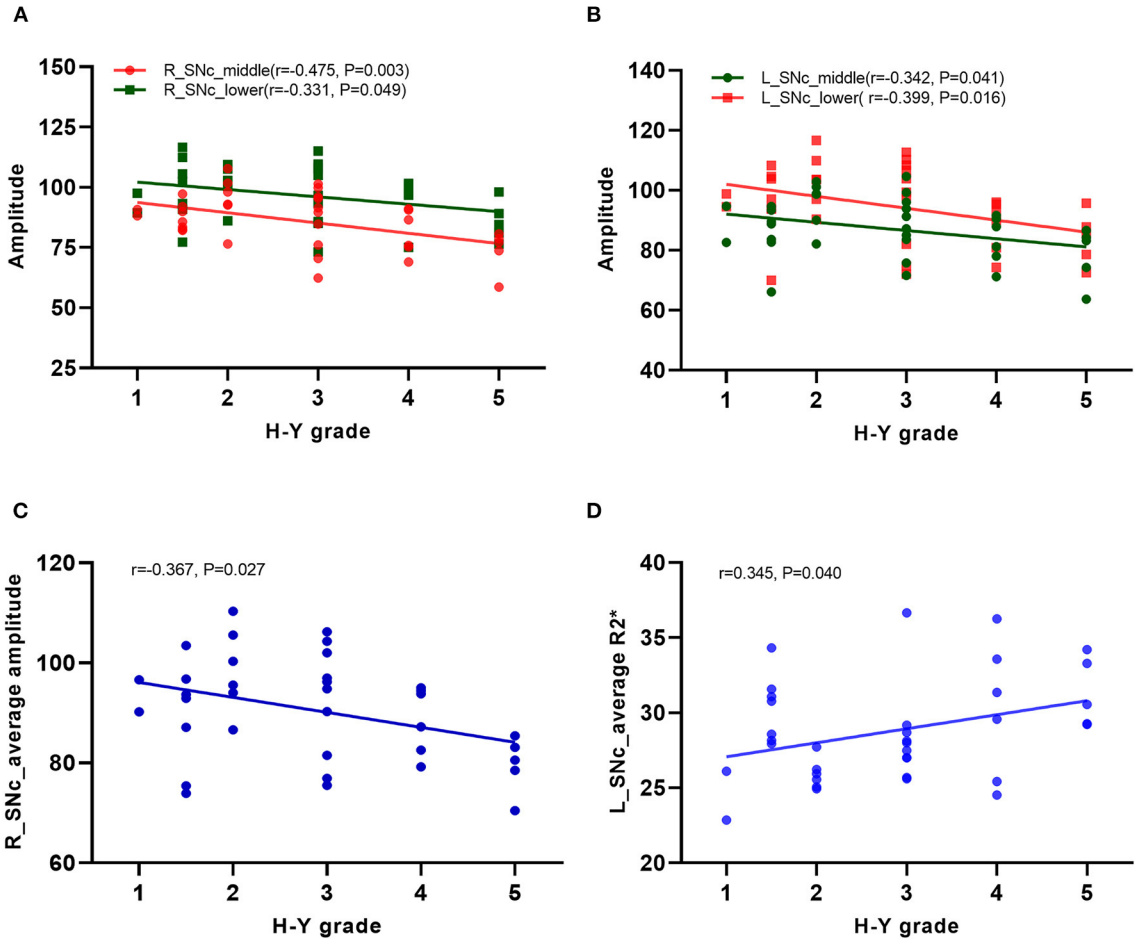

FIGURE 5
Correlation analysis in PD patients. **(A)** Correlation analysis between the amplitudes of the middle and lower parts of the right side of the substation nigra compact zone and H–Y scale; **(B)** Correlation analysis between the amplitudes of the middle and lower parts of the left side of the substation nigra compact zone and H–Y scale; **(C)** Correlation analysis between the average amplitude on the right side of the substation nigra compact zone and H–Y scale; **(D)** Correlation analysis between the the average R2* value on the left side of the substation nigra compact zone and H–Y scale.

and development of disease were understood. The sensitivity of each parameter to its internal iron deposition was compared and analyzed, providing a reference for the subsequent research in the sub-region.

To understand the effect of iron deposition on neuronal degeneration in the entire substantia nigra compact zone, the mean of the measured values in Sanya were used in the analysis. The results showed that the mean values of amplitude, phase, and R2* of the right substantia nigra compact zone were significantly different between the PD and healthy control groups. This indicates that the overall iron deposition in the substantia nigra compact zone was more significant in the PD group than in the healthy control group, consistent with previous findings. For values in the left substantia nigra compact zone, the phase value, but not the amplitude and R2* values, were significantly different between the two groups. The overall analysis indicates that the phase value is more sensitive to iron deposition than is the amplitude and R2* values. Du Guangwei et al. also mentioned in the study that during the 18 months follow-up, the substantia nigra pars compacta R2* showed a faster increase in PD compared with controls. Through ROC curve analysis, we found that the average value of R2* in the right substantia nigra compact zone has higher diagnostic energy efficiency, in line with previous results (2, 20, 22).

The study also analyzed the correlation of the measured values of each sub-region and the whole dense zone of the substantia nigra with the course and degree (H–Y grade) of the disease. The results showed that the amplitude of the middle and lower parts of the bilateral substantia nigra dense zone was negatively correlated with the H–Y stage, while the value measured at the upper part was not correlated with the disease course and degree. This indicates that the more iron deposition

in the middle and lower parts of the substantia nigra dense zone, the more severe is PD. Moreover, the change in iron deposition in the middle and lower parts of the substantia nigra dense zone may highlight the severity of PD. Correlation analysis of the overall average value of the substantia nigra dense zone with the disease course and degree (H–Y grade) showed that the average amplitude value in the right and the average R2* value in the left of the substantia nigra dense zone were correlated with the H–Y grade. This supported that an abnormal increase in iron deposition in the substantia nigra dense zone was correlated with the severity of PD (23). Different measurement methods obtained the same results, consistent with previous results (24, 25).

The study findings show that iron deposition in the upper part of the dense zone of the substantia nigra is more obvious in the PD group than in the healthy control group, but the severity of PD could not be evaluated. The results of quantitative analysis of iron deposition in the middle and lower parts of the right substantia nigra compact zone and in the middle part of the left substantia nigra compact zone both showed a difference in iron deposition according to PD severity. This indicated that the analysis of iron deposition in sub-regions is helpful for early PD diagnosis and the evaluation of disease progression. In particular, the amplitude value is sensitive to quantitative iron deposition. The amplitude, phase, and R2* values of the three sub-regions showed significant differences in iron deposition in PD patients. The right amplitude and left R2* value was correlated with disease severity in PD patients. This indicated that iron deposition in the overall or sub-regions of the substantia nigra compact zone is related to neuronal degeneration in this zone, and thus, its analysis clinically significant for the evaluation of disease in PD patients (6). The analysis and comparison of different measurement methods of iron deposition highlight the clinical value of different parameters, which can provide a basis for more accurate imaging biological indicators for clinical PD diagnosis (26, 27).

This study had some limitations. First, patients were required to be highly cooperative during the examination process. Only when a complete sequence is acquired at one time and the image meets the diagnostic requirements can the subsequent image fusion process be guaranteed. The resolution was relatively high, and the acquisition time was relatively long. Second, in the fusion process, the required sequence images are fused in pairs, not all sequence parameters are fused together. Because the distribution of high signals in the substantia nigra dense zone varies greatly among individuals, the images are manually delineated by the high signal areas on the NM-MRI image, which cannot be analyzed based on voxels or atlases, and it is inevitable to cause certain deviation to the results. However, we also involved two physicians to jointly confirm and delineate the regions of interest to reduce the artificial influence on the results. Third, due to individual differences in the size of the substantia nigra dense zone, layer selection was measured at the defined sub-region level. Some parts of the substantia nigra dense zone with larger or smaller volumes that exceeded the sub-region were measured twice, and the average value of the lower sub-region was included in the analysis, which may have a certain impact on the results. However, the two physicians discussed the findings during data processing to reach an agreement, minimizing this impact.

In summary, this study improved the method of magnetic resonance multiparameter display in the substantia nigra dense zone area and iron deposition measurement and analysis to evaluate iron distribution and deposition in the substantia nigra dense zone. This can help PD diagnosis and the evaluation of disease severity. Further, exploratory research was conducted to identify additional biological imaging indicators for clinical PD diagnosis, with the value of each indicator in the clinical diagnosis and evaluation of PD described.

Data availability statement

The original contributions presented in the study are included in the article/supplementary material, further inquiries can be directed to the corresponding authors.

Ethics statement

The studies involving human participants were reviewed and approved by the Ethics Committee of Guangzhou Xinhai Hospital. The patients/participants provided their written informed consent to participate in this study. Written informed consent was obtained from the individual (s) for the publication of any potentially identifiable images or data included in this article.

Author contributions

All authors listed have made a substantial, direct, and intellectual contribution to the work and approved it for publication.

Funding

This study was supported by funding from Two New Projects of Guangzhou Health Science and Technology (No.: 20211A040003) and 2021 Yancheng Medical Science and Technology Development Project Grants-Yancheng Health Planning [2021] No. 47 (YK2021017).

Conflict of interest

The authors declare that the research was conducted in the absence of any commercial or financial relationships that could be construed as a potential conflict of interest.

Publisher's note

References

1. Kalia Lorraine V, Lang Anthony E. Parkinson disease in 2015: evolving basic, pathological and clinical concepts in PD. *Nat Rev Neurol.* (2016) 12:65–6. doi: 10.1038/nrneurol.2015.249

2. Lehéricy S, Bardinet E, Poupon C, Vidailhet M, François C. 7 Tesla magnetic resonance imaging: a closer look at substantia nigra anatomy in Parkinson's disease. *Movement Disord Off J Movement Disord Soc.* (2014) 29:1574–81. doi: 10.1002/mds.26043

3. Zeng XS, Geng WS, Jia JJ, Chen L, Zhang PP. Cellular and molecular basis of neurodegeneration in Parkinson disease. *Front Aging Neurosci.* (2018) 10:109. doi: 10.3389/fnagi.2018.00109

4. Braak H, Del Tredici K, Rüb U, De Vos RA, Steur EN, Braak E. Staging of brain pathology related to sporadic Parkinson's disease. *Neurobiol Aging.* (2003) 24:197–211. doi: 10.1016/S0197-4580(02)00065-9

5. Reneman L, van der Pluijm M, Schrantee A, van de Giessen E. Imaging of the dopamine system with focus on pharmacological MRI and neuromelanin imaging. *Eur J Radiol.* (2021) 140:109752. doi: 10.1016/j.ejrad.2021.109752

6. Salzman G, Kim J, Horga G, Wengler K. Standardized data acquisition for neuromelanin-sensitive magnetic resonance imaging of the substantia Nigra. *J Vis Exp.* (2021) 8:e62493. doi: 10.3791/62493

7. Kolpakwar S, Arora AJ, Pavan S, Kandadai RM, Alugolu R, Saradhi MV, et al. Volumetric analysis of subthalamic nucleus and red nucleus in patients of advanced Parkinson's disease using SWI sequences. *Surg Neurol Int.* (2021) 27:2532. doi: 10.25259/SNI_584_2021

8. Wang X, Zhang Y, Zhu C, Li G, Kang J, Chen F, et al. Correction to: The diagnostic value of SNpc using NM-MRI in Parkinson's disease: meta-analysis. *Neurol Sci Off J Ital Neurol Soc Ital Soc Clin Neurophysiol.* (2019) 40:2491. doi: 10.1007/s10072-019-04051-7

9. He N, Chen Y, LeWitt PA, Yan F, Haacke EM. Application of neuromelanin MR imaging in Parkinson disease. *J Magn Reson Imag.* (2022) 26:28414. doi: 10.1002/jmri.28414

10. Kan H, Uchida Y, Ueki Y, Arai N, Tsubokura S, Kunitomo H, et al. R2* relaxometry analysis for mapping of white matter alteration in Parkinson's disease with mild cognitive impairment. *NeuroImage Clin.* (2022) 33:102938. doi: 10.1016/j.nicl.2022.102938

11. Xing Y, Sapuan AH, Martín-Bastida A, Naidu S, Tench C, Evans J, et al. Neuromelanin-MRI to quantify and track nigral depigmentation in parkinson's disease: a multicenter longitudinal study using template-based standardized analysis. *Mov Disord.* (2022) 37:1028–39. doi: 10.1002/mds.28934

12. Ward RJ, Zucca FA, Duyn JH, Crichton RR, Zecca L. The role of iron in brain ageing and neurodegenerative disorders. *Lancet Neurol.* (2014) 13:1045–60. doi: 10.1016/S1474-4422(14)70117-6

13. Thomas GEC, Leyland LA, Schrag A. Brain iron deposition is linked with cognitive severity in Parkinson's disease. *J Neurol Neurosurg Psychiatry.* (2020) 91:418–25. doi: 10.1136/jnnp-2019-322042

14. Fedeli MP, Contarino VE, Siggillino S, Samoylova N, Calloni S, Melazzini L, et al. Iron deposition in Parkinsonisms: a quantitative susceptibility mapping study in the deep grey matter. *Eur J Radiol.* (2020) 133:109394. doi: 10.1016/j.ejrad.2020.109394

15. Mazzucchi S, Frosini D, Costagli M, Del Prete E, Donatelli G, Cecchi P, et al. Quantitative susceptibility mapping in atypical Parkinsonisms. *NeuroImage Clin.* (2019) 24:101999. doi: 10.1016/j.nicl.2019.101999

16. Sung YH, Kim JS, Yoo SW, Shin NY, Nam Y, Ahn TB, et al. A prospective multi-centre study of susceptibility map-weighted MRI for the diagnosis of neurodegenerative parkinsonism. *Eur Radiol.* (2022) 32:1–12. doi: 10.1007/s00330-021-08454-z

17. He N, Ling H, Ding B, Huang J, Zhang Y, Zhang Z, et al. Region-specific disturbed iron distribution in early idiopathic Parkinson's disease measured by quantitative susceptibility mapping. *Hum Brain Map.* (2015) 36:4407–20. doi: 10.1002/hbm.22928

18. Yang L, Cheng Y, Sun Y, Xuan Y, Niu J, Guan J, et al. Combined application of quantitative susceptibility mapping and diffusion kurtosis imaging techniques to investigate the effect of iron deposition on microstructural changes in the brain in Parkinson's disease. *Front Aging Neurosci.* (2022) 2022:14. doi: 10.3389/fnagi.2022.792778

19. Sotoudeh H, Sarrami AH, Wang JX, Saadatpour Z, Razaei A, Gaddamanugu S, et al. Susceptibility-weighted imaging in neurodegenerative disorders: a review. *J Neuroimag.* (2021) 31:459–70. doi: 10.1111/jon.12841

20. Du G, Lewis MM, Sica C, He L, Connor JR, Kong L, et al. Distinct progression pattern of susceptibility MRI in the substantia nigra of Parkinson's patients. *Movement Disord Off J Movement Disord Soc.* (2018) 33:1423–31. doi: 10.1002/mds.27318

21. Arribarat G, Pasternak O, De Barros A, Galitzky M, Rascol O, Péran P. Substantia nigra locations of iron-content, free-water and mean diffusivity abnormalities in moderate stage Parkinson's disease. *Parkinsonism Relat Disord.* (2019) 65:146–52. doi: 10.1016/j.parkreldis.2019.05.033

22. Ben Bashat D, Thaler A, Lerman Shacham H, Even-Sapir E, Hutchison M, Evans KC, et al. Neuromelanin and T2*-MRI for the assessment of genetically at-risk, prodromal, and symptomatic Parkinson's disease. *NPJ Parkinsons Dis.* (2022) 8:1–8. doi: 10.1038/s41531-022-00405-9

23. Wang M, Wang H, Wang J, Lu S, Li C, Zhong X, et al. Modified iron deposition in nigrosomes by pharmacotherapy for the management of Parkinson's disease. *Front Mol Biosci.* (2022) 9:1007. doi: 10.3389/fmolb.2022.908298

24. Pyatigorskaya N, Sanz-Morère CB, Gaurav R, Biondetti E, Valabregue R, Santin M, et al. Iron imaging as a diagnostic tool for Parkinson's disease: a systematic review and meta-analysis. *Front Neurol.* (2020) 11:366. doi: 10.3389/fneur.2020.00366

25. Baudrexel S, Nürnberger L, Rüb U, Seifried C, Klein JC, Deller T, et al. Quantitative mapping of T1 and T2* discloses nigral and brainstem pathology in early Parkinson's disease. *Neuroimage.* (2010) 51:512–20. doi: 10.1016/j.neuroimage.2010.03.005

26. Ghassaban K, He N, Sethi SK, Huang P, Chen S, Yan F, et al. Regional high iron in the substantia Nigra differentiates Parkinson's disease patients from healthy controls. *Front Aging Neurosci.* (2019) 11:106. doi: 10.3389/fnagi.2019.00106

27. Hatano T, Okuzumi A, Kamagata K, Daida K, Taniguchi D, Hori M, et al. Neuromelanin MRI is useful for monitoring motor complications in Parkinson's and PARK2 disease. *J Neural Transm.* (2017) 124:407–15. doi: 10.1007/s00702-017-1688-9

frontiers | Frontiers in Neurology

TYPE Original Research
PUBLISHED 16 May 2023
DOI 10.3389/fneur.2023.1153779

OPEN ACCESS

EDITED BY
Binbin Nie,
Institute of High Energy Physics (CAS), China

REVIEWED BY
Chuantao Zuo,
Huashan Hospital, Fudan University, China
Udunna Anazodo,
McGill University Health Centre, Canada
Fan Hu,
Huazhong University of Science and Technology, China

*CORRESPONDENCE
Chenpeng Zhang
✉ zhangchenpeng1981@126.com
Jianjun Liu
✉ nuclearj@163.com

†These authors have contributed equally to this work and share first authorship

RECEIVED 30 January 2023
ACCEPTED 18 April 2023
PUBLISHED 16 May 2023

CITATION
Xin M, Li L, Wang C, Shao H, Liu J and Zhang C (2023) Pilot study on ^{11}C-CFT dynamic imaging using total-body PET/CT: biodistribution and radiation dosimetry in Parkinson's disease. *Front. Neurol.* 14:1153779. doi: 10.3389/fneur.2023.1153779

Pilot study on ^{11}C-CFT dynamic imaging using total-body PET/CT: biodistribution and radiation dosimetry in Parkinson's disease

Mei Xin†, Lianghua Li†, Cheng Wang, Hongda Shao, Jianjun Liu* and Chenpeng Zhang*

Department of Nuclear Medicine, Renji Hospital, Shanghai Jiao Tong University School of Medicine, Shanghai, China

Objective: Total-body PET/CT equipment, uEXPLORER, is a newly developed imaging technology with a superior resolution, high sensitivity, and high signal-to-noise ratio, providing unique application advantages in the pharmacokinetic evaluation of positron tracers. While ^{11}C-CFT PET/CT has been widely utilized in the early diagnosis of Parkinson's disease (PD), it is limited by the short half-life of the radionuclide and an incomplete understanding of its biological distribution in humans. This study aimed to use a total-body PET/CT dynamic scan with ^{11}C-CFT imaging to describe the real-time internal biodistribution in PD patients and to obtain accurate radiation dosimetry.

Methods: Six male subjects with suspected PD underwent dynamic ^{11}C-CFT total-body PET/CT. Following a bedside intravenous bolus injection of 373.3 ± 71.56 MBq of ^{11}C-CFT, PET acquisition was performed synchronously for 75 min with a maximum axial field of view (AFOV) of 194 cm. Time-activity curves (TACs) were generated by delineating volumes of interest (VOIs) of the sourced organs using PMOD software. Tracer kinetics and cumulative organ activities were calculated, and absorbed doses were calculated and estimated using the OLINDA/EXM software.

Results: In the systemic TAC analysis of ^{11}C-CFT, several unique types of distribution patterns were obtained among several major organs, including a "Fast-in Fast-out" pattern in the kidneys, lungs, spleen, and thyroid, a "Fast-in Slow-out" curve in the heart wall, a "Slow-in Slow-out" mode in the liver, a "Low-level extending" pattern in the whole brain and muscle, and a "Slow-in to plateau" trend in the striatum and bone. The effective dose of ^{11}C-CFT was calculated to be 2.83E-03 mSv/MBq, which is only one-third of the literature value measured by the conventional method. Moreover, this dose is much lower compared to all other doses of DAT radioligands used in PET imaging.

Conclusion: This study is a pioneering application of total-body PET/CT to ^{11}C-CFT dynamic imaging. Our results confirmed that ^{11}C-CFT has a favorable total body biodistribution, an extremely low internal radiation dose, and high imaging quality, making it suitable for reasonable PD diagnosis in patients requiring multiple follow-up examinations.

KEYWORDS

^{11}C-CFT, dopamine transporter, total-body PET/CT, time-activity curve, effective dose

Introduction

Parkinson's disease (PD) is a progressive neurodegenerative disorder that is commonly observed in elderly populations. Despite having been first described two centuries ago, our understanding of the disease has continued to evolve over time (1). The principal pathophysiological characteristic of PD is the degeneration of nigrostriatal neurons and the resultant loss of dopamine, which is responsible for most of the classic motor symptoms, such as bradykinesia, rest tremor, rigidity, and gait instability. Hence, it is crucial to visualize and identify global and regional changes in neurotransmitters related to PD for an accurate diagnosis.

Although dopamine levels cannot be directly measured through imaging, advances in molecular neuroimaging have resulted in the availability of several approaches to mapping the function of dopamine nerve terminals using pre- and post-synaptic ligands (2). Among these tracers, those targeting the dopamine transporter (DAT) in the pre-synaptic membrane are becoming increasingly important as biomarkers for dopaminergic studies. One such representative imaging agent, ^{11}C-2-beta-carbomethoxy-3-beta-(4-fluorophenyl) tropane (^{11}C-CFT), has been used for early PD diagnosis based on standard PET/CT scans (3–5). However, past approaches using so-called "whole-body" multi-bed and multi-timepoint PET/CT imaging may not accurately access the exact pharmacokinetics of ^{11}C-CFT, leading to bias in radiation dose estimates for PD patients.

In this study, we utilized a total-body PET/CT scanner (uEXPLORER, United Imaging Healthcare) to study DAT in a real-time and dynamic mode, enabling evaluation from the "sectional whole body" to the "integral total body." The large equipment's super-long axial field of view (AFOV) and ultra-high resolution, high sensitivity, and high signal-to-noise ratio allowed us to accurately observe tracer biodistribution throughout the entire human body (6). Time-activity curves (TACs) were assessed to determine dosimetry, which is possible with standard PET/CT but would substantially benefit from total-body PET/CT (7). Studies have shown that dynamic scanning and algorithms using total-body PET/CT can effectively yield a much smaller dose estimate value than the previous method (8). Accurate internal dosimetry is not only important for radiation protection, but also helpful for optimizing injection dose, improving image quality, and streamlining clinical workflow. Therefore, we planned to update and optimize the radiation dose estimates of ^{11}C-CFT using the dynamic protocol of total-body PET/CT imaging.

Materials and methods

Radiopharmaceutical preparation

The preparation of ^{11}C-CO2 radionuclide was performed with the medical cyclotron (HM-10, Sumitomo) at the Department of Nuclear Medicine in Renji Hospital, Shanghai, China. The radionuclide was then synthesized, and quality controlled with high efficiency and radiochemical purity of over 95% by following the previous method in detail using CFN-MPS-200 (Sumitomo) (9).

Patients

A total of six patients with suspected Parkinson's disease were retrospectively enrolled in this study between January and April 2021. Prior to the PET/CT imaging, we confirmed that none of the participants were allergic to anhydrous ethanol, which was used as the essential solvent in the synthesis of ^{11}C-CFT. The retrospective study was approved by the Ethics Committee of Renji Hospital, and written informed consent was waived from the patients. The study complied with the principles of the Declaration of Helsinki.

Total-body PET/CT scanning protocol

All six patients underwent ^{11}C-CFT total-body PET/CT imaging using the digital time-of-flight (TOF) uEXPLORER PET/CT scanner after withdrawing from all PD-related medications for at least 12 h. Prior to scanning, subjects were required to empty their urinary bladders and lie comfortably on the examination mattress in a supine position with arms held side-by-side to ensure optimal positioning and reduce motion artifacts during dynamic acquisitions. CT scans from the vertex to the toes was conducted using a fixed tube voltage of 120 kV for attenuation correction and anatomical localization, along with the auto-mAs technique for dose modulation. A bedside intravenous bolus injection of ^{11}C-CFT was administered through a unilateral lower extremity vein, and PET acquisition was launched simultaneously with a maximum axial field of view (AFOV) of 194 cm for a 75-min dynamic PET scan. The raw PET data were reconstructed into 97 frames (24 × 5 s, 20 × 30 s, 48 × 60 s, and 5 × 180 s) using the standard order subset expectation maximization (OSEM) algorithm with TOF, point-spread function (PSF), three iterations, 20 subsets, 256 × 256 matrix, 600-mm FOV, 2.886-mm slice thickness, and a Gaussian postfilter with a full width at half maximum (FWHM) of 3 mm. The PET image reconstruction process also included scatter and random corrections, dead time, and normalization.

Time-activity curves

Image processing of the PET/CT scans was performed by an experienced nuclear physician using PMOD 4.0 software (PMOD Technologies LLC, Zurich, Switzerland) (10). The 97 frames were merged into a single dynamic sequence to quantify tracer dynamics using co-registered dynamic PET and CT images. To account for the partial volume effect, this study involved delineating volumes of interest (VOIs), which were found to be 1–3 mm smaller in all dimensions than the actual region of interest observed in the images. The boundary definition of this VOI should be based on either CT or PET imaging, and we prioritized the smaller area as the more accurate representation of the region of interest. In this study, all organs were rendered to scale as previously specified, except for the skeletal bone, which was represented by the proximal femur. Time-activity curves (TACs) were then automatically generated using the kinetic modeling module of the PMOD software while taking into account the radioactive decay. The generated TACs were used to observe changes in uptake by the source organs.

TABLE 1 Patient characteristics ($n = 6$).

Characteristics	Mean ± SD (range)
Age (years)	59.67 ± 8.89 (48–73)
Height (m)	1.74 ± 0.05 (1.69–1.83)
Weight (kg)	78.83 ± 5.27 (73.00–88.00)
Body mass index (kg/m^2)	26.03 ± 2.10 (22.99–28.73)
Injected dose (MBq)	373.30 ± 71.56 (264.70–479.20)
Injected dose per kg (MBq/kg)	4.78 ± 1.13 (3.44–6.56)

Radiation absorbed dose estimates

The tracer kinetics and cumulative organ activity of the ^{11}C-CFT PET/CT scans were calculated to estimate the absorbed internal radiation dose. The trapezoidal integral over 75 min was employed to obtain the cumulative organ activity (Bq-hr/Bq). Standard organ volumes from OLINDA/EXM 1.0 software (Vanderbilt University, Nashville, TN, USA), as described in a previous study (11), were used to estimate cumulative total organ activity. For each participant, the effective dose and individual organ doses were computed.

Results

Overview of the dynamic PET images

All six patients received the ^{11}C-CFT injection safely and without any immediate discomfort. During the 75-min dynamic scans, decreased uptake of ^{11}C-CFT was observed in the striatum of the brains of all participants. Patient information is listed in Table 1. The reconstructions of the PET images obtained at different time points for the total body and the transverse-sectional brain are depicted in Figure 1.

TAC studies of the main organs

The major organs of all six participants exhibited consistent characteristic biodistribution patterns of ^{11}C-CFT, as shown by the corresponding TAC analyses presented in Table 2 and Figure 2. Tracer uptake displayed a "Fast-in Fast-out" pattern in the kidney, lung, spleen, and thyroid, with rapid increases and decreases observed (Figure 2A). Specifically, the kidney had the highest mean radioactivity count (SUVbw 14.80 ± 3.11 g/mL), while the lung had the shortest time to reach peak activity (57.50 ± 18.64 sec), followed by the thyroid (189.20 ± 68.59 sec). Spleen and kidney shared a similar time of peak arrival (275.00 ± 79.18 s and 268.30 ± 125.40 s, respectively). The heart wall exhibited a rapid tracer uptake but was followed by a slow decline, characterized as "Fast-in Slow-out" uptake (Figure 2B). The liver displayed a "Slow-in Slow-out" pattern, where the ^{11}C-CFT uptake slowly increased until it reached peak activity (1770.00 ± 703.60 sec) and then gradually decreased (Figure 2C). The whole brain and muscle showed generally low degrees of ^{11}C-CFT uptake, resulting in a "Low-level extending" curve pattern over time (Figure 2D). The striatum and bone shared a similar TAC pattern, characterized as "Slow-in to plateau," where the ^{11}C-CFT uptake in the striatum slowly increased and finally reached a plateau activity at 3630.00 ± 345.20 sec (Figure 2E).

Radiation dosimetry analysis

To determine the radiation absorbed doses to the target organs, OLINDA/EXM software was utilized. Based on the data presented in Table 3, the liver had the highest radiation absorbed dose (6.40E-04 mSv/MBq), followed by the urinary bladder (3.41E-04 mSv/MBq), lungs (3.25E-04 mSv/MBq), red bone marrow (2.35E-04 mSv/MBq), stomach (2.31E-04 mSv/MBq), kidney (2.28E-04 mSv/MBq), and thyroid (2.24E-04 mSv/MBq). The estimated mean effective dose was 2.83E-03 mSv/MBq. In Table 4, the reference values of radiation dosimetry for different DAT PET imaging agents from previous literature were also provided for comparison.

Discussion

The abnormal change of dopamine function in the nigrostriatal nuclei has been identified as a sensitive biomarker for the evaluation of degenerative movement disorders (12). Molecular imaging targeting DAT is an effective approach for early diagnosis and progression assessment of PD in recent studies (13, 14).

Although ^{11}C-CFT has been available as a dopaminergic PET tracer for many years, a comprehensive and systematic interpretation of its biological distribution in humans is yet to be established. Prior studies have often used multi-bed and multi-timepoint PET/CT scans to investigate the internal biodistribution and radiation doses of the imaging agent with repeated invasive blood draws (15). However, this imaging procedure is cumbersome, time-consuming, and susceptible to variability in tracer uptake and clearance times in different organs, leading to inaccurate dose estimates, particularly for radionuclides with short half-lives. Conventional PET/CT scans can also miss crucial time points, particularly during the early phase of tracer uptake, which can lead to biased subsequent dose estimation. However, total-body PET can take advantage of the geometric sensitivity gain to scan multiple half-lives after radiotracer administration (7). Notably, there are no previous reports on the use of dynamic total-body PET/CT for ^{11}C-CFT imaging in humans. In this study, we employed a 75-min consecutive acquisition task that fully covered three half-lives of ^{11}C ($t_{1/2}$ = 20 min), allowing real-time evaluation of DAT biodistribution.

The study's findings demonstrated a consistent and uniform biodistribution of ^{11}C-CFT in all participants, with representative curve characteristics observed in the major organs. The kidney, spleen, lungs, and thyroid exhibited a "Fast-in Fast-out" distribution, while the heart wall presented a "Fast-in Slow-out" curve. The muscles and the whole brain displayed a "Low-level extending" trend. Notably, the liver showed a "Slow-in Slow-out" pattern, with a relatively high level of activity retention throughout the scan period. This is due to the liver's physiological control over the removal of peripheral dopamine and its metabolites, effectively limiting access to the systemic circulation of substantial

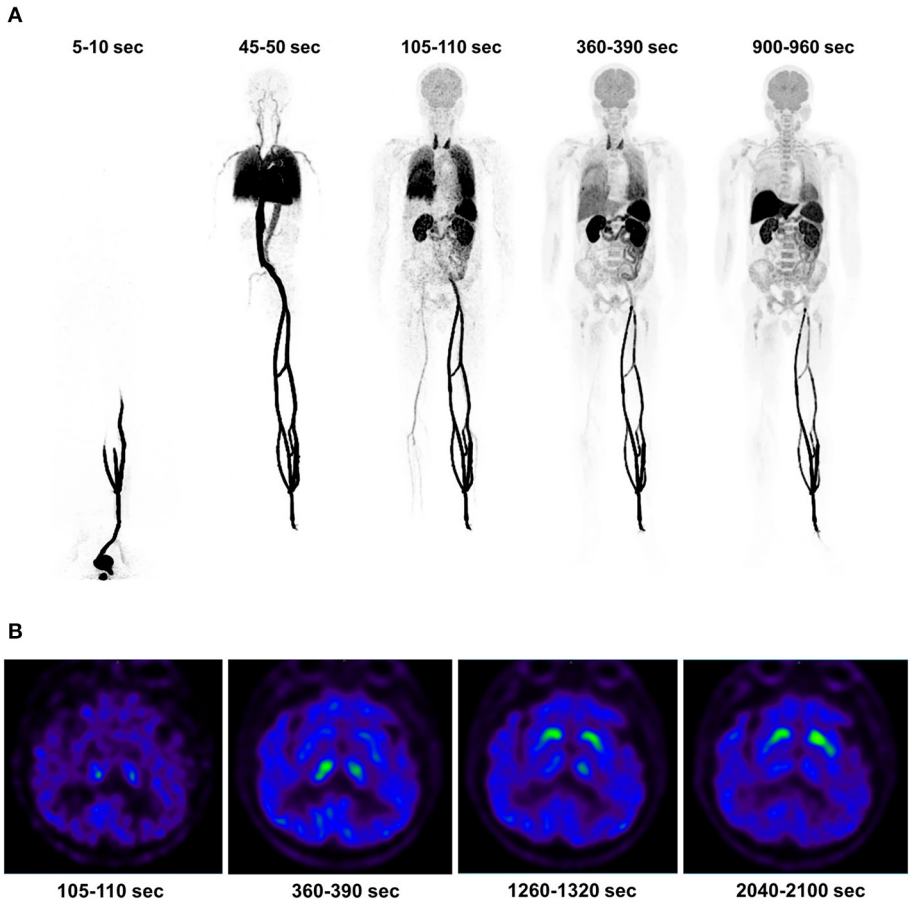

FIGURE 1
The dynamic PET images of a 73-year-old patient with Parkinson's disease were reconstructed, and the maximum intensity projection of the total body uptake at specific time points was generated **(A)**. First, a duration of 5-10 s indicates the ^{11}C-CFT injection and a duration of 45-50 s reflects the distribution in the systemic and pulmonary circulation. A duration of 105-110 s indicates high uptake in the thyroid, while a duration of 360-390 s illustrates the descent of the pulmonary circulation. A duration of 900-960 s indicates high uptake in the liver. Additionally, the cerebral transverse-sectional PET images of the basal ganglia plane displayed the selected time points **(B)**, including a duration of 105-110 s indicating the background uptake of the brain without developing the striatum image. A duration of 360-390 s showed an initial uptake in the striata, followed by a clear outline of the striata at 1,260-1,320 s. Finally, 2,040-2,100 s showed high uptake in the striata.

TABLE 2 Time-activity curve patterns in major organs.

TAC curve pattern	Organ	Time of peak or plateau arrival (s)	Peak or plateau activity (g/mL)
Fast-in Fast-out	Kidney	268.30 ± 125.40	14.80 ± 3.11
	Lung	57.50 ± 18.64	6.06 ± 2.04
	Spleen	275.00 ± 79.18	12.14 ± 1.80
	Thyroid	189.20 ± 68.59	9.30 ± 1.82
Fast-in Slow-out	Heart wall	385.00 ± 87.81	5.75 ± 1.16
Slow-in Slow-out	Liver	1770.00 ± 703.60	12.09 ± 3.72
Low-level extending	Whole brain	2270.00 ± 1335.00	1.91 ± 0.50
	Muscle	3540.00 ± 796.90	0.89 ± 0.25
Slow-in to plateau	Striatum	3630.00 ± 345.20	6.58 ± 1.22
	Bone	4240.00 ± 482.50	3.47 ± 0.90

amounts of dopamine released into the portal circulation from the gastrointestinal organs (16). Of particular interest in PD patients, the striatum showed a "Slow-in to plateau" pattern of ^{11}C-CFT uptake, with an average time tending to plateau at ∼3630 s, which is consistent with the imaging time of static PET scans collected 1 h after ^{11}C-CFT injection in our daily work. Interestingly, a TAC

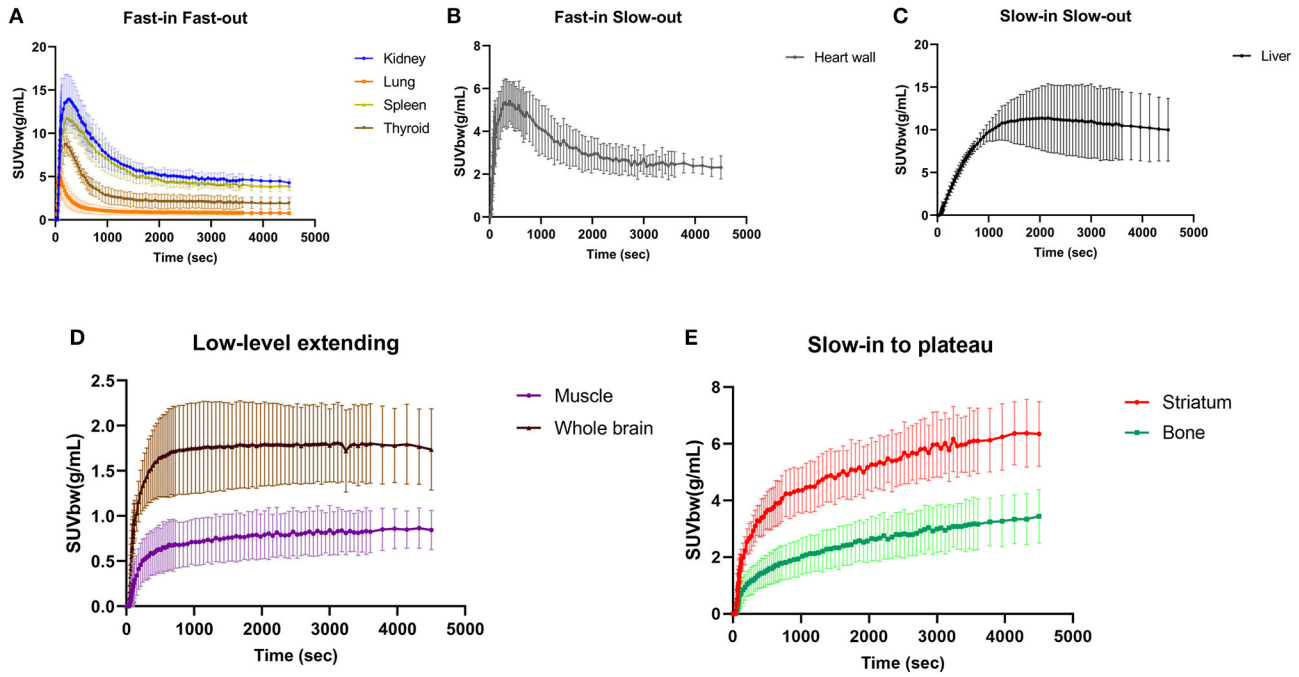

FIGURE 2
Time-activity curves were generated for major organs, such as the kidney, lung, spleen, and thyroid, as shown in panel **(A)**. Panel **(B)** shows the time-activity curve of the heart wall, while panel **(C)** shows the liver. The time-activity curve for the whole brain and muscle is illustrated in panel **(D)**. Finally, panel **(E)** shows the time-activity curves for the striatum and bone.

pattern similar to that in the striatum was unexpectedly discovered in bone. Bone metabolism may be regulated by the nervous system, and dopamine has been reported to stimulate osteoblast proliferation, differentiation, and mineralization (17). The dopamine transporter gene deletion model has been instrumental in elucidating the specific role of dopamine in bone biology (18). Additionally, a research study has shown that the absence of the DAT gene results in impairments in skeletal structure and integrity (19). Dopamine also affects calcium and phosphorus metabolism. Therefore, the synchronous expression of DAT in bone partly reflects the neuroendocrine functions of peripheral dopamine.

Our study, which utilized dynamic, long-time measured TACs and total-body ^{11}C-CFT PET/CT imaging, found that this DAT-targeted agent resulted in an effective dose of 2.83E-03 mSv/MBq in PD patients. Previous radiation dosimetry research on ^{11}C-CFT estimated the effective dose per injected activity to be 8.89E-03 mSv/MBq using conventional multi-bed PET/CT scanning techniques (20), which was more than three times higher than the dose estimates from our study. The observed discrepancies in radiation dose estimates between Huang's study and our study may be due to differences in study design, PET/CT scanning protocols, statistical analysis, and dose estimation methods. In particular, the previous study used a multi-bed repeated acquisition protocol to simulate real-time whole-body PET/CT scans, whereas our study employed an advanced total-body PET/CT scanner to perform true real-time dynamic scans of the entire human body. After calibration for differences in injected tracer activity, the actual effective dose in our study was 1.06 mSv, which is even lower than the previously reported effective radiation dose

TABLE 3 Radiation dose estimates for ^{11}C-CFT *(mSv/MBq, n = 6)*.

Target organ	Mean	SD
Liver	6.40E-04	1.32E-04
Urinary Bladder Wall	3.41E-04	2.61E-04
Lung	3.25E-04	4.64E-05
Red Bone Marrow	2.35E-04	2.18E-05
Stomach Wall	2.31E-04	1.25E-05
Kidney	2.28E-04	2.78E-04
Thyroid	2.24E-04	4.61E-05
*LLI Wall	1.92E-04	2.03E-05
Spleen	4.22E-05	5.34E-06
†ULI Wall	2.46E-05	4.77E-06
Brain	1.24E-05	4.60E-06
Effective Dose	2.83E-03	2.63E-04

*LLI, lower large intestine; †ULI, upper large intestine.

for any comparable radioligands, including ^{18}F-FPCIT (1.20E-02 mSv/MBq) (21), ^{18}F-FE-PE2I (2.30E-02 mSv/MBq) (15), and ^{11}C-PE2I (6.40E-03 mSv/MBq) (22). Although previous studies have indicated that the internal radiation doses of DAT PET tracers are safe and acceptable to the public, our investigation provided substantially lower effective dosimetry for ^{11}C-CFT. The technical advantage of dynamic acquisition and measurement by total-body PET/CT facilitated accurate dose estimation, as previously

TABLE 4 Effective dose for ^{11}C-CFT and other DAT imaging agents.

Imaging agents	Effective dose per injected activity (mSv/MBq)	Injected activity (MBq)	Effective dose (mSv)
^{11}C-CFT (This work)	2.83E-03	373.30	1.06
^{11}C-CFT Huang et al. (20)	8.89E-03	472.06	4.20
^{18}F-FPCIT Robeson et al. (21)	1.20E-02	185.00	2.22
^{18}F-FE-PE2I Lizana et al. (15)	2.30E-02	200.00	4.60
^{11}C-PE2I Ribeiro et al. (22)	6.40E-03	321.00	2.05

described in the ^{18}F-FDG radiation dosimetry study by Hu et al. (8). They have demonstrated that the conventional multi-bed PET/CT scanning method is prone to overestimating the radiation dose to the urinary bladder. Lower radiation exposure coupled with higher image quality will benefit the further application of ^{11}C-CFT in visualizing dopaminergic function and evaluating PD and other related movement disorders. In clinical practice, the routine use of administered activities ranging from 259 to 444 MBq (7 to 12 mCi) in a single ^{11}C-CFT PET scan would yield effective doses of only 0.73 to 1.26 mSv, which is an extremely low radiation burden and more favorable for patients requiring multiple follow-up examinations. Our study shows that the tracer reaches a plateau within 75 min and remains stable thereafter, indicating that prolonged scan times may not be necessary for clinical diagnosis. However, we acknowledge that this plateau phase may result in dose underestimation. Therefore, a further investigation into dose optimization strategies is warranted. In our daily clinical use of ^{11}C-CFT PET/CT imaging, we have not received any feedback concerning toxicity or moderate-to-severe side effects.

Nonetheless, very few patients reported experiencing mild headaches that were transient. Owing to the limited information and duration of the reported headaches, it remains uncertain whether there is a causal relationship between the use of ^{11}C-CFT and this observed effect. Further research is warranted to elucidate the underlying mechanisms of such side effects and to devise strategies to optimize patient safety in nuclear medicine practice.

Given the current limitations of our study, our next steps will involve achieving longer scan times using dynamic ^{11}C-CFT total-body PET/CT in healthy volunteers who demonstrate good compliance. Additionally, in future investigations, we intend to expand our sample size and carefully consider potential gender-based differences in our study design.

Conclusion

Using a novel approach with real-time dynamic total-body PET/CT scans, we have conclusively demonstrated that ^{11}C-CFT has good tissue biodistribution in various human organ systems with effective internal doses that are lower than previously anticipated. The unique features of low radiation doses and high imaging quality make this agent a viable option for PD patients. With such a safer dose range, PET/CT diagnosis and subsequent repeat examinations may become more feasible and clinically practical for individuals in need.

Data availability statement

The original contributions presented in the study are included in the article/supplementary material, further inquiries can be directed to the corresponding authors.

Ethics statement

The studies involving human participants were reviewed and approved by the Shanghai Jiao Tong University School of Medicine, Renji Hospital Ethics Committee. The patients/participants provided their written informed consent to participate in this study. Written informed consent was obtained from the individual(s) for the publication of any potentially identifiable images or data included in this article.

Author contributions

Conceptualization: MX, CZ, and JL. Methodology: LL and CW. Formal analysis, investigation, and Writing—original draft preparation: LL and MX. Writing—review and editing: MX, HS, CZ, and JL. Acquisition of financial support: CW and JL. Supervision: CZ and JL. All authors contributed to the article and approved the submitted version.

Funding

This work was supported by the National Key R&D Program of China (No. 2021YFF0701900), the National Natural Science Foundation of China (No. 82171972), and the Clinical Research Plan of the Shanghai Hospital Development Center (No. 16CR2020A).

Acknowledgments

We thank colleagues in our department for helpful assistance and discussion.

Conflict of interest

The authors declare that the research was conducted in the absence of any commercial or financial relationships that could be construed as a potential conflict of interest.

Publisher's note

References

1. Kalia LV, Lang AE. Parkinson's disease. *Lancet.* (2015) 386:896–912. doi: 10.1016/S0140-6736(14)61393-3

2. Strafella AP, Bohnen NI, Perlmutter JS, Eidelberg D, Pavese N, Van Eimeren T, et al. Molecular imaging to track Parkinson's disease and atypical parkinsonisms: New imaging frontiers. *Mov Disord.* (2017) 32:181–92. doi: 10.1002/mds.26907

3. Zhu S, Ju Z, Wu P, Liu F, Ge J, Zhang H, et al. The Parkinson's Disease Progression Neuroimaging Initiative. *Behav Neurol.* (2021) 2021:2230196. doi: 10.1155/2021/2230196

4. Sun X, Liu F, Liu Q, Gai Y, Ruan W, Wimalarathne DN, et al. Quantitative research of (11)C-CFT and (18)F-FDG PET in Parkinson's disease: a pilot study with neuroq software. *Front Neurosci.* (2019) 13:299. doi: 10.3389/fnins.2019.00299

5. Liu FT, Ge JJ, Wu JJ, Wu P, Ma Y, Zuo CT, et al. Clinical, dopaminergic, and metabolic correlations in Parkinson disease: a dual-tracer PET Study. *Clin Nucl Med.* (2018) 43:562–71. doi: 10.1097/RLU.0000000000002148

6. Badawi RD, Shi H, Hu P, Chen S, Xu T, Price PM, et al. First human imaging studies with the EXPLORER total-body PET scanner. *J Nucl Med.* (2019) 60:299–303. doi: 10.2967/jnumed.119.226498

7. Nardo L, Schmall JP, Werner TJ, Malogolowkin M, Badawi RD, Alavi A. Potential roles of total-body PET/computed tomography in pediatric imaging. *PET Clin.* (2020) 15:271–9. doi: 10.1016/j.cpet.2020.03.009

8. Hu P, Lin X, Zhuo W, Tan H, Xie T, Liu G, et al. Internal dosimetry in F-18 FDG PET examinations based on long-time-measured organ activities using total-body PET/CT: does it make any difference from a short-time measurement? *EJNMMI Physics.* (2021) 8:51. doi: 10.1186/s40658-021-00395-2

9. Tang G, Tang X, Deng H, Wang H, Wen F, Yi C, et al. Efficient preparation of [11C]CH3Br for the labeling of [11C]CH3-containing tracers in positron emission tomography clinical practice. *Nucl Med Commun.* (2011) 32:466–74. doi: 10.1097/MNM.0b013e3283438f9a

10. Sah BR, Sommerauer M, Mu L, Gonzalez GP, Geistlich S, Treyer V, et al. Radiation dosimetry of [(18)F]-PSS232-a PET radioligand for imaging mGlu5 receptors in humans. *EJNMMI Res.* (2019) 9:56. doi: 10.1186/s13550-019-0522-9

11. Stabin MG, Sparks RB, Crowe E. OLINDA/EXM: the second-generation personal computer software for internal dose assessment in nuclear medicine. *J Nucl Med.* (2005) 46:1023–7.

12. Brooks DJ. Molecular imaging of dopamine transporters. *Ageing Res Rev.* (2016) 30:114–21. doi: 10.1016/j.arr.2015.12.009

13. Meles SK, Oertel WH, Leenders KL. Circuit imaging biomarkers in preclinical and prodromal Parkinson's disease. *Mol Med.* (2021) 27:1–18. doi: 10.1186/s10020-021-00327-x

14. Brucke T, Brucke C. Dopamine transporter (DAT) imaging in Parkinson's disease and related disorders. *J Neural Transm.* (2021) 15:1–4. doi: 10.1007/s00702-021-02452-7

15. Lizana H, Johansson L, Axelsson J, Larsson A, Ogren M, Linder J, et al. Whole-body biodistribution and dosimetry of the dopamine transporter radioligand (18)F-FE-PE2I in human subjects. *J Nucl Med.* (2018) 59:1275–80. doi: 10.2967/jnumed.117.197186

16. Eisenhofer G. The role of neuronal and extraneuronal plasma membrane transporters in the inactivation of peripheral catecholamines. *Pharmacol Ther.* (2001) 91:35–62. doi: 10.1016/S0163-7258(01)00144-9

17. Lee DJ, Tseng HC, Wong SW, Wang Z, Deng M, Ko CC. Dopaminergic effects on in vitro osteogenesis. *Bone Res.* (2015) 3:15020. doi: 10.1038/boneres.2015.20

18. Bliziotes M, McLoughlin S, Gunness M, Fumagalli F, Jones SR, Caron MG. Bone histomorphometric and biomechanical abnormalities in mice homozygous for deletion of the dopamine transporter gene. *Bone.* (2000) 26:15–9. doi: 10.1016/S8756-3282(99)00232-X

19. Bliziotes M, Gunness M, Eshleman A, Wiren K. The role of dopamine and serotonin in regulating bone mass and strength: studies on dopamine and serotonin transporter null mice. *J Musculoskelet Neuronal Interact.* (2002) 2:291–5.

20. Huang T, Wang H, Tang G, Liang X, Deng H, Yi C, et al. Human radiation dose estimation of (11)C-CFT using whole-body PET. *Clin Nucl Med.* (2012) 37:1159–62. doi: 10.1097/RLU.0b013e318266cd1b

21. Robeson W, Dhawan V, Belakhlef A, Ma Y, Pillai V, Chaly T, et al. Dosimetry of the dopamine transporter radioligand 18F-FPCIT in human subjects. *J Nucl Med.* (2003) 44:961–6.

22. Ribeiro MJ, Ricard M, Lievre MA, Bourgeois S, Emond P, Gervais P, et al. Whole-body distribution and radiation dosimetry of the dopamine transporter radioligand [(11)C]PE2I in healthy volunteers. *Nucl Med Biol.* (2007) 34:465–70. doi: 10.1016/j.nucmedbio.2007.02.005

frontiers | Frontiers in Neurology

TYPE Original Research
PUBLISHED 13 June 2023
DOI 10.3389/fneur.2023.1195576

OPEN ACCESS

EDITED BY
Binbin Nie,
Chinese Academy of Sciences (CAS),
Beijing, China

REVIEWED BY
Zhenxiang Zang,
Capital Medical University,
Beijing, China
Xun Sun,
Huazhong University of Science and Technology, China

*CORRESPONDENCE
Zhang Ying
✉ zhang_ying99@jlu.edu.cn

†These authors have contributed equally to this work

RECEIVED 28 March 2023
ACCEPTED 25 May 2023
PUBLISHED 13 June 2023

CITATION
Zhihui S, Yinghua L, Hongguang Z, Yuyin D, Xiaoxiao D, Lulu G, Yi L, Kangli F and Ying Z (2023) Correlation analysis between ^{18}F-fluorodeoxyglucose positron emission tomography and cognitive function in first diagnosed Parkinson's disease patients. *Front. Neurol.* 14:1195576. doi: 10.3389/fneur.2023.1195576

Correlation analysis between ^{18}F-fluorodeoxyglucose positron emission tomography and cognitive function in first diagnosed Parkinson's disease patients

Sun Zhihui†, Li Yinghua†, Zhao Hongguang, Dai Yuyin, Du Xiaoxiao, Gao Lulu, Li Yi, Fan Kangli and Zhang Ying*

Department of Neurology, First Hospital of Jilin University, Changchun, China

Objective: Evaluation of the correlation between ^{18}F-fluorodeoxyglucose-positron emission tomography (^{18}F-FDG PET) and cognitive function in first-diagnosed and untreated Parkinson's disease (PD) patients.

Materials and method: This cross-sectional study included 84 first diagnosed and untreated PD patients. The individuals were diagnosed by movement disorder experts based on the 2015 MDS Parkinson's disease diagnostic criteria. The patients also underwent ^{18}F-FDG PET scans and clinical feature assessments including the Montreal Cognitive Assessment (MoCA) scale. Glucose metabolism rates were measured in 26 brain regions using region of interest (ROI) and pixel-wise analyses with displayed *Z* scores. The cognitive function was assessed by professionals using the MoCA scale, which covers five cognitive domains. Spearman's linear correlation and linear regression models were used to compare the correlations between ^{18}F-FDG metabolism in each brain region and cognitive domain, using SPSS 25.0 software.

Result: The results indicated a positive correlation between executive function and glucose metabolism in the lateral prefrontal cortex of the left hemisphere (p=0.041). Additionally, a positive correlation between memory function and glucose metabolism in the right precuneus (p=0.014), right lateral occipital cortex (p=0.017), left lateral occipital cortex (p=0.031), left primary visual cortex (p=0.008), and right medial temporal cortex (p=0.046). Further regression analysis showed that for every one-point decrease in the memory score, the glucose metabolism in the right precuneus would decrease by 0.3 (B=0.30, p=0.005), the glucose metabolism in the left primary visual cortex would decrease by 0.25 (B=0.25, p=0.040), the glucose metabolism in the right lateral occipital cortex would decrease by 0.38 (B=0.38, p=0.012), and the glucose metabolism in the left lateral occipital cortex would decrease by 0.32 (B=0.32, p=0.045).

Conclusion: This study indicated that cognitive impairment in PD patients mainly manifests as changes in executive function, visual-spatial function and memory functions, while glucose metabolism mainly decreases in the frontal and posterior cortex. Further analysis shows that executive function is related to glucose metabolism in the left lateral prefrontal cortex. On the other hand, memory ability involves changes in glucose metabolism in a more extensive brain

region. This suggests that cognitive function assessment can indirectly reflect the level of glucose metabolism in the relevant brain regions.

KEYWORDS

Parkinson's disease, cognitive impairment, ^{18}F-FDG PET, glucose metabolism, cognitive domain, newly diagnosed and untreated PD

1. Introduction

Parkinson's disease (PD) is a degenerative neurological disorder, characterized by the degeneration and loss of dopaminergic neurons in the substantia nigra of the midbrain. This result in reduced dopamine input to the striatum, and typical motor symptoms such as resting tremor, rigidity, bradykinesia, and postural and gait disorder. With the progress of clinical and pathological research, particularly the introduction of the 2003 pathological grading theory (1) providing a basis for a wide range of symptoms in PD, non-motor symptoms of PD have received increasing attention. This include olfactory dysfunction, constipation, sleep disorders, cognitive dysfunction, and autonomic dysfunction that can occur throughout the disease. Currently, the diagnosis of PD relies more on clinical features, and there is still a dearth of a gold standards for diagnosis.

Application of positron emission tomography (PET) using different tracer agents can achieve *in vivo* molecular pathological diagnosis. Dopamine transporter positron emission tomography (DAT-PET) imaging is highly sensitive in testing for presynaptic dopamine neuron functional disorders (2), and molecular imaging showing normal presynaptic dopamine function was listed as one of the exclusion criteria for PD diagnosis in the Movement Disorder Society (MDS) criteria, 2015 (3). Functional abnormalities can help distinguish essential tremor, drug-induced Parkinson's syndrome, and vascular Parkinson's syndrome (4), but DAT-PET imaging has limited value in differentiating PD from other atypical Parkinson's syndromes such as multiple system atrophy (MSA), progressive supranuclear palsy (PSP), and corticobasal degeneration (CBD) (5). Studies have shown that in PD patients, not only is there dopamine dysfunction, but also significant metabolic abnormalities in the brain. Based on this characteristic, scientists have developed ^{18}F-FDG PET specifically for identifying and measuring metabolic abnormalities in PD at the systemic level (6). The ^{18}F-FDG PET imaging can reflect local glucose metabolism. Based on this, a Parkinson's disease-related pattern (PDRP) has been discovered, characterized by a relative increase in metabolism in the pallidum, pons, and cerebellum fibers, and a simultaneous decrease in metabolism in the pre-motor and posterior parietal regions (27). There have been successive studies that have found characteristic metabolic patterns for MSA, PSP, CBD, and DLB. Therefore, glucose metabolism patterns can be used to distinguish between PD and MSA, PSP, and corticobasal syndrome (CBS) (7). However, the factors that affect glucose metabolism in PD are not yet fully understood. There are varying degrees of cognitive impairment in PD, including mild cognitive impairment (MCI) and Parkinson's disease dementia (PDD). Population-based studies have shown that up to 40% of Parkinson's patients eventually develop dementia (8). The development of cognitive impairment involves non-dopaminergic pathways, and further research is needed to investigate whether it is related to brain glucose metabolism. Research has shown that compared to PD patients with normal cognitive function, PD-MCI and PDD patients exhibit a progressive reduction in metabolism in the frontal and parietal cortices (9, 10), and cognitive dysfunction is involved in changes within PD brain metabolism. This study aims to explore the correlation between ^{18}F-glucose metabolism and cognitive function in newly diagnosed and untreated PD patients. Furthermore, we will examine if, the patient's glucose metabolism status can be predicted by the cognitive level. Different cognitive impairment patterns may provide clues for establishing possible glucose metabolic patterns.

2. Materials and methods

2.1. Subjects

The participants in this study were 84 newly-diagnosed and untreated PD patients who had undergone an ^{18}F-FDG PET scan at the Parkinson's Disease Clinic of the First Hospital of Jilin University in northeastern China. Hence, PD was diagnosed by movement disorder experts based on the 2015 MDS Parkinson's disease diagnostic criteria (3). Other organic or psychiatric disorders that may lead to cognitive impairment were excluded, Alzheimer's disease, Lewy body dementia, severe cerebrovascular disease, and major depression. The participants were evaluated using the MoCA cognitive scale and other clinical features by professional individuals.

2.2. Clinical assessments

Clinical assessments were conducted by trained examiners. The patients underwent standardized neurological examinations wherein, the revised Movement Disorder Society Unified Parkinson's Disease Rating Scale Part III (MDS-UPDRS III), and the Hoehn and Yahr (H&Y) staging were employed to grade motor symptoms. Neuropsychological evaluations were performed using the Montreal Cognitive Assessment (MoCA) scale (11), and the Hamilton Anxiety Scale (HAMA) and Hamilton Depression Scale (HAMD). Among them, MoCA was used to clinically assess the five cognitive domains. The specific details of the MoCA items are as follows. The short-term memory recall task (5 points) involved two learning trials of five nouns, followed by delayed recall after approximately 5 min. Visual spatial abilities were evaluated by replicating a three-dimensional cube (1 point). Multiple aspects of executive function were evaluated through the following tasks: an alternate task adapted from the trail making B task (1 point), a drawing a clock task (3 points), phonemic fluency task (1 point), and two verbal abstraction tasks (2 points).

Attention, concentration, and working memory were assessed through multiple tasks such as sustained attention task-detecting targets by tapping (1 point), serial subtraction (3 points), and forward and backward digit span (1 point each). The language was evaluated by a three-item naming task with unfamiliar animals (lion, camel, rhinoceros; 3 points) and repeating two grammatically complex sentences (2 points).

2.3. ^{18}F-FDG PET imaging process

Before PET scanning, all PD patients were required to fast for at least 6 h but had free access to water for at least 12 h before imaging, the blood glucose levels needed to be less than 8 mmol/L. The PET scans were performed with a Siemens Biograph 16HR PET/CT (Siemens) in 3D mode. Before the emission scan, a low-dose CT (tube voltage 120 kV, tube current 50 mAs, rotational speed 0.5 s/r, FOV 812 mm × 812 mm, 512 × 512 matrix, slice thickness 2 mm) transmission scan was performed for attenuation correction. The brain emission scan was acquired at least 60 min after intravenous injection of 185 MBq of [^{18}F] FDG (Sumitomo HM-12, pH 4–8, radioactive purity >95%, radioactive concentration >370 MBq/mL). The PET scan (1-bed positions, FOV 812 mm × 812 mm, 144 × 144 matrix, slice thickness 2 mm) lasted for 10 min. All procedures were carried out on PD patients under standardized circumstances, i.e., in a quiet and dimly lit room with minimal background noise and a resting state with the eyes open.

2.4. Image preprocessing analysis

The FDG images are quantitatively analyzed using Cortex ID Suite software. Cortex ID uses the 3D SSP method developed by Dr. S. Minoshima of the University of Washington. This method first achieves correction and centering of the PET volume using 3D rotation correction, i.e., a symmetry algorithm known as a stochastic sign change (SSC) criterion. Second, stereotactic repositioning of the PET volume with the AC-PC lines is achieved using stereotactic realignment, i.e., iterative matching of the patient image set with a standard atlas template generated by averaging the FDG images of 66 healthy volunteers via linear transformation. Third, the PET volume was matched to a standard image set with a uniform voxel size of 2.25 mm, an interpolation of 60 slices, and a matrix size of 128 × 128 by stretching/compressing it and using a thin-slab spline technique. This way done to nonlinearly distort the PET volume in three dimensions simultaneously along the direction of the major neuronal fiber bundles. This reduces regional mismatches in gray matter locations that remained after linear correction and then automatically standardizes the anatomy of the brain. After that, the algorithm finds the maximum FDG uptake value by "inserting" a 13.5 mm long imaginary 3D vector of the brain in the stereotaxic coordinates of the PET volume with about 16,000 pre-defined cortical surface pixels. Subsequently, these were extracted and assigned to the corresponding surface pixels. The generated uptake maps are normalized pixel-by-pixel to the average metabolic activity across the cerebral cortex. The algorithm uses *Z*-score subtraction to compare the patient's uptake map pixel by pixel with the uptake map of an age-matched average normal brain. The final display shows a metabolic map of 8 directions and 26 brain regions. Eight of this region, include lateral views of the left and right sides, medial views of the left and right sides, anterior view, posterior view, superior view, and inferior view and the 26 brain regions. The 26 brain regions include the left lateral prefrontal lobe, right lateral prefrontal lobe, left medial prefrontal lobe, right medial prefrontal lobe, left sensorimotor, right sensorimotor, left anterior cingulate, right anterior cingulate, left posterior cingulate, right posterior cingulate, left precuneus, right precuneus, left superior parietal lobe, right superior parietal lobe, left inferior parietal lobe, right inferior parietal lobe, left lateral occipital lobe, right lateral occipital lobe, left primary visual cortex, right primary visual cortex, left lateral temporal lobe, right lateral temporal lobe, left mesial temporal lobe, right mesial temporal lobe, cerebellum and pons. This indicated the number of standard deviations in the patient's FDG uptake values differ from those of the age-matched normal brain. Areas of severe hypometabolism are shown in red.

2.5. Statistical analysis

The data were analyzed using SPSS 25.0 software. Normally distributed data were expressed as mean ± standard deviation, while non-normally distributed data were expressed as median and quartile range (IQR) (Tables 1, 2). Spearman correlation analysis was used to examine the correlation between quantitative variables, and variables with $p < 0.05$ were considered significant. After controlling for age, sex, years of education, HAMA, and HAMD, variables with $p < 0.1$ in the correlation analysis were further included in a stepwise linear regression analysis to establish a linear regression model.

3. Result

3.1. Correlation analysis of PD patients

In this study, among the 84 patients, the main glucose metabolism reduction was observed in the prefrontal and posterior cortex, as

TABLE 1 Demographics and clinical characteristics of PD patients.

Characteristic		Total (n =84) median (IQR)
Age		63.5 (23.8)
Gender	Male	38 (45.2)
	Female	46 (54.8)
Age of onset		58.5 (14.7)
Education years		10.5 (6.5)
H&Y stage		2.0 (1.0)
UPDRS III scores		25 (23.5)
Disease duration		4.0 (5.0)
Handedness	Left	3 (3.6)
	Right	81 (96.4)
MoCA		23 (8)
HAMA		9 (9)
HAMD		8 (8)

TABLE 2 Cognitive domain assessment.

Cognitive domain (total scores)	Test items (total scores)	Scores (IQR)
Executive (7)		5 (3)
	TMT-B (1)	1 (1)
	Draw clock (3)	3 (2)
	Semantic fluency (1)	1 (0)
	Abstraction (2)	1 (1)
Visual spatial (1)		0 (1)
	Cube copy (1)	0 (1)
Language (5)		4 (2)
	Naming (3)	3 (1)
	Repeat (2)	1 (2)
Attention (6)		5 (2)
	Digits forward (1)	1 (0)
	Digits backward (1)	1 (0)
	Target detection using tapping (1)	1 (0)
	Serial 7 substraction starting at 100 (3)	2 (1)
Memory (5)		2 (2)
	Delayed recall (5)	2 (2)

(Total execution = 7, total visual-spatial = 1, total verbal = 5, total attention = 6, total memory = 5, TMT-B, the trial making test part B).

shown in Figures 1, 2. The left lateral prefrontal cortex was positively correlated with executive function ($p = 0.041$). The left sensorimotor area ($p = 0.042$), the left superior parietal lobule ($p = 0.034$) and right medial temporal cortex ($p = 0.046$) were negatively correlated with memory function. The right precuneus ($p = 0.014$), right lateral occipital cortex ($p = 0.017$), left lateral occipital cortex ($p = 0.031$) and left primary visual cortex ($p = 0.008$) showed were positive correlation with memory function, as shown in Figure 3. The variables with $p < 0.1$ in the Spearman linear correlation analysis were included in the multiple linear regression analysis with each brain region as the outcome variable using the principle of lenient entry and strict exit. A multiple linear regression model was constructed by controlling for age, gender, education, HAMA, and HAMD. The results showed that for every 1-point decrease in memory score, the metabolism in the right sensorimotor area would increase by 0.32 points ($p = 0.047$, $B = -0.32$). Additionally, the metabolism in the left sensorimotor area would increase by 0.37 points ($p = 0.035$, $B = -0.37$), while the metabolism in the right precuneus would decrease by 0.3 points ($p = 0.005$, $B = 0.30$). The metabolism in the left primary visual cortex would decrease by 0.25 points ($p = 0.040$, $B = 0.25$), the metabolism in the right lateral occipital cortex would decrease by 0.38 points ($p = 0.012$, $B = 0.38$) and the metabolism in the left lateral occipital cortex would decrease by 0.32 points ($p = 0.045$, $B = 0.32$). For every 1-point decrease in attention score, the metabolism in the left precuneus would decrease by 0.33 points ($p = 0.010$, $B = 0.33$) (Table 3). To avoid false-positive results, we qualified the p-values more strictly and reincorporated the independent variables with $p < 0.05$ into the linear regression analysis. We found that only the left sensorimotor area was negatively correlated with memory function, and positive correlations existed between the right precuneus, bilateral occipital lobe, and the left primary visual cortex and memory function (Supplementary Table S1).

4. Discussion

This study suggests that the characteristics of cognitive impairment in PD mainly involve executive function, visuospatial function, and memory function, which is consistent with previous research (12). It is also different from AD, which affects memory function, and DLB, which primarily affects visuospatial and attention functions (13, 14). Impairment in executive function is mainly manifested as cognitive flexibility, planning, and impairment of learning ability. That could be attributed to the disruption in the integrity of the dorsolateral prefrontal-striatal loop (dorsolateral prefrontal cortex, dorsolateral striatum, globus pallidus internus, mediodorsal thalamus of the lateral, and posterior parietal cortex) caused by dopamine deficiency (15). The present study found that PD patients with poor executive function showed decreased glucose metabolism in the left lateral prefrontal cortex. The finding is similar to the results of a study by Duncan et al. in 2015 (16) and also consistent with the current theory that executive function is mainly associated with the frontal cortex. In addition, the lateral prefrontal cortex is more sensitive to spatial position information than the amygdala, ventral striatum, and orbitofrontal cortex in the dorsal region of the frontal-striatal loop (17). The clock drawing and the trial making test part B used in this study to assess executive function are also highly correlated with spatial position, suggesting that PD patients may also have some degree of spatial function impairment (18).

Furthermore, this study also observed that in patients with poor memory function, glucose metabolism was reduced in the right precuneus, bilateral occipital cortex, and left visual cortex. Among them, the right anterior cingulate gyrus, bilateral occipital cortex, and left visual cortex displayed positive linear relation to memory function, indicating the lower the metabolic activity of the related cortex, the more severe the memory function impairment. Existing research has shown that memory function is related to the hippocampal-neocortical circuit function, and the neocortex mainly includes the ventromedial prefrontal cortex and posterior cortex, such as the parietal and occipital lobes. The evaluation of memory function in this study used the delayed recall section of the Montreal Cognitive Assessment Scale (immediate recall was not scored). Participants were asked to recall five words they had heard after a 5 min delay and were allowed to receive prompts. Generally speaking, the process of memory retrieval involves two stages: memory construction and memory refinement. The anatomical basis for the construction stage corresponds to the connection between the ventromedial prefrontal cortex and the anterior hippocampus, while the refinement stage involves the connection between the posterior hippocampus and the posterior neocortex, including the occipital and parietal lobes. The neocortex is often involved in tasks such as somatosensory processing, visual recognition, and spatial tasks (19), while the precuneus is closely related to visual spatial representations, situational memory retrieval, etc. This can explain the reduced metabolism in the right precuneus cortex and bilateral occipital cortex found in memory-impaired patients in this study. Another study has also shown that the

A

Region	Uptake Ratio	Z-Score
Prefrontal Lateral R	0.96	-2.59
Prefrontal Lateral L	0.96	-2.11
Prefrontal Medial R	0.86	-2.19
Prefrontal Medial L	0.88	-1.91
Sensorimotor R	0.83	-4.21
Sensorimotor L	0.84	-3.79
Anterior Cingulate R	0.94	2.07
Anterior Cingulate L	0.96	2.70
Posterior Cingulate R	1.07	-0.29
Posterior Cingulate L	1.06	-0.22
Precuneus R	1.04	-1.19
Precuneus L	0.97	-2.23
Parietal Superior R	0.77	-3.57
Parietal Superior L	0.67	-5.34
Parietal Inferior R	0.85	-4.33
Parietal Inferior L	0.82	-5.03
Occipital Lateral R	0.98	-1.72
Occipital Lateral L	0.88	-4.43
Primary Visual R	1.16	0.44
Primary Visual L	1.09	-0.43
Temporal Lateral R	0.94	1.83
Temporal Lateral L	0.97	3.04
Temporal Mesial R	0.83	4.20
Temporal Mesial L	0.92	7.06
Cerebellum Whole	0.90	1.47
Pons	0.76	1.92
Reference Region: Global		

B

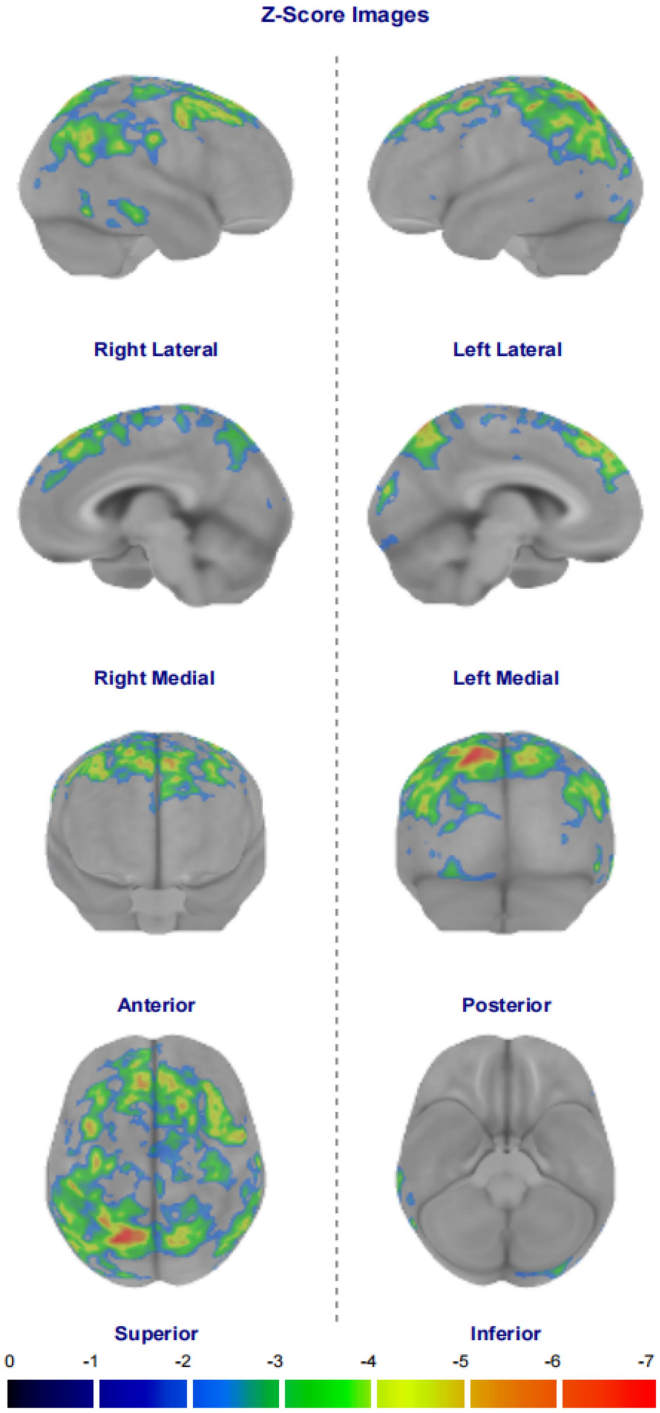

FIGURE 1
(A) Shows the 26 brain regions selected using the region of interest (ROI) method by the Cortex ID Suite program, their respective regional brain glucose uptake rates, and the calculated *Z*-values. **(B)** Are schematic illustrations of the whole-brain glucose metabolism observed in eight directions (lateral views of the left and right sides, medial views of the left and right sides, anterior view, posterior view, superior view, and inferior view). Each unit scale below the image represents a decrease in metabolism of one standard deviation. This image shows brain regions with a decrease in metabolism of two or more standard deviations, with warmer colors indicating greater metabolic deficits.

primary visual cortex is related to memory function (20). Since most of the five words in the MoCA recall task are highly concrete words (such as "red," "face," "church," "velvet," and "chrysanthemum"), perceptual and storage deficits related to visual information can also affect the formation of memory in patients. Therefore, this can also explain why the memory-impaired patients in this study showed reduced metabolism in the left visual cortices. It is worth noting that this study found that although PD patients have significant memory impairment, their attention function is still relatively intact. This is mainly manifested as impaired short-term and immediate memory,

10.3389/fneur.2023.1195576

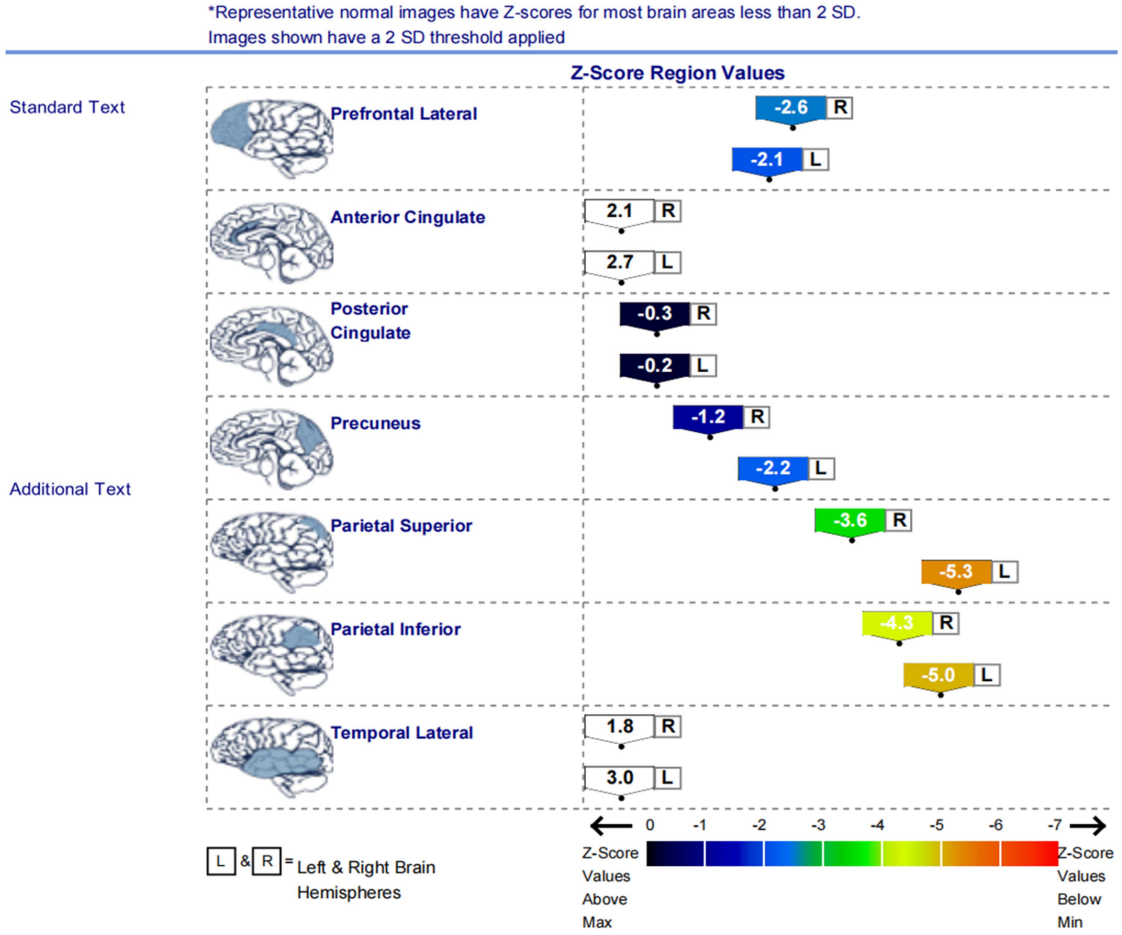

FIGURE 2
The graph displays the *Z* scores of glucose metabolism in the brain regions of the left and right lateral prefrontal cortex, anterior cingulate cortex, posterior cingulate cortex, precuneus, superior parietal lobule, inferior parietal lobule, and lateral temporal cortex. The low metabolism regions in the patients were mainly located in the lateral prefrontal cortex, precuneus, superior parietal lobule, and inferior parietal lobule on both sides of the brain.

TABLE 3 Spearman correlation analysis of glucose metabolism in each cognitive domain and brain region.

Brain region	Cognitive domain	*p*	*B*	95% CI
Prefrontal lateral R	Executive	0.196	–	–
Prefrontal lateral L	Executive	0.171	–	–
Prefrontal medial L	Memory	0.304	–	–
Sensorimotor R	Memory	0.047	−0.32	−0.64, −0.01
Sensorimotor L	Memory	0.035	−0.37	−0.72, −0.03
Anterior cingulate L	Memory	0.822	–	–
Precuneus R	Memory	0.005	0.30	0.09, 0.51
Precuneus L	Attention	0.010	0.33	0.08, 0.58
Parietal superior L	Memory	0.172	–	–
Parietal inferior L	Visual spital	0.492	–	–
Occipital lateral R	Memory	0.012	0.38	0.09, 0.67
Primary visual R	Memory	0.005	−0.06	−0.09, −0.02
Primary visual L	Attention	0.354	–	–
	Memory	0.040	0.25	0.01, 0.50
Temporal lateral L	Memory	0.385	–	–
Temporal mesial R	Memory	0.223	–	–

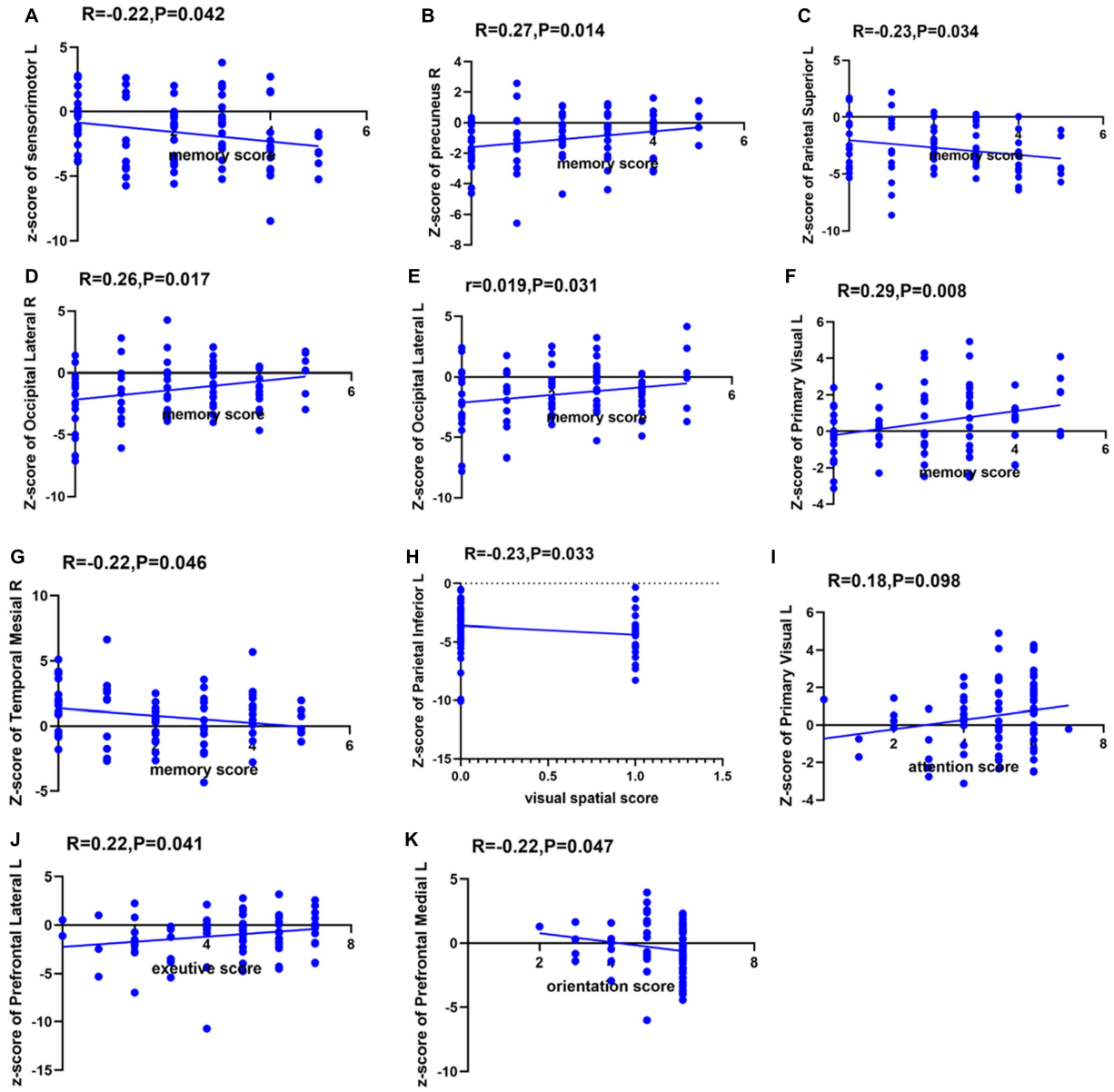

FIGURE 3
Spearman correlation analysis between glucose metabolism in each brain region and each cognitive domain. The ordinates indicate the glucose metabolism in each brain region, with L indicating the left side and R indicating the right side. **(A)** Spearman correlation analysis between glucose metabolism in left sensorimotor cortex and memory function. **(B)** Spearman correlation analysis between glucose metabolism in right precuneus and memory function. **(C)** Spearman correlation analysis between glucose metabolism in left superior parietal cortex and memory function. **(D)** Spearman correlation analysis between glucose metabolism in right lateral occipital cortex and memory function. **(E)** Spearman correlation analysis between glucose metabolism in left lateral occipital cortex and memory function. **(F)** Spearman correlation analysis between glucose metabolism in left primary visual cortex and memory function. **(G)** Spearman correlation analysis between glucose metabolism in right temporal mesial cortex and memory function. **(H)** Spearman correlation analysis between glucose metabolism in left inferior parietal cortex and visual spatial function. **(I)** Spearman correlation analysis between glucose metabolism in left primary visual cortex and attention function. **(J)** Spearman correlation analysis between glucose metabolism in left lateral prefrontal cortex and executive function. **(K)** Spearman correlation analysis between glucose metabolism in left medial prefrontal cortex and orientation function.

while number-related memory (such as digit span forward and backward) remains relatively intact (see Figure 3).

Interestingly, this study found that patients with poor memory function had increased metabolism in the left medial frontal cortex, left sensorimotor areas, left superior parietal cortex, and right medial temporal cortex. On the other hand, patients with worse visuospatial function had hyper-metabolism in the left superior parietal cortex. Among them, there was a negative linear relation between the bilateral sensorimotor areas and memory function. The presence of high metabolism in certain brain regions in neurodegenerative diseases is a highly controversial topic in the current scenario. First, the neuroinflammation present during disease progression may lead to higher glucose metabolism (21, 22). Second, higher glucose metabolism is a compensatory response to PD-related cortical atrophy with less-damaged brain regions, thereby exhibiting higher glucose metabolism and indicating a decline in cognitive ability. In addition,

most of the brain regions with negatively correlated metabolism with cognitive domains belong to the default network. The default network includes the medial prefrontal cortex, medial and lateral parietal cortex, and medial and lateral temporal cortex. Brain regions within the default network exhibit decreased metabolism during task execution. Although patients in this study did not perform cognitive tasks during ^{18}F-FDG PET scanning, studies have shown that brain regions with decreased metabolism during novel tasks are not activated during the rest period (23). This suggests that the increased metabolism in the brain regions during PD is related to memory impairment.

This study found that cognitive impairment in PD patients is mainly manifested as changes in executive, visual-spatial and memory function, with decreased glucose metabolism primarily in the frontal and posterior cortex. Among them, the executive ability is related to glucose metabolism in the left lateral prefrontal cortex, while memory ability involves a more extensive range of metabolic changes in the left medial prefrontal cortex, bilateral sensorimotor areas, left primary visual cortex, bilateral occipital cortex, right precuneus, left superior parietal cortex, and right medial temporal cortex. This is broadly consistent with previous studies (24). So, is the pattern of glucose metabolism in the brain of PD patients different from that of other types of cognitive impairment? Vander et al. found that both PDD and Alzheimer's disease (AD) show a global reduction in glucose metabolism, with similar cortical metabolism in the bilateral parietal, temporal, and frontal lobes (20, 25). When comparing PDD and AD, PDD patients showed a greater decrease in visual cortex metabolism, while metabolism in the medial temporal cortex was relatively preserved (20, 26). In a longitudinal study that lasted for 8 years and used SVM to predict the conversion rate from MCI to PDD, it was found that the SVM-supported PDD classifier was used to classify Lewy body dementia (DLB) patients, with 94.12% of DLB patients predicted to convert to PDD. This suggests that there is no phenotypic difference between PDD and DLB. Therefore, FDG-PET can detect small regional changes in areas such as the frontal lobe, parietal lobe, and occipital lobe at the voxel level and establish a metabolic brain network related to PD cognitive impairment. However, there may still be significant difficulties in using glucose metabolism to differentiate between DLB and PD cognitive impairment.

We believe that this study will help clinicians to predict alterations in glucose metabolism in relevant brain regions by using the patients' cognitive scores. Additionally, it is also predict possible patterns of glucose metabolism in PD by different impaired cognitive domains to assist in the clinical diagnosis and differential diagnosis of PD.

This study has certain limitations. First, this study adopted a cross-sectional design with a small sample size from a single center. This may have biases in terms of geographic location, race, examination, and evaluation. In the future, we plan to expand the sample size and conduct a longitudinal study with multi-center collaboration to further validate the results. Second, the testing of visual spatial function in this study is relatively limited. We plan to add more tests of visual spatial function to verify the results. Third, we used automatic region of interest (ROI) segmentation, which reduced time and labor costs but was not as accurate as manual delineation. We aim to achieve more accurate, stable, and intelligent automatic sketching and brain partitioning methods in the future.

Data availability statement

The original contributions presented in the study are included in the article/Supplementary material, further inquiries can be directed to the corresponding author.

Ethics statement

The studies involving human participants were reviewed and approved by Ethics Committee of First Hospital of Jilin University First Hospital of Jilin University. The patients/participants provided their written informed consent to participate in this study.

Author contributions

All authors listed have made a substantial, direct, and intellectual contribution to the work and approved it for publication.

Funding

The work was supported by grants from the National Natural Science Foundation of China (no. 81974194) and the Natural Science Foundation of Jilin Province (no. YDZJ202201ZYTS116) to YZ.

Acknowledgments

The authors thank to Wu Yanhua from the First Hospital of Jilin University for her statistical guidance on this study.

Conflict of interest

The authors declare that the research was conducted in the absence of any commercial or financial relationships that could be construed as a potential conflict of interest.

Publisher's note

Supplementary material

The Supplementary material for this article can be found online at: https://www.frontiersin.org/articles/10.3389/fneur.2023.1195576/full#supplementary-material

References

1. Braak H, Del Tredici K, Rub U, de Vos RA, Jansen Steur EN, Braak E. Staging of brain pathology related to sporadic Parkinson's disease. *Neurobiol Aging*. (2003) 24:197–211. doi: 10.1016/s0197-4580(02)00065-9

2. Stoessl AJ. Neuroimaging in Parkinson's disease: from pathology to diagnosis. *Parkinsonism Relat Disord*. (2012) 18:S55–9. doi: 10.1016/S1353-8020(11)70019-0

3. Postuma RB, Berg D, Stern M, Poewe W, Olanow CW, Oertel W, et al. MDS clinical diagnostic criteria for Parkinson's disease. *Mov Disord*. (2015) 30:1591–601. doi: 10.1002/mds.26424

4. Kagi G, Bhatia KP, Tolosa E. The role of DAT-SPECT in movement disorders. *J Neurol Neurosurg Psychiatry*. (2010) 81:5–12. doi: 10.1136/jnnp.2008.157370

5. Liu FT, Ge JJ, Wu JJ, Wu P, Ma Y, Zuo CT, et al. Clinical, dopaminergic, and metabolic correlations in Parkinson disease: a dual-tracer pet study. *Clin Nucl Med*. (2018) 43:562–71. doi: 10.1097/RLU.0000000000002148

6. Behnke S, Berg D, Naumann M, Becker G. Differentiation of Parkinson's disease and atypical parkinsonian syndromes by transcranial ultrasound. *J Neurol Neurosurg Psychiatry*. (2005) 76:423–5. doi: 10.1136/jnnp.2004.049221

7. Hoglinger GU, Respondek G, Stamelou M, Kurz C, Josephs KA, Lang AE, et al. Clinical diagnosis of progressive supranuclear palsy: the Movement Disorder Society criteria. *Mov Disord*. (2017) 32:853–64. doi: 10.1002/mds.26987

8. Aarsland D, Andersen K, Larsen JP, Lolk A, Nielsen H, Kragh-Sorensen P. Risk of dementia in Parkinson's disease: a community-based, prospective study. *Neurology*. (2001) 56:730–6. doi: 10.1212/wnl.56.6.730

9. Folstein MF, Folstein SE, McHugh PR. "Mini-mental state". A practical method for grading the cognitive state of patients for the clinician. *J Psychiatr Res*. (1975) 12:189–98. doi: 10.1016/0022-3956(75)90026-6

10. Emre M, Aarsland D, Brown R, Burn DJ, Duyckaerts C, Mizuno Y, et al. Clinical diagnostic criteria for dementia associated with Parkinson's disease. *Mov Disord*. (2007) 22:1689–707. doi: 10.1002/mds.21507

11. Dalrymple-Alford JC, MacAskill MR, Nakas CT, Livingston L, Graham C, Crucian GP, et al. The MoCA: well-suited screen for cognitive impairment in Parkinson disease. *Neurology*. (2010) 75:1717–25. doi: 10.1212/WNL.0b013e3181fc29c9

12. Dujardin K, Leentjens AF, Langlois C, Moonen AJ, Duits AA, Carette AS, et al. The spectrum of cognitive disorders in Parkinson's disease: a data-driven approach. *Mov Disord*. (2013) 28:183–9. doi: 10.1002/mds.25311

13. Jellinger KA, Korczyn AD. Are dementia with Lewy bodies and Parkinson's disease dementia the same disease? *BMC Med*. (2018) 16:34. doi: 10.1186/s12916-018-1016-8

14. Dubois B, Feldman HH, Jacova C, Hampel H, Molinuevo JL, Blennow K, et al. Advancing research diagnostic criteria for Alzheimer's disease: the IWG-2 criteria. *Lancet Neurol*. (2014) 13:614–29. doi: 10.1016/S1474-4422(14)70090-0

15. Obeso JA, Rodriguez-Oroz MC, Stamelou M, Bhatia KP, Burn DJ. The expanding universe of disorders of the basal ganglia. *Lancet*. (2014) 384:523–31. doi: 10.1016/S0140-6736(13)62418-6

16. Duncan GW, Firbank MJ, Yarnall AJ, Khoo TK, Brooks DJ, Barker RA, et al. Gray and white matter imaging: a biomarker for cognitive impairment in early Parkinson's disease? *Mov Disord*. (2016) 31:103–10. doi: 10.1002/mds.26312

17. Yong SW, Yoon JK, An YS, Lee PH. A comparison of cerebral glucose metabolism in Parkinson's disease, Parkinson's disease dementia and dementia with Lewy bodies. *Eur J Neurol*. (2007) 14:1357–62. doi: 10.1111/j.1468-1331.2007.01977.x

18. Williams-Gray CH, Evans JR, Goris A, Foltynie T, Ban M, Robbins TW, et al. The distinct cognitive syndromes of Parkinson's disease: 5 year follow-up of the campaign cohort. *Brain*. (2009) 132:2958–69. doi: 10.1093/brain/awp245

19. Robin J, Moscovitch M. Details, gist and schema: hippocampal–neocortical interactions underlying recent and remote episodic and spatial memory. *Curr Opin Behav Sci*. (2017) 17:114–23. doi: 10.1016/j.cobeha.2017.07.016

20. Pappata S, Santangelo G, Aarsland D, Vicidomini C, Longo K, Bronnick K, et al. Mild cognitive impairment in drug-naive patients with PD is associated with cerebral hypometabolism. *Neurology*. (2011) 77:1357–62. doi: 10.1212/WNL.0b013e3182315259

21. Schroeter M, Dennin MA, Walberer M, Backes H, Neumaier B, Fink GR, et al. Neuroinflammation extends brain tissue at risk to vital peri-infarct tissue: a double tracer [^{11}C]PK11195- and [^{18}F]FDG-PET study. *J Cereb Blood Flow Metab*. (2009) 29:1216–25. doi: 10.1038/jcbfm.2009.36

22. Jeong YJ, Yoon HJ, Kang DY. Assessment of change in glucose metabolism in white matter of amyloid-positive patients with Alzheimer disease using F-18 FDG PET. *Medicine*. (2017) 96:e9042. doi: 10.1097/MD.0000000000009042

23. Raichle ME. The brain's default mode network. *Annu Rev Neurosci*. (2015) 38:433–47. doi: 10.1146/annurev-neuro-071013-014030

24. Firbank MJ, Yarnall AJ, Lawson RA, Duncan GW, Khoo TK, Petrides GS, et al. Cerebral glucose metabolism and cognition in newly diagnosed Parkinson's disease: ICICLE-PD study. *J Neurol Neurosurg Psychiatry*. (2017) 88:310–6. doi: 10.1136/jnnp-2016-313918

25. Gonzalez-Redondo R, Garcia-Garcia D, Clavero P, Gasca-Salas C, Garcia-Eulate R, Zubieta JL, et al. Grey matter hypometabolism and atrophy in Parkinson's disease with cognitive impairment: a two-step process. *Brain*. (2014) 137:2356–67. doi: 10.1093/brain/awu159

26. Libby LA, Ekstrom AD, Ragland JD, Ranganath C. Differential connectivity of perirhinal and parahippocampal cortices within human hippocampal subregions revealed by high-resolution functional imaging. *J Neurosci*. (2012) 32:6550–60. doi: 10.1523/JNEUROSCI.3711-11.2012

27. Wu P, Wang J, Peng S, Ma Y, Zhang H, Guan Y, et al. Metabolic brain network in the Chinese patients with Parkinson's disease based on ^{18}F-FDG PET imaging. *Parkinsonism Relat Disord*. (2013) 19:622–7. doi: 10.1016/j.parkreldis.2013.02.013

frontiers | Frontiers in Neurology

TYPE Original Research
PUBLISHED 06 July 2023
DOI 10.3389/fneur.2023.1195577

OPEN ACCESS

EDITED BY
Lihong Bu,
Renmin Hospital of Wuhan University, China

REVIEWED BY
Emanuele Camerucci,
Mayo Clinic, United States
Piotr Alster,
Medical University of Warsaw, Poland

*CORRESPONDENCE
Zhang Ying
✉ zhang_ying99@jlu.edu.cn

†These authors have contributed equally to this work and share first authorship

RECEIVED 28 March 2023
ACCEPTED 19 June 2023
PUBLISHED 06 July 2023

CITATION
Kangli F, Hongguang Z, Yinghua L, Xiaoxiao D, Yuyin D, Lulu G, Yi L, Zhihui S and Ying Z (2023) Characteristics and influencing factors of ^{11}C-CFT PET imaging in patients with early and late onset Parkinson's disease.
Front. Neurol. 14:1195577.
doi: 10.3389/fneur.2023.1195577

Characteristics and influencing factors of ^{11}C-CFT PET imaging in patients with early and late onset Parkinson's disease

Fan Kangli†, Zhao Hongguang†, Li Yinghua, Du Xiaoxiao, Dai Yuyin, Gao Lulu, Li Yi, Sun Zhihui and Zhang Ying*

Department of Neurology, First Hospital of Jilin University, Changchun, China

Objective: This study aims to explore the difference between ^{11}C-methyl-N-2β-carbomethoxy-3β-(4-fluorophenyl)-tropanel (^{11}C-CFT) positron emission tomography (PET) imaging in the early-onset Parkinson's disease (EOPD) and late-onset Parkinson's disease (LOPD), and to analyze the correlation between ^{11}C-CFT PET imaging and disease duration, Hoehn & Yahr (H&Y) stage, motor symptoms, and non-motor symptoms in patients with idiopathic Parkinson's disease (PD), so as to explore its application value in assessing the severity of Parkinson's disease.

Materials and methods: A total of 113 patients with idiopathic PD were included in this study. The patients were divided into EOPD and LOPD groups according to the age of 60years, of which 58 were early-onset and 55 were late-onset. All patients underwent ^{11}C-CFT PET imaging and manually sketched regions of interest (ROI) to delineate the caudate nucleus, anterior putamen, and posterior putamen ROI layer-by-layer, and the corresponding values were recorded. Clinical data [age of onset, disease duration, H&Y stage, total Unified Parkinson's Disease Rating Scale (UPDRS) score, UPDRS III score, tremor score, postural instability/gait difficulty (PIGD) score, rigidity score, bradykinesia score, and Montreal Cognitive Assessment (MoCA) score] were collected from all patients. The differences in striatal ^{11}C-CFT uptake between patients with EOPD and LOPD were compared, and the correlation between striatal ^{11}C-CFT uptake and the clinical data of patients with idiopathic PD was evaluated.

Results: The caudate nucleus ^{11}C-CFT uptake was higher in EOPD than in the LOPD group (t=3.002, p=0.003). ^{11}C-CFT uptake in the caudate nucleus in patients with PD was negatively correlated with the age of onset, H&Y stage, disease duration, total UPDRS score, UPDRS III score, rigidity score, and bradykinesia score (p<0.05). The anterior and posterior putamen ^{11}C-CFT uptake was negatively correlated with H&Y stage, disease duration, total UPDRS score, UPDRS III score, PIGD score, rigidity score, and bradykinesia score (p<0.05).

Conclusion: ^{11}C-CFT PET provides an objective molecular imaging basis for the difference in disease progression rates between patients with EOPD and LOPD. Secondly, ^{11}C-CFT PET can be used as an important objective indicator to assess disease severity and monitor disease progression.

KEYWORDS

Parkinson's disease, the early-onset Parkinson's disease, the late-onset Parkinson's disease, ^{11}C-CFT PET, dopamine transporter, motor symptoms, non-motor symptoms

1. Introduction

Parkinson's disease (PD) is the second most common neurodegenerative disease worldwide after Alzheimer's disease (AD) (1), and the main pathological changes are: degeneration and loss of nigrostriatal dopaminergic neurons, formation of Lewy bodies in the remaining neurons and reduction of striatal dopamine levels. The clinical manifestations of PD are predominantly motor symptoms, including rest tremor, rigidity, bradykinesia, and postural imbalance. With the progress of clinical and pathological research, PD has been found to be accompanied by some non-motor symptoms. Braak et al. classified the pathological changes in PD into six stages according to the different sites of α-synuclein deposition and the time and order of PD pathology in 2003, among which non-motor symptoms included: cognitive, olfactory, sleep, autonomic dysfunctions, anxiety and depression and mental and behavioral dysfunction (2). Although imaging and genetic research for the diagnosis of Parkinson's disease have made great progress in recent years, the diagnosis of PD still depends mainly on the comprehensive assessment of medical history, symptoms and signs, and response to levodopa drugs, which lacks a gold standard for diagnosis. The pathogenesis of PD is very complex, and the pathophysiological mechanism includes: oxidative stress, mitochondrial dysfunction, neuroinflammation, etc. Based on the above pathophysiological changes, the current research hotspot is mainly to find effective biomarkers for PD diagnosis. Among them, great progress has been made in the study of biomarkers of the central nervous system and peripheral blood, and it plays an important role in the diagnosis and differential diagnosis of PD and Parkinson's syndrome (3–5). However, it is still difficult to reflect the essential characteristics of PD. Moreover, most patients with PD have atypical clinical symptoms in the early stages, that are difficult to detect and diagnose. At the same time, a reliable objective assessment index for evaluating PD severity is lacking.

Positron emission computed tomography (PET/CT) is an *in vivo* molecular imaging technique. By combining with different radiotracers, systemic or local metabolic, functional and structural information can be obtained to achieve early detection, early diagnosis and early treatment of diseases. Different radiotracers in PET indicate different features. PET/CT is also increasingly used for the diagnosis and evaluation of PD because of its specific advantages, such as the dopamine transporter (DAT)-PET. DAT-PET imaging is based on the principle that ^{11}C-methyl-N-2β-carbomethoxy-3β-(4-fluorophenyl)-tropanel (^{11}C-CFT) tracers specifically bind to striatal DAT to visualize the caudate nucleus and putamen, while DAT-deficient regions such as the cerebellum and cortex do not bind to the tracer, in order to assess the density of presynaptic dopaminergic neurons in the striatum and reflect the severity of neuronal degeneration in the dense substantia nigra (6). Therefore, a reduction of ^{11}C-CFT uptake in the caudate nucleus and putamen plays an important role in the early diagnosis and differential diagnosis of PD (7, 8).

DAT-PET imaging is clinically useful for differentiating PD from conditions unrelated to dopaminergic dysfunction, such as essential tremor, dystonia, drug-induced parkinsonism and vascular parkinsonism. (9, 10). However, the ^{11}C-CFT uptake in different parts of the striatum in patients with PD is different, and whether it is related to the age of onset and disease severity of patients with PD, especially the correlation with motor and non-motor symptoms, needs to be further investigated. In this study, the correlation between striatal ^{11}C-CFT uptake and clinical data [including age of onset, disease duration, H&Y stage, total UPDRS score, UPDRS III score, tremor score, postural instability/gait difficulty (PIGD) score, rigidity score, bradykinesia score, and the Montreal Cognitive Assessment (MoCA) score] in patients with idiopathic PD was analyzed in the Chinese population, with the aim of exploring the application value of DAT-PET in assessing PD severity. In addition, the incidence of Parkinson's disease increases with age, and the cut-off age varies by age group, distinguished by the ages of 40, 45, 50, 60, or 70 years; the terms used in the literature, such as juvenile, young, and late-onset Parkinson's disease, are defined differently (11). In this study, PD was defined as early-onset Parkinson's disease (EOPD) or late-onset Parkinson's disease (LOPD) by taking the age of onset of 60 years as the limit, and the difference between ^{11}C-CFT uptake in EOPD and LOPD was preliminarily explored using DAT-PET imaging.

2. Materials and methods

2.1. Subjects

One hundred thirteen patients with a definite diagnosis of idiopathic PD who underwent ^{11}C-CFT PET imaging at the Parkinson's Disease Specialized Clinic, Department of Neurology, First Hospital of Jilin University from January 2020 to October 2022 were included in this study, including 58 patients with EOPD and 55 patients with LOPD. All patients were definitively diagnosed by an experienced Parkinson's disease specialist according to the clinical diagnostic criteria for Parkinson's disease established by the International Parkinson and Movement Disorders Society in 2015 (12).

Inclusion criteria were: ① clinically diagnosed idiopathic PD; ② can cooperate with ^{11}C-CFT DAT-PET scan and there are no contraindications; ③ complete clinical data (including MDS-UPDRS, MoCA).

Exclusion criteria were: ① Non-idiopathic PD; ② Associated with brain diseases such as stroke, head trauma, and cranial surgery.

2.2. Clinical assessment

2008 MDS Revised Unified Parkinson's Disease Rating Scale (MDS-UPDRS) was used to assess motor symptoms of PD patients (13). Among them, tremor scores included: UPDRS II 2.10, UPDRS III 3.15–3.18; rigidity scores included: UPDRS III.3.3; bradykinesia scores included: UPDRS II 2.4–2.9, UPDRS III.3.2 3.4–3.8 3.14; PIGD scores included: UPDRS II 2.12–2.13, UPDRS III.3.10–3.12 (14). Montreal Cognitive Assessment (MoCA) was used to assess cognition (15). All assessments were performed in the "on" state of the patients. The MDS-UPDRS score was performed by a professional in the patient's "off" state, and the MoCA score was performed in the patient's "on" state, within 1 week of the DAT PET scan.

2.3. ^{11}C-CFT PET imaging process

The ^{11}C-CFT is produced by the HM-12 cyclotron of Sumitomo Heavy Machinery Co., Ltd. in Japan with a purity of ≥95% for radiochemistry. A Siemens Discovery 16HR PET/CT scanner was used. Patients discontinued PD medications for at least 12 h before the

examination, and all patients were injected intravenously with ^{11}C-CFT at a uniform standard of 3.7 MBq/Kg via the back of the hand. The PET/CT examinations were performed under calm breathing after a 60-min waiting period in a quiet environment. The patient position was supine on the examination bed, the head was fixed in the head rest, and the scan area included the entire head. CT images were acquired first for attenuation correction, and PET imaging was performed in the same field of view in the three-dimensional mode for 15 min. Image reconstruction was performed using an iterative method to obtain CT, PET, and PET/CT fusion images of the brain in the transverse, coronal, and sagittal views, respectively.

2.4. Image analysis methods

Three consecutive images with the clearest striatal structures on the PET/CT fusion images were selected, and the regions of interest (ROI) method was used to delineate the caudate nucleus, anterior putamen and posterior putamen ROI layer-by-layer; the maximum radioactivity counts of each nucleus were recorded. The parieto-occipital cortex, which lacks DAT distribution, was selected as the background reference area, and the distribution of each ROI was semi-quantitatively calculated using the following formula: ^{11}C-CFT uptake value = (ROI radioactivity count/occipital radioactivity count)-1 (16). ^{11}C-CFT uptake in the caudate nucleus, anterior putamen, and posterior putamen was the average radioactivity uptake on the left and right sides.

2.5. Statistical analysis

SPSS26.0 software was used for the data analysis. Normally distributed data are expressed as X^- ± S, and non-normally distributed data are expressed as M (P25, P75). The *t*-test was used for comparisons between data groups that conformed to a normal distribution and the rank-sum test was used for comparisons between data groups that did not conform to a normal distribution. Analysis of covariance was used to correct the influence of confounding variables. Spearman's correlation analysis was used to evaluate the correlation between striatal 11C-CFT uptake and the clinical data of patients with PD. $P < 0.05$ indicated a statistically significant difference.

3. Results

3.1. Subject characteristics

A total of 113 patients were included in this study, with a mean age of onset of 57.11 ± 11.53 years, and a median duration of disease of 4 (2, 6) years. They were divided into EOPD group and LOPD group according to whether the age of onset was greater than 60 years old, including 58 patients in EOPD group and 55 patients in LOPD group. There was no significant difference between groups in gender, duration of disease, H&Y stage, total UPDRS score, UPDRS III score, tremor score, PIGD score, rigidity score, and bradykinesia score. MoCA score ($p = 0.010$) and ^{11}C-CFT uptake in the caudate nucleus ($p = 0.008$) were significantly higher in EOPD group than in LOPD group (Table 1).

3.2. Covariance analysis of striatal ^{11}C-CFT uptake in EOPD group and LOPD group after correcting for disease duration

The results of the covariance analysis after correcting for disease duration showed that ^{11}C-CFT uptake in the caudate nucleus in the EOPD group was significantly higher than in the LOPD group ($t = 3.002$, $p = 0.003$). There was no significant difference between the anterior and posterior putamen ^{11}C-CFT uptake between the EOPD and LOPD groups (Table 2 and Figures 1, 2).

3.3. Correlation analysis of striatal ^{11}C-CFT uptake in patients with PD with clinical data

In patients with PD, the caudate nucleus ^{11}C-CFT uptake was negatively correlated with the age of onset, H&Y stage, disease duration, total UPDRS score, UPDRS III score, rigidity score, and bradykinesia score ($p < 0.05$) (Figures 3A–G), while the anterior and posterior putamen ^{11}C-CFT uptake was negatively correlated with

TABLE 1 Demographics and clinical characteristics of PD patients.

Characteristic	PD (*n*=113)	EOPD (*n*=58)	LOPD (*n*=55)	*P*
Participants (Male/Female)	113 (49/64)	58 (23/35)	55 (26/29)	0.165
Age of onset (year)	57.11 ± 11.53	48.41 ± 9.18	66.27 ± 4.47	<0.001
Disease duration (year)	4 (2, 6)	4 (2, 8)	3 (2, 5)	0.154
H&Y stage	2 (1, 2)	2 (1, 2)	2 (1.5, 2)	0.088
Total UPDRS score	44 (32, 67)	42.5 (31, 70)	47 (32.5, 66)	0.881
UPDRS III score	25 (18, 40)	24 (17, 40)	27 (18.5, 39)	0.419
Tremor score	7 (3, 12)	6.5 (3, 11)	9 (4.5, 13.5)	0.206
PIGD score	3 (2, 6)	3 (2, 5)	3 (2, 6)	0.582
Rigidity score	3 (2, 6)	3 (1, 7)	4 (2, 6)	0.799
Bradykinesia score	19 (12, 30)	19 (13, 31)	20 (12, 29.5)	0.847
Education (year)	11.1 ± 3.82	10.64 ± 3.44	11.58 ± 4.16	0.191
MoCA score	21.58 ± 5.06	22.86 ± 5.09	20.42 ± 4.82	0.010
Caudate nucleus	1.40 ± 0.45	1.51 ± 0.51	1.29 ± 0.35	0.008
Anterior putamen	1.20 ± 0.48	1.22 ± 0.56	1.18 ± 0.38	0.657
Posterior putamen	0.71 ± 0.46	0.73 ± 0.52	0.70 ± 0.39	0.691

TABLE 2 Comparation of striatal ^{11}C-CFT uptake in EOPD and LOPD after correction for the disease duration.

Characteristic	Group	X±S	*B*	*t*	*P*
Caudate nucleus	EOPD	1.527 ± 0.058	0.252	3.002	0.003
	LOPD	1.275 ± 0.059			
Anterior putamen	EOPD	1.243 ± 0.063	0.084	0.918	0.361
	LOPD	1.159 ± 0.065			
Posterior putamen	EOPD	0.742 ± 0.061	0.059	0.667	0.506
	LOPD	0.683 ± 0.063			

H&Y stage, disease duration, total UPDRS score, UPDRS III score, PIGD score, rigidity score, and bradykinesia score ($p < 0.05$) (Figures 3H–U). There was no significant correlation between striatal ^{11}C-CFT uptake and tremor score and MoCA score (Table 3).

4. Discussion

PD is a chronic neurodegenerative disease characterized by the degeneration and progressive loss of dopaminergic neurons in the substantia nigra-striatum. Its prevalence increases progressively with age. DAT is located on the cell membrane of presynaptic neurons and can transport dopamine from the synaptic cleft to the presynaptic membrane for reuse or further degradation after dopaminergic neurons release impulses, thus regulating the amount of dopamine released from presynaptic nerve endings to ensure normal physiological function of the synapses. ^{11}C-CFT is mainly distributed in the bilateral caudate nucleus and putamen, whereas radioactivity distribution in other regions of the brain is extremely low, indicating that dopamine in the brain is mainly concentrated in the bilateral striatal region, as consistent with the neuroanatomical dopaminergic nerve fiber projection pathway. Dopaminergic neuronal projections are mainly located in the substantia nigra-striatum pathway. Animal studies have shown that DAT significantly correlates with the levels of synaptic dopamine transmitters (17) and residual nigrostriatal dopaminergic neurons (18), which can accurately reflect the severity of nigrostriatal dopaminergic neuronal damage. The number of DAT is closely related to the occurrence and progression of PD.

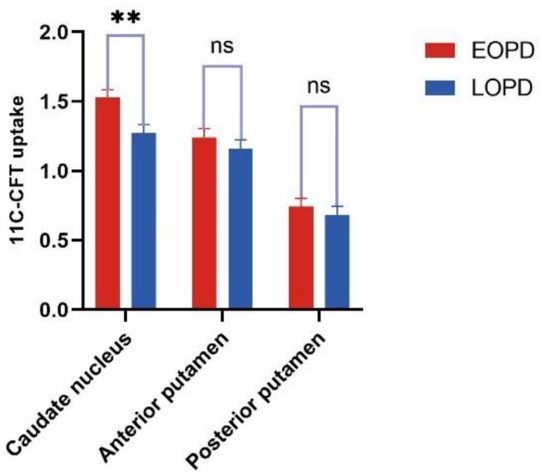

FIGURE 1
Comparation of striatal ^{11}C-CFT uptake in EOPD and LOPD (**$p \leq 0.01$; ns: $p > 0.05$).

First, this study found that patients with EOPD had a higher cognitive score than those with LOPD. And the ^{11}C-CFT uptake in the caudate nucleus was also higher in patients with EOPD than in those with LOPD. These are consistent with the findings of Yang et al. (19). Controlling for the effects of disease duration, patients with early onset PD have higher caudate nucleus ^{11}C-CFT uptake, resulting in less damage to dopaminergic neurons. It can be hypothesized that EOPD has a slower rate of disease progression, which is in agreement with Schrag et al. (20). It is also consistent with the pathological characteristics of PD, where the ventral lateral substantia nigra is most affected, dopaminergic neurons are the most deficient, and the middle and posterior parts of the putamen may receive the most projections from the ventral lateral substantia nigra; therefore, the lesion initially involves the middle and posterior parts of the putamen. As the disease progresses, the anterior putamen and caudate nucleus become progressively more involved (21). The higher ^{11}C-CFT uptake in the caudate nucleus of patients with EOPD indicates less damage to dopaminergic neurons in the caudate nucleus and later involvement of the caudate nucleus, resulting in slower disease progression. Patients with EOPD sshow better cognitive function, consistent with the findings of Wickremaratchi et al. (22). Analysis of the causes, in addition to age, may be due to the unequal involvement of the caudate nucleus and putamen in parallel basal ganglia-thalamus-cortex circuits. The dopaminergic circuits associated with the putamen are primarily responsible for motor functions, and lesions in the putamen nucleus are mainly associated with motor symptoms and symptom severity (23). The cholinergic pathways associated with the caudate

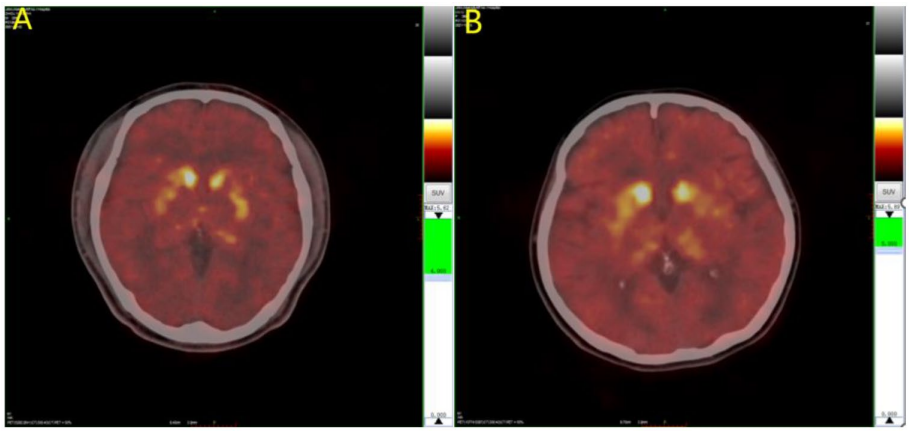

FIGURE 2
^{11}C-CFT PET images of Parkinson's disease. **(A)** LOPD; **(B)** EOPD. ^{11}C-CFT PET metabolic model for EOPD and LOPD: ^{11}C-CFT uptake in the caudate nucleus in patient with EOPD was significantly higher than LOPD, and there was no significant difference between the anterior and posterior putamen between patients with EOPD and LOPD.

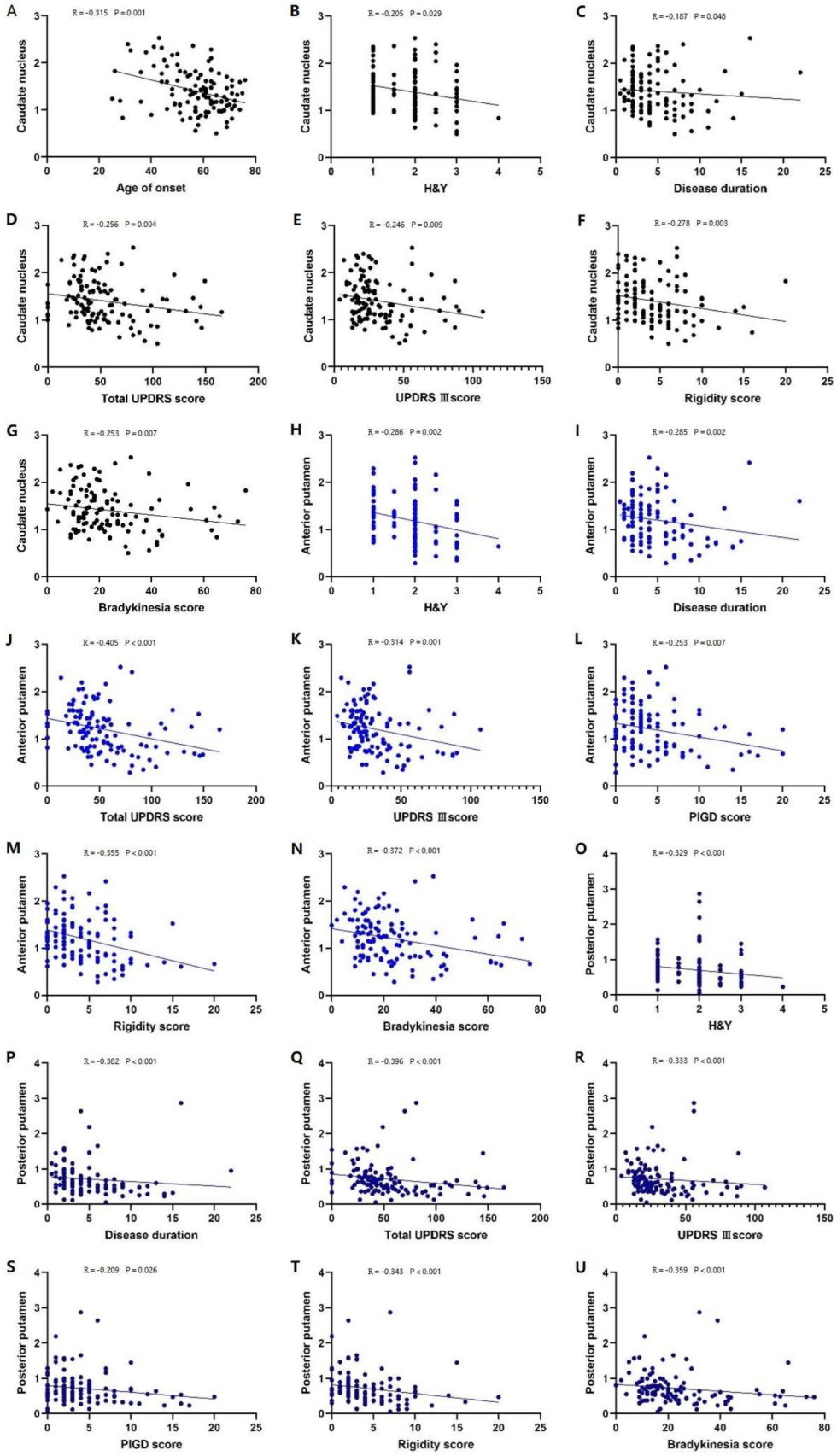

FIGURE 3
Correlation analysis of PD patients. Correlation analysis between the caudate nucleus 11C-CFT uptake and: **(A)** age of onset; **(B)** H-Y stage; **(C)** disease duration; **(D)** total UPDRS score; **(E)** UPDRS III score; **(F)** rigidity score; **(G)** bradykinesia score. Correlation analysis between the anterior putamen

(Continued)

Figure 3 (Continued)
11C-CFT uptake and: **(H)** H-Y stage; **(I)** disease duration; **(J)** total UPDRS score; **(K)** UPDRS III score; **(L)** PIGD score; **(M)** rigidity score; **(N)** bradykinesia score. Correlation analysis between the posterior putamen 11C-CFT uptake and: **(O)** H-Y stage; **(P)** disease duration; **(Q)** total UPDRS score; **(R)** UPDRS III score; **(S)** PIGD score; **(T)** rigidity score; **(U)** bradykinesia score.

TABLE 3 Spearman correlation analysis of striatal ^{11}C-CFT uptake in PD patients with clinical data.

Characteristic	Caudate nucleus		Anterior putamen		Posterior putamen	
	R	*P*	*R*	*P*	*R*	*P*
Age of onset	−0.315	0.001	−0.091	0.339	−0.079	0.403
H&Y stage	−0.205	0.029	−0.286	0.002	−0.329	<0.001
Disease duration	−0.187	0.048	−0.285	0.002	−0.382	<0.001
Total UPDRS score	−0.256	0.004	−0.405	<0.001	−0.396	<0.001
UPDRS III score	−0.246	0.009	−0.314	0.001	−0.333	<0.001
Tremor score	−0.079	0.408	−0.01	0.914	−0.114	0.230
PIGD score	−0.151	0.110	−0.253	0.007	−0.209	0.026
Rigidity score	−0.278	0.003	−0.355	<0.001	−0.343	<0.001
Bradykinesia score	−0.253	0.007	−0.372	<0.001	−0.359	<0.001
MoCA score	0.065	0.495	0.068	0.477	−0.038	0.691

nucleus are more likely to be involved in cognitive and emotional functions, and patients with lesions in the caudate nucleus have cognitive changes (24). Patients with EOPD have better preservation of the caudate nucleus, and therefore, better cognition. Significant differences were observed between patients with EOPD and LOPD in terms of clinical presentation, response to medication, progression rate, and prognosis. The results of this study provide an objective molecular imaging basis for determining the differences in progression rate between the two.

Second, in this study, ^{11}C-CFT uptake in the caudate nucleus, anterior putamen, and posterior putamen was negatively correlated with H&Y stage, disease duration, total UPDRS score, and UPDRS III score, consistent with previous study fundings (25, 26). In addition, this study divided the UPDRS score for movement into four subdomains: tremor, rigidity, bradykinesia, and PIGD, and found that ^{11}C-CFT uptake in the caudate nucleus, anterior putamen, and posterior putamen was negatively correlated with rigidity and bradykinesia scores. ^{11}C-CFT uptake in the anterior and posterior putamen negatively correlated with the PIGD score. This is related to the dysfunction of the cortex-basal ganglia-thalamus-cortex loop, in which the striatum receives fiber projections from the sensorimotor cortex and transmits them via the "direct pathway" and the "indirect pathway" (27) to the medial globus pallidus/substantia nigra pars reticulate in the output nucleus of the basal ganglia. Patients with PD have reduced substantia nigra-striatal dopaminergic, which causes inhibition of the "direct pathway" and excitation of the "indirect pathway," resulting in motor symptoms such as reduced movement and rigidity (28). Thus, the longer the disease course, the more advanced the H&Y stage, the higher the motor symptom score, and the lower the striatal ^{11}C-CFT uptake, indicating severe dopaminergic neuronal damage. Therefore, DAT PET imaging can be used to assess the severity of PD. This study also found that ^{11}C-CFT uptake in the caudate nucleus, anterior putamen, and posterior putamen was not significantly correlated with tremor score, which is consistent with most previous studies suggesting that tremor is not associated with dopamine loss in the substantia nigra striatum (29–35). This may be due to the fact that the loop involved in PD tremor is not the same as the loop involved in the reduced movement and rigidity. Huang et al. showed that subthalamic burst discharges are dependent on input from the motor cortex, resulting in erroneous re-entrant information relays from the cortico-subthalamic nucleus to the pallido-thalamocortical loops, and thus Parkinsonian tremor (36). The caudate nucleus and putamen are not part of this loop, which explains why striatal ^{11}C-CFT uptake does not correlate with tremor scores. In addition, pathological studies have shown that patients with tremor-type Parkinson's disease have less degeneration in the substantia nigra, which projects mainly to the striatum, and more degeneration in the posterior region of the red nucleus, which projects mainly to the pallidus. This may also explain the lack of correlation between tremor scores and caudate-putamen DAT uptake (37).

Undeniably, ^{18}F-DOPA PET is the first *in vivo* assessment of dopaminergic function in PD. ^{18}F-Dopa is a fluorinated analog of levodopa that follows the same presynaptic dopamine (DA) synthesis pathway. It is decarboxylated by aromatic L-amino acid decarboxylase (AADC) and stored in presynaptic vesicles in the form of ^{18}F-labeled dopamine, providing an *in vivo* measure of AADC activity and presynaptic DA storage capacity. However, in the pathological state, levodopa decreases, and AADC activity compensatively increases as a compensatory response to progressive DA cell death. Upregulated AADC activity may lead to ^{18}F-dopa overestimation nerve terminal density and underestimation of the disease severity in early PD. In addition, most AADC-containing neurons are capable of taking up and converting ^{18}F-dopa. ^{11}C-CFT has been used to label DAT to assess dopaminergic neuron function, which may more sensitively reflect disease severity in early PD. Therefore, we chose DAT-PET in this study (38).

In conclusion, ^{11}C-CFT DAT-PET provides an objective molecular imaging basis for the difference in the rate of disease progression between patients with EOPD and those with LOPD. At the same time, DAT-PET can also be used as an important objective indicator to assess disease severity and monitor disease progression. The loss of striatal DAT is closely related to the clinical manifestations, especially motor symptoms. With the help of this study, clinicians can also preliminarily estimate the extent of DAT loss and dopaminergic neuronal damage in the patient's brain based on the patient's medical history, symptoms, signs and scale scores to predict the severity and progression rate of the disease, which is helpful in guiding clinical treatment and prognosis. What's more, this study provides an objective basis for screening patients for intermediate and advanced surgical indications for deep brain stimulation (DBS), and also provides an objective basis for accurate screening of patients in clinical drug trials. It is expected to promote early diagnosis and accurate treatment of Parkinson's disease.

This study has several limitations. First, this was a single-center, small-sample study, and there may have been bias in terms of

geography, race, examination, and assessment. Expansion of the sample size should be considered to conduct a multicenter study and further validate the findings. Second, DAT binding is susceptible to the effects of drugs (e.g., amantadine and modafinil) and normal aging, which may overestimate disease severity. This is intended for further validation in patients with PD who undergo DTBZ imaging.

Equations

$$11\text{C CFT uptake} = (\text{ROI radioactivity count / occipital radioactivity count}) - 1$$

Data availability statement

The original contributions presented in the study are included in the article/Supplementary material, further inquiries can be directed to the corresponding author.

Ethics statement

The studies involving human participants were reviewed and approved by Ethics Committee of the First Hospital of Jilin University. The patients/participants provided their written informed consent to participate in this study.

Author contributions

All authors listed have made a substantial, direct, and intellectual contribution to the work and approved it for publication.

Funding

This work was supported by grants from the National Natural Science Foundation of China (No. 81974194) and the Natural Science Foundation of Jilin Province (No. YDZJ202201ZYTS116) to ZY.

Acknowledgments

Thanks to Wu Yanhua from the First Hospital of Jilin University for her statistical guidance on this study.

Conflict of interest

The authors declare that the research was conducted in the absence of any commercial or financial relationships that could be construed as a potential conflict of interest.

Publisher's note

Supplementary material

The Supplementary material for this article can be found online at: https://www.frontiersin.org/articles/10.3389/fneur.2023.1195577/full#supplementary-material

References

1. Tolosa E, Garrido A, Scholz SW, Poewe W. Challenges in the diagnosis of Parkinson's disease. *Lancet Neurol.* (2021) 20:385–97. doi: 10.1016/s1474-4422(21)00030-2

2. Braak H, Del Tredici K, Rub U, de Vos RAI, Steur E, Braak E. Staging of brain pathology related to sporadic Parkinson's disease. *Neurobiol Aging.* (2003) 24:197–211. doi: 10.1016/s0197-4580(02)00065-9

3. Madetko N, Migda B, Alster P, Turski P, Koziorowski D, Friedman A. Platelet-to-lymphocyte ratio and neutrophil-to-lymphocyte ratio may reflect differences in Pd and Msa-P neuroinflammation patterns. *Neurol Neurochir Pol.* (2022) 56:148–55. doi: 10.5603/PJNNS.a2022.0014

4. Pedersen CC, Ushakova A, Skogseth RE, Alves G, Tysnes O-B, Aarsland D, et al. Inflammatory biomarkers in newly diagnosed patients with Parkinson disease and related neurodegenerative disorders. *Neurol Neuroimmunol Neuroinflamm.* (2023) 10:e200132. doi: 10.1212/nxi.0000000000200132

5. Schwab C, Klegeris A, McGeer PL. Inflammation in transgenic mouse models of neurodegenerative disorders. *Biochim Biophys Acta Mol Basis Dis.* (2010) 1802:889–902. doi: 10.1016/j.bbadis.2009.10.013

6. Stoessl AJ. Developments in neuroimaging: positron emission tomography. *Parkinsonism Relat Disord.* (2014) 20:S180–3. doi: 10.1016/s1353-8020(13)70042-7

7. Marshall V, Grosset D. Role of dopamine transporter imaging in routine clinical practice. *Mov Disord.* (2003) 18:1415–23. doi: 10.1002/mds.10592

8. Huang TT, Wang HL, Tang GH, Liang X, Shi XC, Zhang XS. The influence of residual nor-Beta-Cft in C-11 Cft injection on the Parkinson disease diagnosis a C-11 Cft pet study. *Clin Nucl Med.* (2012) 37:743–7. doi: 10.1097/RLU.0b013e31824c5fae

9. Postuma RB, Berg D, Stern M, Poewe W, Olanow CW, Oertel W, et al. Mds clinical diagnostic criteria for Parkinson's disease. *Mov Disord.* (2015) 30:1591–601. doi: 10.1002/mds.26424

10. Massa J, Chahine LM. Revision of diagnosis in early parkinsonism with abnormal dopamine transporter imaging. *J Parkinsons Dis.* (2019) 9:327–34. doi: 10.3233/jpd-181517

11. Mehanna R, Moore S, Hou JG, Sarwar AI, Lai EC. Comparing clinical features of young onset, middle onset and late onset Parkinson's disease. *Parkinsonism Relat Disord.* (2014) 20:530–4. doi: 10.1016/j.parkreldis.2014.02.013

12. Berg D, Postuma RB, Adler CH, Bloem BR, Chan P, Dubois B, et al. Mds research criteria for prodromal Parkinson's disease. *Mov Disord.* (2015) 30:1600–11. doi: 10.1002/mds.26431

13. Goetz CG, Tilley BC, Shaftman SR, Stebbins GT, Fahn S, Martinez-Martin P, et al. Movement Disorder Society-sponsored revision of the unified Parkinson's disease rating scale (Mds-Updrs): scale presentation and clinimetric testing results. *Mov Disord.* (2008) 23:2129–70. doi: 10.1002/mds.22340

14. Stebbins GT, Goetz CG, Burn DJ, Jankovic J, Khoo TK, Tilley BC. How to identify tremor dominant and postural instability/gait difficulty groups with the Movement Disorder Society unified Parkinson's disease rating scale: comparison with the unified Parkinson's disease rating scale. *Mov Disord.* (2013) 28:668–70. doi: 10.1002/mds.25383

15. Nasreddine ZS, Phillips NA, Bedirian V, Charbonneau S, Whitehead V, Collin I, et al. The Montreal Cognitive Assessment, Moca: A Brief Screening Tool for Mild Cognitive Impairment. *J Am Geriatr Soc.* (2019) 62:1991. doi: 10.1111/jgs.15925

16. Zhang Weishan JC, Wu Ping W, Jianjun GJ, Yihu G. 11c-Cft pet imaging to evaluate the distribution characteristics of dopamine transporters in the brain of patients with Parkinson's disease and multiple system atrophy P-type. *Chinese Clin Neurosci.* (2017) 25:652–8.

17. de la Fuente-Fernandez R, Sossi V, McCormick S, Schulzer M, Ruth TJ, Stoessl AJ. Visualizing vesicular dopamine dynamics in Parkinson's disease. *Synapse.* (2009) 63:713–6. doi: 10.1002/syn.20653

18. Sossi V, Dinelle K, Topping GJ, Holden JE, Doudet D, Schulzer M, et al. Dopamine transporter relation to levodopa-derived synaptic dopamine in a rat model of Parkinson's: an in vivo imaging study. *J Neurochem*. (2009) 109:85–92. doi: 10.1111/j.1471-4159.2009.05904.x

19. Yang YJ, Ge JJ, Liu FT, Liu ZY, Zhao J, Wu JJ, et al. Preserved caudate function in young-onset patients with Parkinson's disease: a dual-tracer pet imaging study. *Ther Adv Neurol Disord*. (2019) 12:11. doi: 10.1177/1756286419851400

20. Schrag A, Ben-Shlomo Y, Brown R, Marsden CD, Quinn N. Young-onset Parkinson's disease revisited--clinical features, natural history, and mortality. *Mov Disord*. (1998) 13:885–94. doi: 10.1002/mds.870130605

21. Ishibashi K, Oda K, Ishiwata K, Ishii K. Comparison of dopamine transporter decline in a patient with Parkinson's disease and normal aging effect. *J Neurol Sci*. (2014) 339:207–9. doi: 10.1016/j.jns.2014.01.015

22. Wickremaratchi MM, Ben-Shlomo Y, Morris HR. The effect of onset age on the clinical features of Parkinson's disease. *Eur J Neurol*. (2009) 16:450–6. doi: 10.1111/j.1468-1331.2008.02514.x

23. DeLong MR, Wichmann T. Basal ganglia circuits as targets for neuromodulation in Parkinson disease. *JAMA Neurol*. (2015) 72:1354–60. doi: 10.1001/jamaneurol.2015.2397

24. Mendez MF, Adams NL, Lewandowski KS. Neurobehavioral changes associated with caudate lesions. *Neurology*. (1989) 39:349–54. doi: 10.1212/wnl.39.3.349

25. Troiano AR, Schulzer M, De La Fuente-Fernandez R, Mak E, McKenzie J, Sossi V, et al. Dopamine transporter pet in normal aging: dopamine transporter decline and its possible role in preservation of motor function. *Synapse*. (2010) 64:146–51. doi: 10.1002/syn.20708

26. Liu SY, Wu JJ, Zhao J, Huang SF, Wang YX, Ge JJ, et al. Onset-related subtypes of Parkinson's disease differ in the patterns of striatal dopaminergic dysfunction: a positron emission tomography study. *Parkinsonism Relat Disord*. (2015) 21:1448–53. doi: 10.1016/j.parkreldis.2015.10.017

27. Miocinovic S, Somayajula S, Chitnis S, Vitek JL. History, applications, and mechanisms of deep brain stimulation. *JAMA Neurol*. (2013) 70:163–71. doi: 10.1001/2013.jamaneurol.45

28. Poewe W, Seppi K, Tanner CM, Halliday GM, Brundin P, Volkmann J, et al. Parkinson disease. *Nat Rev Dis Primers*. (2017) 3:21. doi: 10.1038/nrdp.2017.13

29. Benamer HTS, Patterson J, Wyper DJ, Hadley DM, Macphee GJA, Grosset DG. Correlation of Parkinson's disease severity and duration with I-123-Fp-Cit Spect striatal uptake. *Mov Disord*. (2000) 15:692–8. doi: 10.1002/1531-8257(200007)15:4<692::Aid-mds1014>3.0.Co;2-v

30. Benamer HTS, Oertel WH, Patterson J, Hadley DM, Pogarell O, Hoffken H, et al. Prospective study of presynaptic dopaminergic imaging in patients with mild parkinsonism and tremor disorders: part 1. Baseline and 3-month observations. *Mov Disord*. (2003) 18:977–84. doi: 10.1002/mds.10482

31. Pirker W. Correlation of dopamine transporter imaging with parkinsonian motor handicap: how close is it? *Mov Disord*. (2003) 18:S43–51. doi: 10.1002/mds.10579

32. Isaias IU, Benti R, Cilia R, Canesi M, Marotta G, Gerundini P, et al. I-23 Fp-Cit striatal binding in early Parkinson's disease patients with tremor vs. akinetic-rigid onset. *Neuroreport*. (2007) 18:1499–502. doi: 10.1097/WNR.0b013e3282ef69f9

33. Spiegel J, Hellwig D, Samnick S, Jost W, Mollers MO, Fassbender K, et al. Striatal Fp-Cit uptake differs in the subtypes of early Parkinson's disease. *J Neural Transm*. (2007) 114:331–5. doi: 10.1007/s00702-006-0518-2

34. Helmich RC, Janssen MJR, Oyen WJG, Bloem BR, Toni I. Pallidal dysfunction drives a cerebellothalamic circuit into Parkinson tremor. *Ann Neurol*. (2011) 69:269–81. doi: 10.1002/ana.22361

35. Helmich RC, Hallett M, Deuschl G, Toni I, Bloem BR. Cerebral causes and consequences of parkinsonian resting tremor: a tale of two circuits? *Brain*. (2012) 135:3206–26. doi: 10.1093/brain/aws023

36. Huang CS, Wang GH, Chuang HH, Chuang AY, Yeh JY, Lai YC, et al. Conveyance of cortical pacing for parkinsonian tremor-like hyperkinetic behavior by subthalamic dysrhythmia. *Cell Rep*. (2021) 35:21. doi: 10.1016/j.celrep.2021.109007

37. Jellinger KA. Post mortem studies in Parkinson's disease - is it possible to detect brain areas for specific symptoms? *J Neural Transm Suppl*. (1999) 56:1–29. doi: 10.1007/978-3-7091-6360-3_1

38. Li WH, Lao-Kaim NP, Roussakis AA, Martin-Bastida A, Valle-Guzman N, Paul G, et al. C-11-Pe2i and F-18-Dopa pet for assessing progression rate in Parkinson's: a longitudinal study. *Mov Disord*. (2018) 33:117–27. doi: 10.1002/mds.27183

frontiers | Frontiers in Neurology

TYPE Correction
PUBLISHED 21 September 2023
DOI 10.3389/fneur.2023.1289550

OPEN ACCESS

APPROVED BY
Frontiers Editorial Office,
Frontiers Media SA, Switzerland

*CORRESPONDENCE
Zhang Ying
zhang_ying99@jlu.edu.cn

†These authors have contributed equally to this work and share first authorship

RECEIVED 06 September 2023
ACCEPTED 07 September 2023
PUBLISHED 21 September 2023

CITATION
Kangli F, Hongguang Z, Yinghua L, Xiaoxiao D, Yuyin D, Lulu G, Yi L, Zhihui S and Ying Z (2023) Corrigendum: Characteristics and influencing factors of ^{11}C-CFT PET imaging in patients with early and late onset Parkinson's disease. *Front. Neurol.* 14:1289550. doi: 10.3389/fneur.2023.1289550

Corrigendum: Characteristics and influencing factors of ^{11}C-CFT PET imaging in patients with early and late onset Parkinson's disease

Fan Kangli†, Zhao Hongguang†, Li Yinghua, Du Xiaoxiao, Dai Yuyin, Gao Lulu, Li Yi, Sun Zhihui and Zhang Ying*

Department of Neurology, First Hospital of Jilin University, Changchun, China

KEYWORDS

Parkinson's disease, the early-onset Parkinson's disease, the late-onset Parkinson's disease, ^{11}C-CFT PET, dopamine transporter, motor symptoms, non-motor symptoms

A corrigendum on

Characteristics and influencing factors of ^{11}C-CFT PET imaging in patients with early and late onset Parkinson's disease

by Kangli, F., Hongguang, Z., Yinghua, L., Xiaoxiao, D., Yuyin, D., Lulu, G., Yi, L., Zhihui, S., and Ying, Z. (2023). *Front. Neurol.* 14:1195577. doi: 10.3389/fneur.2023.1195577

In the published article, there was an error in the author list. Fan Kangli and Zhao Hongguang are both equal and first authors.

The authors apologize for this error and state that this does not change the scientific conclusions of the article in any way. The original article has been updated.

Publisher's note

All claims expressed in this article are solely those of the authors and do not necessarily represent those of their affiliated organizations, or those of the publisher, the editors and the reviewers. Any product that may be evaluated in this article, or claim that may be made by its manufacturer, is not guaranteed or endorsed by the publisher.

frontiers | Frontiers in Neurology

TYPE Original Research
PUBLISHED 18 July 2023
DOI 10.3389/fneur.2023.1149577

OPEN ACCESS

EDITED BY
Binbin Nie,
Chinese Academy of Sciences (CAS), China

REVIEWED BY
Ane Murueta-Goyena,
University of the Basque Country, Spain
Marcelo Mendonça,
Champalimaud Foundation, Portugal

*CORRESPONDENCE
Erhe Xu
✉ xuerhe@163.com
Lichun Zhou
✉ lichunzhou@bjcyh.com

†These authors have contributed equally to this work and share first authorship
‡These authors have contributed equally to this work

RECEIVED 22 January 2023
ACCEPTED 27 March 2023
PUBLISHED 18 July 2023

CITATION
Xue X, Huang A, Zeng J, Song H, Xing Y, Chan P, Xu E and Zhou L (2023) The mechanism of impaired delayed recall verbal memory function in Parkinson's disease with orthostatic hypotension: a multiple imaging study. *Front. Neurol.* 14:1149577. doi: 10.3389/fneur.2023.1149577

The mechanism of impaired delayed recall verbal memory function in Parkinson's disease with orthostatic hypotension: a multiple imaging study

Xiaofan Xue[1,2†], Anqi Huang[2†], Jingrong Zeng[2], Haixia Song[3], Yingqi Xing[2], Piu Chan[2], Erhe Xu[2*‡] and Lichun Zhou[1*‡]

[1]Department of Neurology, Beijing Chaoyang Hospital, Capital Medical University, Beijing, China, [2]Department of Neurology, Beijing Xuanwu Hospital, Capital Medical University, Beijing, China, [3]Department of Neurology, The People's Hospital of Shijiazhuang, Shijiazhuang, Hebei, China

Introduction: Orthostatic hypotension (OH) frequently accompanies autonomic dysfunction and is an important risk factor for cognitive impairment in Parkinson's disease (PD). However, the association between different cognitive functions and OH in PD patients is not yet fully understood.

Methods: This study aimed to evaluate the scores of different cognitive domains and multiple parameters using different imaging techniques on PD patients with or without OH. A total number of 31 PD patients with OH ($n = 20$) and without OH ($n = 11$) were recruited from the Department of Neurology, Beijing Xuanwu Hospital for this study. All patients underwent beat-to-beat non-invasive blood pressure recordings and an active standing test to evaluate neurogenic OH and a global neuropsychological test to assess cognitive function. All patients underwent dynamic cerebral autoregulation (dCA) measurement, brain magnetic resonance imaging (MRI), and brain 18fluorine-fluorodeoxyglucose positron emission tomography/computed tomography (18F-FDG PET/CT).

Results: The results showed that OH patients had poor delayed recall verbal memory when compared with the PD patients without OH (1.75 ± 1.59 vs. 3.10 ± 1.73, $p = 0.042$). The dCA test indicated a significant difference in the right very low-frequency (VLF) gain between two groups (1.27 ± 0.17 vs. 1.10 ± 0.26, $p = 0.045$) and the brain 18F-FDG PET/CT indicated a significant difference in the SUV (right medial temporal lobe) to SUV (occipital lobe) ratio (0.60 ± 0.08 vs. 0.67 ± 0.11, $p = 0.049$). Meanwhile, these two imaging parameters were negatively correlated ($p < 0.001$). Furthermore, the score of a delayed recall verbal memory in the OH group was positively correlated with the right medial temporal lobe to occipital lobe ratio ($p < 0.001$) and was negatively correlated with the right VLF gain ($p = 0.023$).

Discussion: PD with OH patients had poor delayed recall memory, which might have been caused by the decreased metabolic dysfunction of specific medial temporal lobe due to the impaired dCA ability.

KEYWORDS

Parkinson's disease, orthostatic hypotension, cognitive impairment, imaging technique, memory function

1. Introduction

Parkinson's disease (PD) is commonly accepted to be associated with various non-motor symptoms, including sleep disturbance, cognitive impairment, and autonomic dysfunction (1). Autonomic impairment associated with PD is characterized by clinical features of constipation, sweating, orthostatic hypotension (OH), and postprandial hypotension (PPH), even in the early phase (2). Cognitive impairment and OH are among the most frequent and troublesome non-motor symptoms in PD. In a community cohort of PD patients who survived 20 years from diagnosis, 83% had dementia and 48% had symptomatic OH (3, 4).

Orthostatic hypotension (OH) and cognitive dysfunction often coexist; however, whether the relationship is causative or associative is still unclear (5–8). Recently, there is growing evidence to suggest that several cognitive domains were reported to be associated with OH in PD, such as visuospatial, verbal memory, and attention (5, 9–13). Memory was the most consistent domain among the reports, and in particular, verbal memory was the only domain associated with OH in the patients before medication (14). However, these studies were based on limited data and were mainly cross-sectional, and these studies had often failed to adjust for important covariates such as age, disease severity, and disease duration.

Neuroimaging studies have provided considerable insight into the neurobiological basis of PD and its cognitive function (15). In a previous study, we investigated the impaired dynamic cerebral autoregulation (dCA) ability, which was obtained by transcranial doppler ultrasound (TCD) and beat-to-beat technology in PD patients with OH (16). Moreover, the impaired dCA is also associated with OH and Parkinson's disease dementia (PDD) (17). Meanwhile, there are some studies which indicated that PD patients with OH had a more severe impairment on tests of verbal immediate and delayed memory, and there were higher white matter lesion scores recorded by brain magnetic resonance imaging (MRI) in the OH group, which supported the vascular hypothesis (14, 18). Compared with dCA and MRI, 18fluorine-fluorodeoxyglucose positron emission tomography (18F-FDG-PET) provides more information on the underlying pathophysiology by highlighting the metabolic dysfunction of specific anatomical structures which can then be correlated with cognitive impairment (19). However, there are limited studies on the relationship between the cognitive impairment and PD with or without OH patients as shown by brain 18F-FDG PET patterns.

This cross-sectional cohort study aimed to investigate the characteristics of cognitive impairment with or without OH using the beat-to-beat and TCD technology by clinically defined PD and explore the associated dCA parameters, white matter hyperintensity (WMH) scores by brain MRI, and cerebral glucose metabolism with 18F-FDG-PET computed tomography (18F-FDG-PET/CT) among these patients. We aimed to (1) find out the relationship between the clinical or imaging indicators and PD-associated OH; (2) compare the characteristics of seven different cognitive domains (visuospatial/executive, naming, delayed recall verbal memory, attention, repetition/lexical fluency, similarities, and orientation) from the Montreal Cognitive Assessment (MoCA) Scale in PD patients with or without OH; and (3) figure out the correlation between imaging parameters and impaired cognitive domains of PD patients.

2. Methods and materials

2.1. Participants

Parkinson's disease patients ($n = 31$) were enrolled consecutively from the Department of Neurology of the Xuanwu Hospital, Capital Medical University in Beijing, China, from January 2021 to December 2021. All patients were diagnosed as under clinical diagnosis or probable diagnosis of PD according to the UK Brain Bank criteria, regardless of their disease severity. All diagnoses were established by two independent neurologists. The exclusion criteria were arterial hypertension, diabetes mellitus, arrhythmia, old myocardial infarction, cerebral vascular diseases, sleep disorders (i.e., rapid eye movement sleep behavior disorder, RBD), visual hallucinations and other mental diseases, dehydration, anemia or infection, severe systemic diseases, and poor cooperation. All the PD patients received dopaminergic therapy and without OH therapy. We evaluated the motor symptoms by Hoehn–Yahr (H–Y) stages and Movement Disorder Society Unified Parkinson's Disease Rating Scale (MDS-UPDRS) Part 3 scores. We evaluated all the PD patients for non-motor symptoms using the Non-Motor Symptom Scale (NMSS). We used MoCA to assess cognitive impairment [a total MoCA score cutoff < 26, which has 90% sensitivity and 75% specificity for PD mild cognitive impairment (MCI), a total MoCA score < 21, which has 81% sensitivity and 95% specificity for PD-dementia (20)] and the Hamilton Depression Scale (HAMD) to assess the severity of depression. All tests were performed in a quiet and temperature-controlled room to minimize stress and its effects on the patients.

2.2. Active standing test

Blood pressure (BP) measurements were performed in a silent, temperature-controlled room and the participants were asked to avoid alcohol, caffeine, nicotine, discontinue dopamine and vasoactive medications for 24 h before the examination. After 10 min of relaxation in the supine position, they were asked to take the active standing test, which involved lying in the supine position on the bed for 10 min and standing for 10 min (21). OH is defined as at least 20 mmHg drop in systolic BP and/or a 10 mmHg drop in diastolic BP within 3 min after standing (22). We distinguished neurogenic OH from non-neurogenic OH using the neurogenic OH ratio based on the active standing test (23), where the neurogenic OH was characterized by the Δheart rate/Δsystolic blood pressure (ΔHR/ΔSBP) ratio of <0.492 during the active standing test (16). Based on these results, the participants were allocated either to the OH positive [OH(+)] group to the normal active standing test [OH(-)] group.

2.3. dCA measurement

Baseline brachial blood pressure was measured by a sphygmomanometer (Omron HBP-1300, Kyoto, Japan) in the supine position. During a 10-min supine period, three blood pressure readings were recorded. We used a servocontrolled plethysmograph (Finometer, Enschede, Netherlands) at middle finger to record the non-invasive continuous beat-to-beat BP (NIBP) and used a TCD (EMS-9D PRO, Shenzhen Delica Medical Equipment Co., Ltd., Shenzhen, China) to measure the cerebral blood flow velocity (CBFV) simultaneously in both the supine and standing positions during the entire procedure. Doppler probes were placed over the temporal window and fixed with an adjustable head frame. Continuous CBFV was measured in the left and right middle cerebral arteries (MCAs) at a depth of 50–65 mm (16, 17). All procedures were performed by a professional ultrasound doctor.

Based on the recommendations of the Cerebrovascular Research Network (CARNet) (24), the stored and processed data were adopted using the transfer function analysis (TFA) method to reflect the oscillations in BP and cerebral blood flow at a range of frequencies (17). With the assumption of linear correlation, it quantifies how much NIBP was reflected in the CBFV, and the regulator between NIBP and CBFV was indicated as cerebral autoregulation (16). The computer output parameters included the bilateral hemisphere phase, normalized gain (%/mmHg), absolute gain (cm/s/mmHg), and coherence at very low frequency (VLF, 0.02–0.07 Hz) and low frequency (LF, 0.07–0.2 Hz) separately. In general, the phase and gain reflect the temporal and amplitude relationship between BP and CBFV at the same frequency, whereas coherence approaches 1.0, reflected the linear relationship between oscillations in BP and CBFV (17). Thus, a lower phase and a higher gain represent a more impaired dCA ability. For the frequency domain, we evaluated within a VLF range, which was considered to reflect the most relevant real-time dynamic dCA behavior (25). We only estimated dCA parameters if the coherence $\geq$0.5 because a previous study had shown that a low coherence indicates that the linearity condition relating changes in velocity to pressure may be violated in this frequency range (26).

2.4. Brain MRI

A total of 31 patients underwent 3.0-T MRI (Magnetom Verio 3T; Siemens, Erlangen, Germany). Fluid-attenuated inversion recovery MRI sequences were reviewed for white matter changes and rated as per the modified Fazekas scale (27–29) as follows: grade 0, no white matter change; grade 1, minimal patchy white matter foci; grade 2, start of confluence of white matter disease; grade 3, large confluent areas; grade 4, confluence of white matter changes with cortical and subcortical involvement; grade 5, diffuse leukoencephalopathy with widespread and diffuse white matter disease.

2.5. PET/CT imaging

All PET/CT scans were performed on a uMI 510 PET/CT scanner (United Imaging Healthcare, Shanghai, China). 18F-FDG was produced in a radiochemistry laboratory, and the radiochemical purity of the tracer was >98%. After 40 min of intravenous injection of the radiotracer 18F-FDG (3.7 MBq/kg), 18F-FDG PET/CT brain scans were acquired. All patients were asked to fast for 4 to 6 h before injection. After injection, the patients were asked to have their eyes closed and keep quiet during the 40-min uptake period. The CT imaging thickness was 3.0 mm per slice and scanning time was 11.4 s. A single PET bed position was subsequently acquired for 15 min. Iterative reconstruction was performed with a 128 × 128 matrix and a 2.44-mm-thick slice. Two nuclear medicine physicians analyzed the 18F-FDG PET/CT images by visual assessment. The regions of interest (ROIs) are bilateral hippocampus and medial temporal lobes. Semiquantitative analysis was then completed by two experienced scientists (one from the Department of Nuclear Medicine and another from the Department of Radiology) who were double blinded to the results of the qualitative analysis. The ROI of each brain region was drawn along the outline of the gray matter cortex and mirrored to the contralateral side manually. The mean standard uptake value (SUV) of each ROI was quantitatively measured and recorded. To avoid individualized differences, the SUV of occipital lobe was treated as a reference, and we calculated the SUV (ROI) to SUV (occipital lobe) ratio.

2.6. Statistics

This research was designed as a single-center cross-sectional cohort study. Statistical analyses were performed using IBM SPSS v26 (IBM Corp., Armonk, NY, USA) and two-sided $p < 0.05$ were considered significant. Normally distributed continuous variables were expressed as the mean ± standard deviation (SD) and compared using *t*-tests, whereas skewed continuous variables were expressed as the median with interquartile range (IQR) and compared using the Mann–Whitney U test. Categorical variables, such as sex and cognitive function (i.e., the percentage of MCI/dementia), were expressed as percentages and analyzed using chi-square tests and a Fisher's exact test. Imaging parameters and the score of cognitive domains were tested with the Pearson correlation.

3. Results

3.1. Demographic information and cognition in PD patients with or without OH

Among our 31 PD patients (45.2% male), 20 (40% male) had OH and 11 (54.5% male) did not have OH. There were no significant differences ($p > 0.05$) between two groups in terms of sex, age, education years, disease duration, LED, H–Y stages, UPDRS Part 3 scores, NMSS scores, HAMD scores, MMSE scores, MoCA scores, and the percentage of MCI/dementia (Table 1).

TABLE 1 Demographic and clinical characteristics.

	OH(+) ($n = 20$)	OH(-) ($n = 11$)	P
Age, years	60.65 ± 8.18	58.64 ± 6.96	0.496
Sex, male (%)	8 (40.0%)	6 (54.5%)	0.532
Education, years	11.05 ± 3.50	10.73 ± 6.42	0.879
Disease duration, years	3.19 ± 3.17	3.55 ± 2.66	0.756
LED, mg	295.00 ± 299.26	256.80 ± 182.70	0.704
Hoehn and Yahr score	1.80 ± 0.73	2.18 ± 0.60	0.152
MDS-UPDRS Part 3 score	27.21 ± 15.45	30.40 ± 8.26	0.550
NMSS score	27.89 ± 30.20	27.40 ± 34.98	0.969
HAMD score	3.85 ± 3.18	6.45 ± 5.72	0.185
MMSE score	27.60 ± 2.91	27.91 ± 3.18	0.786
MoCA score	23.00 ± 5.04	23.55 ± 5.73	0.785
MCI (%)	2 (10.0%)	4 (36.4%)	0.151
Dementia (%)	8 (40.0%)	2 (18.2%)	0.202

OH, orthostatic hypotension; OH(+), OH positive; OH(-), OH negative; LED, levodopa equivalent dose; MDS-UPDRS, Movement Disorder Society Unified Parkinson's Disease Rating Scale; NMSS, Non-Motor Symptom Scale; HAMD, Hamilton Depression Scale; MMSE, Mini-mental State Examination; MoCA, Montreal Cognitive Assessment; MCI, mild cognitive impairment. Values are means (±SD), except sex (percentage of men), of the percentage of MCI and dementia (a total MoCA score cutoff < 26, which shows 90% sensitivity and 75% specificity for PD mild cognitive impairment (MCI) and a total MoCA score < 21, which shows 81% sensitivity and 95% specificity for PD-dementia).

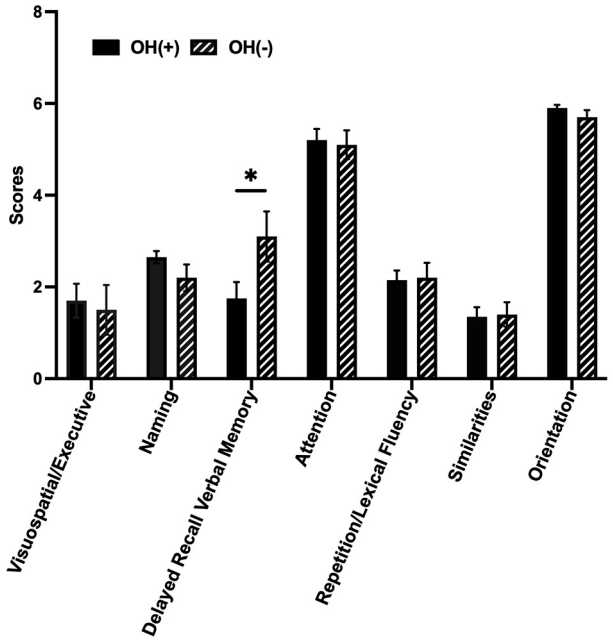

FIGURE 1
Cognitive domains of PD with or without OH. Column bars represent the scores of seven different cognitive domains by MoCA. The OH(+) group scored lower than the OH(-) group on delayed recall verbal memory function (1.75 ± 1.59 vs. 3.10 ± 1.73, $p = 0.042$, $p < 0.05$). OH, orthostatic hypotension; OH(+), OH positive; OH(-), OH negative. OH(+) ($n = 20$), OH(-) ($n = 11$). *p < 0.05.

3.2. Cognitive domains in the MoCA of PD patients with and without OH

Among our 31 PD patients, the OH(+) group scored lower than the OH(-) group on delayed recall verbal memory function (1.75 ± 1.59 vs. 3.10 ± 1.73, $p = 0.042$); however, the scores on other six subdomains (visuospatial/executive, naming, attention, repetition/lexical fluency, similarities, and orientation) between two groups were not significantly different (Figure 1).

3.3. The characteristics of multiple imaging methods in PD patients with or without OH

The data of imaging methods including dCA parameters (left and right VLF phase, left and right VLF gain) and the Fazekas scores by brain MRI and SUV (ROI) to SUV (occipital lobe) ratio calculated from the brain 18F-FDG PET/CT are presented in Table 2. The degree of bilateral VLF phase of patients with OH(+) was lower than that of OH(-) patients. At the same time, the bilateral VLF gain of patients with OH(+) was higher than that of OH(-) patients. Particularly, there was a significant difference in the right VLF gain between two groups (1.27 ± 0.17 vs. 1.10 ± 0.26, $p = 0.045$). The scores of WMH with OH(+) patients were higher than those of OH(-) PD patients, but there was no significant difference between two groups ($p > 0.05$). For the images (Figure 2) and parameters of the brain 18F-FDG PET/CT, the bilateral SUV (medial temporal lobe) to SUV (occipital lobe) ratio and the bilateral SUV (hippocampus) to SUV (occipital lobe) ratio were lower than those of OH(-) patients. Furthermore, there was a significant difference in the SUV (right medial temporal lobe) to SUV (occipital lobe) ratio (0.60 ± 0.08 vs. 0.67 ± 0.11, $p = 0.049$).

3.4. The correlation between the delayed recall verbal memory function and imaging parameters in PD patients with or without OH

Our Pearson correlation analysis showed that the right VLF gain was negatively correlated with the SUV (right medial temporal lobe) to SUV (occipital lobe) ratio within the two groups ($r = -0.844$, $p < 0.001$) (Figure 3A). In the OH(+) group, the score of delayed recall verbal memory was positively correlated with the SUV (right medial temporal lobe) to SUV (occipital lobe) ratio ($r = 0.774$, $p < 0.001$), and the score of delayed recall verbal memory was negatively correlated with the right VLF gain ($r = -0.504$, $p = 0.039$) (Figure 3B), and such correlations were not found in the OH(-) group ($p > 0.05$).

4. Discussion

The major findings of this study are as follows: (1) delayed recall verbal memory deficits were the most prominent feature in

TABLE 2 Multiple imaging characteristics of PD with or without OH.

	OH(+) (n = 20)	OH(-) (n = 11)	P
dCA parameters (MCA)			
Left very low-frequency phase (degree)	56.47 ± 31.34	67.29 ± 9.05	0.120
Right very low-frequency phase (degree)	61.61 ± 21.07	64.82 ± 10.13	0.401
Left very low-frequency gain (%/mmHg)	1.30 ± 0.22	1.18 ± 0.20	0.417
Right very low-frequency gain (%/mmHg)	1.27 ± 0.17	1.10 ± 0.26	**0.045***
Brain MRI			
Fazekas score	0.77 ± 0.66	0.55 ± 0.69	0.368
Brain 18F-FDG-PET/CT (ratio, SUV/SUV)			
Left medial temporal lobe/occipital lobe	0.61 ± 0.09	0.64 ± 0.89	0.334
Right medial temporal lobe/occipital lobe	0.60 ± 0.08	0.67 ± 0.11	**0.049***
Left hippocampus/occipital lobe	0.79 ± 0.11	0.83 ± 0.10	0.261
Right hippocampus/occipital lobe	0.78 ± 0.16	0.84 ± 0.11	0.254

OH, orthostatic hypotension; OH(+), OH positive; OH(-), OH negative; dCA, dynamic cerebral autoregulation; MCA, middle cerebral artery; MRI, magnetic resonance imaging; 18F-FDG-PET/CT, 18fluorine-fluorodeoxyglucose positron emission tomography/computed tomography; SUV, standard uptake value. Values are means (±SD). *$p < 0.05$. There was a significant difference in the right very low-frequency gain between OH(+) and OH(-) groups (1.27 ± 0.17 vs. 1.10 ± 0.26, $p = 0.045$) and there was a significant difference in the SUV (right medial temporal lobe) to SUV (occipital lobe) ratio (0.60 ± 0.08 vs. 0.67 ± 0.11, $p = 0.049$) between two groups.

OH(+) PD patients compared with OH(-) PD patients, (2) more impaired dCA ability and lower SUV (ROI) to SUV (occipital lobe) ratio by the brain 18F-FDG PET/CT were observed in PD patients with OH, especially the right VLF gain and the SUV (right medial temporal lobe) to SUV (occipital lobe) ratio, (3) the right VLF gain and the SUV (right medial temporal lobe) to SUV (occipital lobe) ratio were negatively correlated. In the OH(+) group, the score of delayed recall verbal memory was positively correlated with the SUV (right medial temporal lobe) to SUV (occipital lobe) ratio and was negatively correlated with the right VLF gain.

The delayed recall verbal memory function is thought to be dependent on the integrity of the Papez circuit, which includes the hippocampus, parahippocampal gyrus, medial temporal lobe, mammillary bodies, insula, and cingulate gyrus (30). Why was the delayed recall verbal memory impairment between OH(+) and OH(-) different? A possible mechanism for the contributory relationship was proposed to show that the intermittent cerebral hypoperfusion caused by episodic hypotension might induce brain key region ischemia (31–36). The cerebral hypoperfusion and anoxic damage in these vulnerable areas will lead to WMH and memory dysfunction (35, 36). Previous studies indicated that PD patients with OH had a more severe impairment on tests of verbal immediate and delayed memory, and there were higher WMH scores in the OH(+) group (14, 18). However, another study failed to find any difference in WMH between PD with and without OH (9). Our study showed that the score of WMH was higher in the OH(+) group than in the OH(-) group, but there was no significant difference between two groups ($p > 0.05$). The reason why the score of WMH did not show a significant difference within two groups might be attributed to the fact that the severity of WMH was rated using the semiquantitative visual rating system of Scheltens et al. by MRI (37), which is not the best approach to investigate the microstructure of deep brain white matter (30). The second reason may be that the severity of WMH could not represent the neuronal damage directly. Future studies should consider OH and WMH burdens in the pathological context of PD with more advanced neuroimaging approaches, such as diffusion kurtosis imaging (DKI) or diffusion tensor imaging (DTI). Although the role of WMH burdens in OH(+) PD patients is not clear, we still think that it could be a potential pathological mechanism for OH and cognitive impairment. As a result of WMH, PD patients may have had an early stage of cognitive impairment that was not detected yet.

As we all know, PD patients with OH appear to have poor cerebrovascular autoregulation (38). We attempted to use the dCA measurement to explain the reason why a delayed recall verbal memory impairment is more seriously experienced in OH(+) patients with PD. The dCA ability was obtained by the TCD and beat-to-beat technology. The TCD probes were placed over the temporal window and fixed with an adjustable head frame. The parameters of dCA represented the flow regulation function of the left and right MCAs that mainly supply blood to the temporal lobe and part of hippocampus (16). We evaluated the bilateral phase and gain within a VLF range, which was considered to reflect the most relevant real-time dynamic dCA behavior (25). Phase could be the representation of the time delay in the CBFV response to NIBP, where a higher phase means a better cerebral autoregulation ability. Gain represented the damping effect of dCA on the magnitude of BP oscillation. Absolute gain represents the absolute changes in NIBP and CBFV, whereas normalized gain represents relative changes in CBFV and NIBP, regardless of the baseline values of NIBP and CBFV. A higher gain represents a more impaired dCA ability. Our research showed there were more impaired dCA parameters in the OH(+) group, especially the right VLF gain, which indicated that CBFV was greatly influenced by NIBP on the right side. The result of cerebral autoregulation dysfunction might be attributed to the unstable flow through the distal capillary and injury to the cerebral microcirculation. This, in turn, will damage the microvascular system and induce several downstream sequelae, namely, the disruption of the blood–brain barrier, neuroinflammation, cerebral microbleeds, and white matter lesions (16). It is consistent with our hypothesis again that WMH burdens induced by dCA impairment might be the potential mechanism for memory dysfunction in PD with OH.

However, it is not enough to analyze the dCA ability alone, we also used the brain 18F-FDG PET/CT that focused on the regions of hippocampus and medial temporal lobe to clarify the relationship between the vascular mechanism and the memory impairment in OH(+) patients. As a diagnostic aid, 18F-FDG PET provides information that is currently considered as an additional feature for the diagnosis of PD (39). The previous 18F-FDG PET study showed that PD patients with visual hallucinations, indeed, show occipital

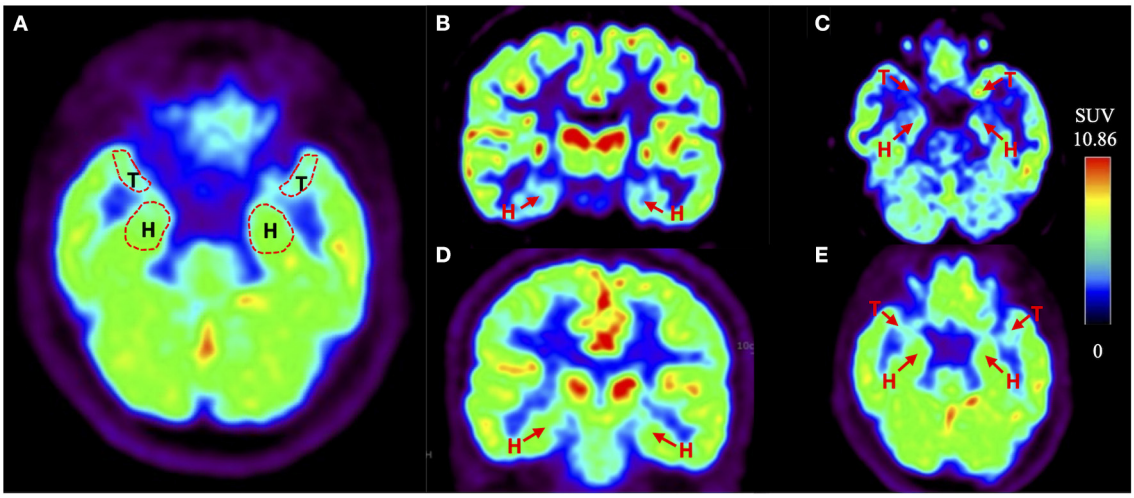

FIGURE 2
Example of the brain 18F-FDG PET/CT of PD with or without OH. **(A)** The red dotted line indicates the regions of interest (ROIs), which are bilateral hippocampus (H) and medial temporal lobes (T). **(B, C)** Shown are coronal and transverse sections of the brain 18F-FDG PET /CT of PD-OH(+) patients. The red arrow points the bilateral hippocampus (H) and medial temporal lobes (T). **(D, E)** Shown are coronal and transverse sections of the brain 18F-FDG PET/CT of PD-OH(-) patients. The red arrow points the bilateral hippocampus (H) and medial temporal lobes (T).

hypometabolism and a high risk of developing dementia than patients without visual hallucinations (22, 23, 40). Likewise, PD patients with the RBD showed a lower cognitive performance and a higher likelihood of MCI and posterior cortical hypometabolism than PD patients without this disorder (39). The occipital lobe was chosen as the reference because we excluded diseases that might affect occipital lobe metabolism, for example RBD and visual hallucinations. Another reason was that we analyzed the metabolism of occipital lobe within two groups, and there was no significant difference between them ($p > 0.05$). Our research showed a lower SUV (right medial temporal lobe) to SUV (occipital lobe) ratio in the OH(+) group compared with the OH(-) group. The right VLF gain was negatively correlated with the SUV (right medial temporal lobe) to SUV (occipital lobe) ratio within two groups, which indicated the potential causal relationship between these two parameters. The brain 18F-FDG PET/CT provided an important information on the underlying pathophysiology that metabolic dysfunction of specific medial temporal lobe may be correlated with dCA dysfunction. Moreover, the score of delayed recall verbal memory was positively correlated with the SUV (right medial temporal lobe) to SUV (occipital lobe) ratio and was also negatively correlated with the right VLF gain in the OH(+) group, whereas such correlations were not found in the OH(-) group. The aforementioned conclusions suggested that the delayed recall verbal memory dysfunction in PD patients with OH might have been caused by the decreased metabolic dysfunction of specific medial temporal lobe due to the impaired dCA; however, it might not be the potential mechanism for the OH(-) group. Furthermore, we did not find any obvious metabolic dysfunction in the hippocampus region. The reason might be attributed to the fact that not only MCAs supply blood to the hippocampus, but also the posterior cerebral arteries (PCAs), and these dCA parameters cannot represent the autoregulation ability of PCAs. The reason why we only found significant differences in the imaging parameters on the right side is still not well explained. A previous study showed that pathological attenuation of neural activities within the right-lateralized cortical network is a neurophysiological biomarker of speech and limb movement timing deficits in PD (41). There is another study which found that memory-impaired PD patients demonstrated a more significant reduction in D2 receptor binding in the right medial temporal lobe compared to healthy controls and PD patients with no MCI (42). Future studies are needed to confirm whether PD with OH patients have right-lateralized reduction in D2 receptor binding, moreover, if there is any relationship between the memory impairment and speech or motor timing control in PD with OH.

Furthermore, animal models also suggested that cerebral hypoperfusion may decrease vascular clearance, increase cleavage of amyloid precursor protein, and promote beta amyloid accumulation (43). It is known that the beta amyloid protein is a well-recognized pathological biomarker for Alzheimer's disease (AD), whose typical symptoms are short-term memory deficits in the early stage (44, 45). Moreover, PD patients with coexisting AD pathology tend to have a higher level of α-synuclein accumulation in limbus and neocortex (46, 47). Additionally, hippocampus and medial temporal lobe are thought to play a prominent role in human episodic memory, and this pattern is often observed during verbal memory recall (48). Based on aforementioned studies and our conclusion, we suggest that another reason for an earlier delayed recall verbal memory dysfunction in OH with PD is that it is possible for OH to have overlapped pathological changes with AD, especially on certain areas related to the medial temporal–hippocampal circuit.

To the best of our knowledge, this is the first study to have elaborated on the relationship between the cognitive domain impairment of OH(+) and OH(-) in patients with PD using multiple neuroimaging parameters (dCA measurement, brain MRI,

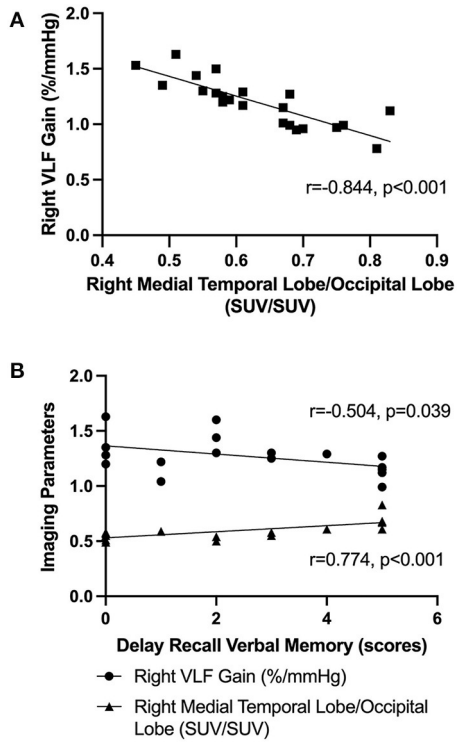

FIGURE 3
The Pearson correlation analysis. **(A)** The Pearson correlation analysis of the right VLF gain and the SUV (right medial temporal lobe) to SUV (occipital lobe) ratio in OH(+) and OH(-) groups. **(B)** The Pearson correlation analysis about the score of delay recall verbal memory function, the right VLF gain, and the SUV (right medial temporal lobe) to SUV (occipital lobe) ratio in OH(+) groups.

and 18F-FDG PET/CT). This study will provide new ideas for further research on the pathological mechanism of OH and cognitive impairment in PD. However, there are still limitations to this study. First, this study was based on limited data because we ruled out diseases that might affect the cerebral perfusion. Moreover, it was only a single-center cross-sectional study that cannot directly observe the progress of different cognitive domains in PD patients. Therefore, a larger longitudinal study is required to confirm our conclusion. Second, we did not distinguish the asymptomatic OH from symptomatic OH within the OH group, and healthy controls were not included in this study. Third, the assessment of MoCA is simple and feasible; however, it does not differentiate visuospatial function from executive function very well, and it also cannot well stratify with the memory dysfunction. More specific tests on memory function should be considered in future. Moreover, the other part of the Papez circuit of brain 18F-FDG PET/CT and AD-related biomarkers should be considered to further study the internal causes of impairment in different cognitive domains with OH in PD patients.

In conclusion, we found that PD with OH patients had poor delayed recall verbal memory function, which might have been caused by the decreased metabolic dysfunction of specific medial temporal lobe due to the impaired dCA of MCAs. An understanding of which of these mechanisms contributes to the link between the OH and cognitive function in PD may help clinicians to identify the most effective therapeutic strategy for OH patients with PD.

Data availability statement

The original contributions presented in the study are included in the article/supplementary material, further inquiries can be directed to the corresponding authors.

Ethics statement

The studies involving human participants were reviewed and approved by the Board of the Ethics Committee of Beijing Xuanwu Hospital, Capital Medical University. The patients/participants provided their written informed consent to participate in this study.

Author contributions

XX and AH collected and conducted data analysis, interpreted the data, and drafted the manuscript for intellectual content. JZ and HS analyzed the data and interpreted the data. YX and PC revised the manuscript. LZ and EX acquired the study data, designed, and conceptualized the study. All authors contributed to the article and approved the submitted version.

Acknowledgments

The authors thank the patients for their participation.

Conflict of interest

The authors declare that the research was conducted in the absence of any commercial or financial relationships that could be construed as a potential conflict of interest.

Publisher's note

All claims expressed in this article are solely those of the authors and do not necessarily represent those of their affiliated organizations, or those of the publisher, the editors and the reviewers. Any product that may be evaluated in this article, or claim that may be made by its manufacturer, is not guaranteed or endorsed by the publisher.

References

1. Oka H, Umehara T, Nakahara A, Matsuno H. Comparisons of cardiovascular dysautonomia and cognitive impairment between de novo Parkinson's disease de novo dementia with Lewy bodies. *BMC Neurol.* (2020) 20:350. doi: 10.1186/s12883-020-01928-5

2. Goldstein DS. Orthostatic hypotension as an early finding in Parkinson disease. *Clin Auton Res.* (2006) 16:46–54. doi: 10.1007/s10286-006-0317-8

3. Lim SY, Lang AE. The nonmotor symptoms of Parkinson's disease–an overview. *Mov Disord.* (2010) 25:S123–30. doi: 10.1002/mds.22786

4. Hely MA, Morris JGL, Reid WGJ, Trafficante R. Sydney multicenter study of Parkinson's disease: non-L-dopa-response problems dominate at 15 years. *Mov Disord.* (2005) 20:190–9. doi: 10.1002/mds.20324

5. Allcock LM, Kenny RA, Mosimann UP, Tordoff S, Wesnes KA, Hildreth AJ, et al. Orthostatic hypotension in Parkinson's disease: association with cognitive decline? *Int J Geriatr Psychiatry.* (2006) 21:778–83. doi: 10.1002/gps.1562

6. Idiaquez J, Benarroch EE, Rosales H, Milla P, Ríos L. Autonomic and cognitive dysfunction in Parkinson's disease. *Clin Auton Res.* (2007) 17:93–8. doi: 10.1007/s10286-007-0410-7

7. Peralta C, Stampfer-Kountchev M, Karner E, Köllensperger M, Geser F, Wolf E, et al. Orthostatic hypotension and attention in Parkinson's disease with and without dementia. *J Neural Transm.* (2007) 114:585–8. doi: 10.1007/s00702-006-0615-2

8. Hohler AD, Zuzuarregui JR, Katz DI, Depiero TJ, Hehl CL, Leonard A, et al. Differences in motor and cognitive function in patients with Parkinson's disease with and without orthostatic hypotension. *Int J Neurosci.* (2012) 122:233–6. doi: 10.1080/00207454.2012.642038

9. Pilleri M, Facchini S, Gasparoli E, Biundo R, Bernardi L, Marchetti M, et al. Cognitive and MRI correlates of orthostatic hypotension in Parkinson's disease. *J Neurol.* (2013) 260:253–9. doi: 10.1007/s00415-012-6627-y

10. Centi J, Freeman R, Gibbons CH, Neargarder S, Canova AO, Cronin-Golomb A. Effects of orthostatistic hypotension on cognition in Parkinson disease. *Neurology.* (2016) 88:17–24. doi: 10.1212/WNL.0000000000003452

11. Bae H-J, Lim J-H, Cheon S-M. Orthstatic hypotension and cognitive impairment in de novo patients with Parkinson's disease. *J Mov Disord.* (2014) 7:102–4. doi: 10.14802/jmd.14016

12. Udow SJ, Robertson AD, MacIntosh BJ, Espay AJ, Rowe JB, Lang AE, et al. 'Under pressure': is there a link between orthostatic hypotension and cognitive impairment in α-synucleinopathies? *J Neurol Neurosurg Psychiatry.* (2016) 87:1311–21. doi: 10.1136/jnnp-2016-314123

13. Cicero CE, Raciti L, Monastero R, Mostile G, Donzuso G, Sciacca G, et al. Cardiovascular autonomic function and MCI in Parkinson's disease. *Parkinsonism Relat Disord.* (2019) 69:55–8. doi: 10.1016/j.parkreldis.2019.10.023

14. Oh YS, Kim JS, Lee KS. Orthostatic and supine blood pressures are associated with white matter hyperintensities in Parkinson disease. *J Mov Disord.* (2013) 6:23–7. doi: 10.14802/jmd.13006

15. Weingarten CP, Sundman MH, Hickey P, Chen NK. Neuroimaging of Parkinson's disease: expanding views. *Neurosci Biobehav Rev.* (2015) 59:16–52. doi: 10.1016/j.neubiorev.2015.09.007

16. Xing Y, Li Q, Xu E, Zeng J, Li Q, Mei S, et al. Impaired cerebral autoregulation in Parkinson's disease: an orthostatic hypotension analysis. *Front Neuro.* (2022) 13:811698. doi: 10.3389/fneur.2022.811698

17. Chen H, Xu E, Zhou F, Li Q, Zeng J, Mei S, et al. Impaired dynamic cerebral autoregulation: a potential mechanism of orthostatic hypotension and dementia in Parikinson's disease. *Front Aging Neurosci.* (2022) 14:927009. doi: 10.3389/fnagi.2022.927009

18. Kim J-S, Oh Y-S, Lee K-S, Kim Y-I, Yang D-W, Goldstein DS. Association of cognitive dysfunction with neurocirculatory abnormalities in early Parkinson disease. *Neurology.* (2012) 79:1323–31. doi: 10.1212/WNL.0b013e31826c1acd

19. Perani D, Bressi S, Testa D, Grassi F, Cortelli P, Gentrini S, et al. Clinical/metabolic correlations in multiple system atrophy. A fludeoxyglucose F 18 positron emission tomographic study. *Arch Neurol.* (1995) 52:179–85. doi: 10.1001/archneur.1995.00540260085021

20. Dalrymple-Alford JC, MacAskill MR, Nakas CT, Livingston L, Graham C, Crucian GP, et al. The MoCA: well-suited screen for cognitive impairment in Parkinson's disease. *Neurology.* (2010) 75:1717–25. doi: 10.1212/WNL.0b013e3181fc29c9

21. Aydin AE, Soysal P, Isik AT. Which is preferable for orthostatic hypotension diagnosis in older adults: active standing test or head-up tilt table test? *Clin Interv Aging.* (2017) 12:207–12. doi: 10.2147/CIA.S129868

22. Freeman R, Wieling W, Axelrod FB, Benditt DG, Benarroch E, Biaggioni I, et al. Consensus statement on the definition of orthostatic hypotension, neurally mediated syncope and the postural tachycardia syndrome. *Clin Auto Res.* (2011) 21:69–72. doi: 10.1007/s10286-011-0119-5

23. Fanciulli A, Kerer K, Leys F, Seppi K, Kaufmann H, Norcliffe-Kaufmann L, et al. Validation of the neurogenic orthostatic hypotension ratio with active standing. *Ann Neurol.* (2020) 88:643–5. doi: 10.1002/ana.25834

24. Claassen JA, Meel-van den Abeelen AS, Simpson DM, Panerai RB, international Cerebral Autoregulation Research Network (CARNet). Transfer function analysis of dynamic cerebral autoregulation: a white paper from the International Cerebral Autoregulation Research Network. *J Cereb Blood Flow Metab.* (2016) 36:665–80. doi: 10.1177/0271678X15626425

25. Haubrich C, Wendt A, Diehl RR, Klötzsch C. Dynamic autoregulation testing in the posterior cerebral artery. *Stroke.* (2004) 35:848–52. doi: 10.1161/01.STR.0000120729.99039.B6

26. Zhang R, Zuckerman JH, Giller CA, Levine BD. Transfer function analysis of dynamic cerebral autoregulation in humans. *Am J Physiol.* (1998) 274:H233–41. doi: 10.1152/ajpheart.1998.274.1.H233

27. Fazekas F, Chawluk JB, Alavi A, Hurtig HI, Zimmerman RA. MR signal abnormalities at 15 T in Alzheimer's dementia and normal aging AJR. *Am J Roentgenol.* (1987) 149:351–6. doi: 10.2214/ajr.149.2.351

28. Correa DD, Shi W, Abrey LE, Deangelis LM, Omuro AM, Deutsch MB, et al. Cognitive functions in primary CNS lymphoma after single or combined modality regimens. *Neuro Oncol.* (2012) 14:101–8. doi: 10.1093/neuonc/nor186

29. Corn BW, Yousem DM, Scott CB, Rotman M, Asbell SO, Nelson DF, et al. White matter changes are correlated significantly withradiation dose: observations from a randomized dose-escalation trial for malignant glioma (Radiation Therapy Oncology Group 83-02). *Cancer.* (1994) 74:2828–35.

30. Papez JW. A proposed mechanism of emotion. *J Neuropsychiatry Clin Neurosci.* (1937) 7:103–12.

31. Espay AJ, LeWitt PA, Kaufmann H. Norepinephrine deficiency in Parkinson's disease: the case for noradrenergic enhancement. *Mov Disord.* (2014) 29:1710–9. doi: 10.1002/mds.26048

32. Vazey EM, Aston-Jones G. The emergine role of norepinephrine in cognitive dysfunctions of Parkinson's disease. *Front Behav Neurosci.* (2012) 6:48. doi: 10.3389/fnbeh.2012.00048

33. Braak H, Tredici KD, Rüb U, de Vos RA, Jansen Steur EN, Braak E. Staging of brain pathology related to sporadic Parkinson's disease. *Neurobiol Aging.* (2003) 24:197–211. doi: 10.1016/S0197-4580(02)00065-9

34. Carlsson A. Evidence for a role of dopamine in extrapyramidal functions. *Acta Neuroveg.* (1964) 26:484–93. doi: 10.1007/BF01252144

35. Pantoni L, Garcia JH. Pathogenesis of leukoaraiosis: a review. *Stroke.* (1997) 28:652–9. doi: 10.1161/01.STR.28.3.652

36. Bowler JV. Editorial comment- the progression of leukoaraiosis. *Stroke.* (2003) 34:1916–7. doi: 10.1161/01.STR.0000080940.16070.5B

37. Scheltens P, Barkhof F, Leys D, Pruvo JP, Nauta JJ, Vermersch P, et al. A semiquantative rating scale for the assessment of signal hyperintensities on magnetic resonance imaging. *J Neurol Sci.* (1993) 114:7–12. doi: 10.1016/0022-510X(93)90041-V

38. Palma JA. Norcliffe-Kaufmann. Orthostatic hypotension in Parkinson disease. *Clin Geriatr Med.* (2020) 36:53–67. doi: 10.1016/j.cger.2019.09.002

39. Arnaldi D, Morbelli S, Brugnolo A, Girtler N, Picco A, Ferrara M, et al. Functional neuroimaging and clinical features of drug naïve patients with de novo Parkinson's disease and probable RBD. *Parkin Rel Dis.* (2016) 29:47–53. doi: 10.1016/j.parkreldis.2016.05.031

40. Marinus J, Zhu K, Marras C, Aarsland D, van Hilten JJ. Risk factors for non-motor symptoms in Parkinson's disease. *Lancet Neurol.* (2018) 17:559–68. doi: 10.1016/S1474-4422(18)30127-3

41. Roozbeh B, Karim J. Pathological attenuation of the right prefrontal cortex activity predicts speech and limb motor timing disorder in Parkinson's disease. *Behav Bra Res.* (2019) 369:111939. doi: 10.1016/j.bbr.2019.111939

42. Christopher L, Duff-Canning S, Koshimori Y, Segura B, Boileau I, Chen R, et al. Salience network and parahippocampal dopamine dysfunction in memory-impaired Parkinson disease. *Ann Neuro.* (2014) 2:269–80. doi: 10.1002/ana.24323

43. Iadecola C. The overlap between neurodegenerative and vascular factors in the pathogenesis of dementia. *Acta Neuropathol.* (2010) 120:287–96. doi: 10.1007/s00401-010-0718-6

44. Mathis CA, Wang Y, Holt DP, Huang G-F, Debnath ML, Klunk WE. Synthesis and evaluation of 11C-labeled 6-substituted 2-arylbenzothiazoles as amyloid imaging agents. *J Med Chem.* (2003) 46:2740–54. doi: 10.1021/jm030026b

45. Nebes R. Semantic memory in Alzheimer's disease. *Psychol Bull.* (1989) 106:377–94. doi: 10.1037/0033-2909.106.3.377

46. Smith C, Malek N, Grosset K, Cullen B, Gentleman S, Grosset DG. Neuropathology of dementia in patients with Parkinson's disease: a systematic review of autopsy studies. *J Neurol Neurosurg Psychiatry*. (2019) 90:1234–43. doi: 10.1136/jnnp-2019-321111

47. Toledo JB, Gopal P, Raible K, Irwin DJ, Brettschneider J, Sedor S, et al. Pathological alpha-synuclein distribution in subjects with coincident Alzheimer's and Lewy body pathology. *Acta Neuropathol*. (2016) 131:393–409. doi: 10.1007/s00401-015-1526-9

48. Das A, Menon V. Asymmetric frequency-specific feedforward and feedback information flow between hippocampus and prefrontal cortex during verbal memory encoding and recall. *J Neurosci*. (2021) 41:8427–40. doi: 10.1523/JNEUROSCI.0802-21.2021

frontiers | Frontiers in Aging Neuroscience

TYPE Brief Research Report
PUBLISHED 22 September 2023
DOI 10.3389/fnagi.2023.1232387

OPEN ACCESS

EDITED BY
Francesca Mancini,
Fondazione Don Carlo Gnocchi Onlus (IRCCS), Italy

REVIEWED BY
Sebastian Heinzel,
University of Kiel, Germany
Benjamin Roeben,
University of Tübingen, Germany

*CORRESPONDENCE
Gennaro Pagano
✉ gennaro.pagano@roche.com

RECEIVED 05 June 2023
ACCEPTED 08 September 2023
PUBLISHED 22 September 2023

CITATION
Jackson H, Anzures-Cabrera J, Simuni T, Postuma RB, Marek K and Pagano G (2023) Identifying prodromal symptoms at high specificity for Parkinson's disease. *Front. Aging Neurosci.* 15:1232387. doi: 10.3389/fnagi.2023.1232387

Identifying prodromal symptoms at high specificity for Parkinson's disease

Holly Jackson[1,2], Judith Anzures-Cabrera[1], Tanya Simuni[3], Ronald B. Postuma[4], Kenneth Marek[5] and Gennaro Pagano[6,7]*

[1]Roche Products Ltd, Welwyn Garden City, United Kingdom, [2]Department of Mathematics and Statistics, Lancaster University, Lancaster, United Kingdom, [3]Department of Neurology, Northwestern University Feinberg School of Medicine, Chicago, IL, United States, [4]Department of Neurology, Montreal Neurological Institute, McGill University, Montreal, QC, Canada, [5]Institute for Neurodegenerative Disorders, New Haven, CT, United States, [6]Roche Pharma Research and Early Development (pRED), Neuroscience and Rare Diseases Discovery and Translational Area, Roche Innovation Center Basel, Basel, Switzerland, [7]University of Exeter Medical School, London, United Kingdom

Introduction: To test drugs with the potential to prevent the onset of Parkinson's disease (PD), it is key to identify individuals in the general population at high risk of developing PD. This is often difficult because most of the clinical markers are non-specific, common in PD but also common in older adults (e.g., sleep problems).

Objective: We aimed to identify the clinical markers at high specificity for developing PD by comparing individuals with PD or prodromal PD to healthy controls.

Methods: We investigated motor and non-motor symptoms (Movement Disorder Society Unified Parkinson's Disease Rating Scale Part 1 and 2 items) in 64 prodromal PD and 422 PD individuals calculating the odds ratios, adjusting for age and gender, for PD and prodromal PD versus 195 healthy controls. Symptoms at high specificity were defined as having an adjusted odds ratio ≥ 6.

Results: Constipation had an adjusted odds ratio, 6.14 [95% CI: 2.94–12.80] showing high specificity for prodromal PD, and speech difficulties had an adjusted odds ratio, 9.61 [95% CI: 7.88–48.81] showing high specificity for PD. The proportion of participants showing these specific markers was moderate (e.g., prevalence of constipation was 43.75% in prodromal PD, and speech difficulties was 33.89% in PD), suggesting these symptoms may make robust predictors of prodromal PD and PD, respectively.

Discussion: Clinical markers at high specificity for developing PD could be used as tools in the screening of general populations to identify individuals at higher risk of developing PD.

KEYWORDS

Parkinson's disease, prodromal symptoms, specificity, prevalence, observational study

1. Introduction

Parkinson's disease (PD) diagnosis is clinical, based on the presence of motor features, such as bradykinesia, rigidity and resting tremor (de Lau and Breteler, 2006). Prodromal Parkinson's disease is a stage of PD wherein neurodegeneration has started but the full motor signs (bradykinesia, rigidity, and resting tremor) are not fully established yet and hence, PD has not

been clinically diagnosed (Postuma et al., 2012). Drugs that aim to slow disease progression should be started as soon as neurodegeneration begins, thus the need to identify prodromal PD for future clinical trials.

Currently, prodromal PD is very difficult to diagnose in the general population (Postuma et al., 2016), as there is no 100% reliable, ready and available test to identify this condition (Berg et al., 2014) as no biological definition of PD has been accepted yet. A proposal put forward by the International Parkinson and Movement Disorders Society task force suggested that diagnostic criteria for prodromal PD should be probabilistic and it should include clinical motor and non-motor markers, and non-clinical biomarkers (Berg et al., 2014). A Bayesian method to predict the probability of diagnosis was explored by sequentially adding diagnostic information. The method starts with an initial prior probability of diagnosis, using an age-adjusted prevalence of prodromal PD and this probability is updated using likelihood ratios based on the strength of the diagnostic test (Berg et al., 2015). This method is however difficult to use in clinical practice or in screening of the general population.

In the last ten years, there has been a notable increase in the research into prodromal PD and into the potential markers which could be used in a biological diagnosis of PD (Postuma and Berg, 2019). Several predictive models for PD have been suggested in the last decade, ten of which were critically appraised in a systematic review by Chen et al. (2023). Three models: Mahlknecht et al. (2016), Faust et al. (2020), and Karabayir et al. (2022) were recommended by Chen et al. (2023), which consisted of 12, 17, and 541 predictors, respectively, including age and smoking status. The following non-motor symptoms: daytime sleepiness and cognitive impairment were included in Karabayir et al. (2022), urinary dysfunction, constipation and depression were included in Mahlknecht et al. (2016) and Faust et al. (2020) included 536 diagnosis or procedure codes. However, there is still much to learn and uncover on this journey towards a specific diagnostic test for PD. Ultimately, the goal is to develop a highly specific, sensitive, and feasible PD screening biomarker battery. While alpha-synuclein seed amplification assay has shown high sensitivity/specificity in the spinal fluid, the matrix for analysis (CSF) and cost preclude scaling for general population screening. As such clinical screening remains of paramount significance.

Here, we aimed to investigate whether any of the ready clinical markers of PD, such as motor and non-motor symptoms measured with the Movement Disorder Society Unified Parkinson's Disease Rating Scale (MDS-UPDRS), might be highly specific of PD (common in PD but rare in an age-matched healthy population). This is key as many of the currently used clinical markers of prodromal PD are also common in comparably aged healthy individuals (Pfeiffer, 2016), including depression, sleep problems and hyposmia (Pellicano et al., 2007). Clinical markers specific to prodromal PD (i.e., common in prodromal PD and PD but rare in the comparably aged healthy population) could be used to identify people at high risk of developing PD in the screening of general populations.

We used the Parkinson's Progression Markers Initiative (PPMI) to investigate and compare the prevalence of clinical markers of PD in participants with prodromal PD, with PD in comparison to healthy controls. Symptoms at high specificity were defined based on a high odds ratio.

2. Methods

2.1. Study design

The PPMI is an observational, international multi-center study designed to improve the understanding of PD and enhance the success of new experimental treatments (Marek et al., 2011). One commitment of PPMI is to allow the research community to access publicly available PD study data. The participants in this dataset are followed over the course of 5 years. This PPMI dataset was obtained from the LONI Image data archive.[1] Demographic information, clinical characteristics and results of clinical tests were downloaded from the PPMI database in January, 2021.

The MDS-UPDRS is a clinical rating scale for Parkinson's disease (Goetz et al., 2008). It is split into four parts:

- Part I, non-motor experiences of daily living,
- Part II, motor experiences of daily living,
- Part III, motor examination,
- Part IV, motor complications.

Potential clinical markers of PD were defined from both motor and non-motor experiences of daily living by measuring each of the individual items from the MDS-UPDRS Part I questionnaire, in addition to the first three items from the MDS-UPDRS Part II questionnaire, speech difficulties, excessive drooling and swallowing difficulties. We chose these items because they describe patient reported symptoms rather than the functional impact of motor symptoms on the activity of daily living (e.g., dressing, hygiene etc.). Item 1.1 focuses on the patient's cognitive impairment, 1.2 hallucinations and psychosis, 1.3 depressed mood, 1.4 anxious mood, 1.5 apathy, 1.7 sleep problems (insomnia), 1.8 daytime sleepiness, 1.9 pain and other sensations, 1.10 urinary problems, 1.11 constipation, 1.12 lightheadedness on standing, 1.13 fatigue, 2.1 speech difficulties, 2.2 excessive saliva and drooling, and 2.3 chewing and swallowing difficulties.

To investigate the prevalence of each marker we used baseline data from the PPMI database. In our analysis, we included all the participants from the PPMI database who were labeled as healthy controls, participants with prodromal PD or individuals with PD, who had an enrollment date and who had data available for all 15 markers. The inclusion criteria for each cohort within the PPMI database has been described elsewhere (Marek et al., 2011; Mollenhauer et al., 2019; PPMI, 2023a). Briefly, healthy controls were at least 30 years old, had no current or active clinically significant neurological disorder at baseline, and no first-degree relatives diagnosed with PD. The PD cohort consists of participants aged 30 years or older, with a recent clinical diagnosis of PD who are drug naive at baseline and who had a positive dopamine transporter (DAT) single-photon emission computed tomography. The prodromal PD cohort included volunteers aged 60 years or older, with rapid eye movement (REM) sleep behavior disorder (RBD) confirmed by polysomnography, clinically diagnosed by the site investigator, or with hyposmia based on the University of

1 https://ida.loni.usc.edu/login.jsp

Pennsylvania Smell Identification Test, with DAT deficit. All inclusion and exclusion criteria are noted in the study protocol (PPMI, 2023b).

In order to calculate the prevalence of each marker, the MDS-UPDRS scale was categorized into two groups: symptom present or not: a score of "1–4" implied the presence of the symptom, whereas a score of '0' indicated that the symptom was not present.

2.2. Statistical methods

The standardized mean difference (SMD) in baseline and demographic characteristics was used to assess differences between baseline data for the prodromal and healthy controls, PD and healthy controls, and for the prodromal PD and PD participant groups. The SMD was calculated as the absolute value in the difference in means of a covariate across the population groups, divided by the pooled standard deviation (SD). SMDs larger than 0.25 indicate that the populations were different from one another in that variable (Stuart et al., 2013; Pagano et al., 2021). Differences in symptom prevalence could be caused by an imbalance of baseline characteristics across the populations. If that is the case, such baseline characteristics should be accounted for in the model.

To account for the imbalance in baseline characteristics between the three cohorts, we used logistic regression to calculate adjusted odds ratios for each symptom (Sperandei, 2014). The dependent binary variable was the population cohort (HC, Prodromal or PD) and the independent covariates were the symptom, age and gender. A separate model was calculated for each symptom and for each cohort comparison (prodromal versus healthy controls and PD versus healthy controls). The adjusted odds ratio between two cohorts was obtained by exponentiating the coefficient of the specific symptom. All adjusted odds ratios are reported together with a 95% confidence interval. Specificity of a symptom to each population was determined in terms of the adjusted odds ratio. A symptom was categorized as having "high" specificity if the adjusted odds ratio ≥ 6, "moderate" if the adjusted odds ratio ≥ 3 but < 6, or "low" specificity, if the adjusted odds ratio < 3. The prevalence of each symptom was calculated by adding up all the cases when the symptom was present (score 1–4) and dividing it by the total number of subjects in each population (healthy controls, prodromal PD, PD).

3. Results

3.1. Patient characteristics

A total of 195 healthy controls, 64 prodromal PD and 422 PD individuals were included in the analysis from the PPMI database. The baseline characteristics of the PPMI groups are displayed in Table 1.

3.1.1. Prodromal vs. healthy controls

Prodromal participants were on average older than the healthy controls [Mean (SD)] [68.9 (5.8) years vs. 60.8 (11.2) years respectively; SMD: 0.8]. The proportion of Caucasians was higher in the healthy control group (92.3%) than in the prodromal group (60.9%). However more Hispanics/Latinos were observed in the prodromal group than in the healthy controls (31.25% vs. 1.54% respectively). The prodromal group had higher progression of disease at baseline with mean (SD) MDS-UPDRS Part I 6.36 (3.92), MDS-UPDRS Part II 2.14 (2.54), MDS-UPDRS Part III 3.84 (3.81), and MDS-UPDRS Total (Sum Part I + II + III) 12.34 (7.76) (Supplementary Figure S1).

3.1.2. PD vs. healthy controls

The majority of the healthy controls were on Hoehn and Yahr Stage 0 (98.9%), whereas the PD participants were distributed among Hoehn and Yahr Stages 1 and 2 (45.8% and 55.6% respectively). The PD group had higher progression of disease at baseline with mean (SD) MDS-UPDRS Part I 5.57 (4.07), MDS-UPDRS Part II 5.90 (4.19), MDS-UPDRS Part III 20.88 (8.86), and MDS-UPDRS Total 32.35 (13.14). All other baseline characteristics were balanced between PD and healthy control groups (Supplementary Figure S2).

3.1.3. Prodromal vs. PD

Prodromal participants were on average older than the PD participants [68.9 (5.8) years vs. 61.6 (9.6) years respectively; SMD: −0.79]. Almost all the participants in the prodromal group were in Hoehn and Yahr Stage 0 (95.3%). MDS-UPDRS Part I was balanced among the two groups (SMD: −0.20). However the PD group presented higher mean values of MDS-UPDRS Part II (SMD: 0.94), MDS-UPDRS Part III (SMD: 2.03), and MDS-UPDRS Total (SMD: 1.59) (Supplementary Figure S3).

3.2. Specificity of clinical markers of PD

To determine which symptoms were more specific to each of the groups under investigation (prodromal PD and PD); we ordered the odds ratios and plotted them in a forest plot (Figure 1). The symptoms classified as highly specific for prodromal PD were visual hallucinations (odds ratio, 8.64 [95% CI: 0.83–90.45]) and constipation (odds ratio, 6.14 [95% CI: 2.94–12.80]). For PD individuals, speech difficulties (odds ratio, 19.61 [95% CI: 7.88–48.81]), excessive drooling (odds ratio, 12.81 [95% CI: 6.04–24.59]), swallowing difficulties (odds ratios, 9.51 [95% CI: 2.94–30.82]) and visual hallucinations (odds ratio, 6.19 [95% CI: 0.81–47.62]) were highly specific. However, the prevalence of visual hallucinations is very small for all three populations, particularly the healthy controls (see Table 2). This is why their adjusted odds ratios are so large, they have very large confidence intervals and they do not have a significant p-value for either comparison. Due to these small prevalence, we must be careful when drawing conclusions.

3.3. Prevalence of clinical markers of PD

We further investigated the prevalence of each symptom in individuals with prodromal PD and PD (Table 2). Prevalence was plotted against the odds ratio of each symptom in Figure 2. The three symptoms with the largest prevalence in prodromal PD individuals were excessive daytime sleepiness (65.63%), insomnia (60.94%) and urinary problems (53.13%). For individuals with PD, the most prevalent symptoms were insomnia (53.08%), pain (52.37%), and

10.3389/fnagi.2023.1232387

TABLE 1 Demographics and baseline characteristics of PPMI participants.

Baseline characteristic	HCs (*n* = 195)	Prodromal (*n* = 64)	PD (*n* = 422)	SMD (95% C.I.) Prodromal vs HC	SMD (95% C.I.) PD vs HC	SMD (95% C.I.) Prodromal vs PD
Mean age (SD)	60.84 (11.26)	68.97 (5.80)	61.65 (9.68)	0.80 (0.51–1.09)	0.08* (−0.09–0.25)	−0.79 (−1.06 to −0.52)
Gender: men (%)	125 (64.1)	50 (78.12)	277 (65.64)	0.14* (0.02–0.26)	0.02* (−0.07–0.10)	−0.12* (−0.24 to −0.01)
Race: white (%)	180 (92.31)	39 (60.94)	388 (91.94)	−0.30 (−0.4 to −0.2)	0.00* (−0.04–0.04)	0.30 (0.18–0.42)
Hispanic/latino	3 (1.54)	20 (31.25)	9 (2.13)	0.31 (0.19–0.42)	0.01* (−0.02–0.03)	−0.30 (−0.42 to −0.19)
American Indian/Alaska native	0 (0)	1 (1.56)	4 (0.95)	0.02* (−0.01–0.05)	0.01* (0.00–0.02)	−0.01* (−0.04–0.03)
Black/African American	10 (5.13)	2 (3.12)	7 (1.66)	−0.02* (−0.07–0.03)	−0.03* (−0.07–0.00)	−0.02* (−0.06–0.03)
Asian	1 (0.51)	0 (0)	10 (2.37)	−0.01* (−0.02–0.00)	0.02* (0.00–0.04)	0.02* (0.01–0.04)
Not Specified	1 (0.51)	2 (3.12)	4 (0.95)	NA	NA	NA
Mean time since diagnosis in months (SD)	NA	NA	6.53 (6.46)	NA	NA	NA
Hoehn and Yahr stage: 0 (%)	193 (98.97)	61 (95.31)	0 (0)	−0.04* (−0.09–0.02)	−0.99 (−1.00 to −0.98)	−0.95 (−1.00 to −0.90)
1	2 (1.03)	2 (3.12)	185 (43.84)	0.02* (−0.02–0.07)	0.43 (0.38–0.48)	0.41 (0.34–0.47)
2	0 (0)	1 (1.56)	235 (55.69)	0.02* (−0.01–0.05)	0.56 (0.51–0.60)	0.54 (0.48–0.60)
3	0 (0)	0 (0)	2 (0.47)	NA	0.00* (0.00–0.01)	0.00* (0.00–0.01)
Mean MDS-UPDRS part I (SD)	2.95 (2.96)	6.36 (3.92)	5.57 (4.07)	1.06 (0.76–1.35)	0.70 (0.52–0.87)	−0.20* (−0.46–0.07)
Mean MDS-UPDRS part II (SD)	0.46 (1.02)	2.14 (2.54)	5.90 (4.19)	1.09 (0.79–1.39)	1.55 (1.36–1.74)	0.94 (0.67–1.21)
Mean MDS-UPDRS part III (SD)	1.21 (2.19)	3.84 (3.81)	20.88 (8.86)	0.98 (0.69–1.28)	2.64 (2.42–2.87)	2.03 (1.74–2.33)
Mean Total MDS-UPDRS (SD)	4.56 (4.4)	12.34 (7.76)	32.35 (13.14)	1.43 (1.13–1.74)	2.49 (2.27–2.71)	1.59 (1.31–1.87)

PD, Parkinson's disease; HC, healthy controls; SD, standard deviation; SMD, standardized mean difference; C.I., confidence intervals; MDS-UPDRS, movement disorder society-unified Parkinson's disease rating scale. *SMD within the range of (−0.25, 0.25).

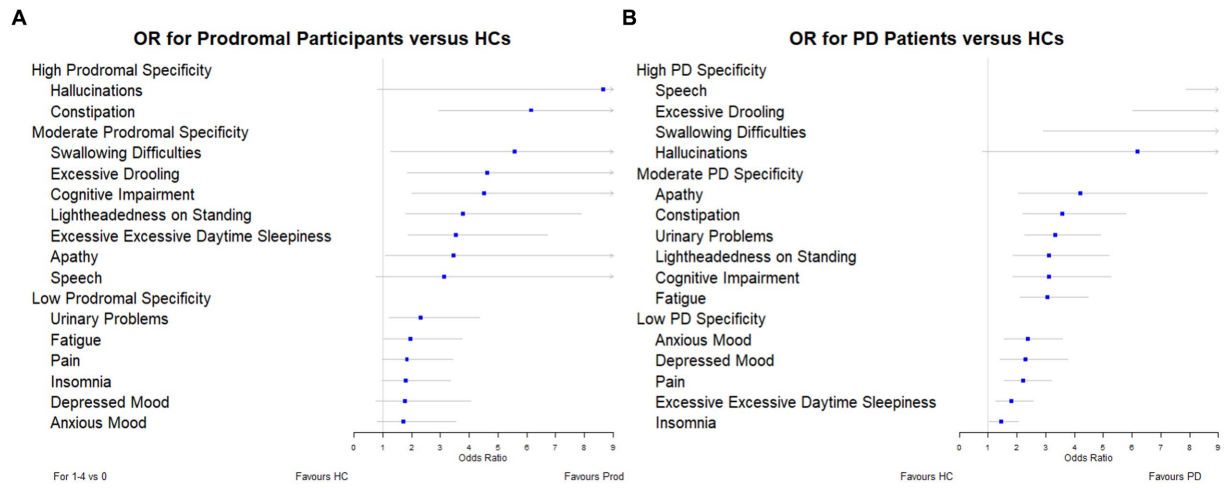

FIGURE 1
Forest plots showing the adjusted odds ratios for each symptom: **(A)** prodromal participants versus healthy controls, and **(B)** PD individuals versus healthy controls.

TABLE 2 Adjusted odds ratios and prevalence of each symptom.

Symptom	OR: prodromal PD vs HC (95% C.I.)	*p*-value of symptom in LR	OR: PD vs HC (95% C.I.)	*p*-value of symptom in LR	Prev in HCs	Prev in prodromal PD	Prev in PD
Hallucinations	8.64 (0.83–90.45)	0.07	6.19 (0.81–47.62)	0.08	0.51% (1/195)	4.69% (3/64)	3.08% (13/422)
Constipation	6.14 (2.94–12.80)	<0.01	3.58 (2.22–5.78)	<0.01	12.31% (24/195)	43.75% (28/64)	33.18% (140/422)
Swallowing difficulties	5.57 (1.28–24.12)	0.02	9.51 (2.94–30.82)	<0.01	1.54% (3/195)	9.38% (6/64)	13.03% (55/422)
Excessive drooling	4.62 (1.86–11.45)	<0.01	12.81 (6.04–24.59)	<0.01	4.62% (9/195)	26.56% (17/64)	36.49% (154/422)
Cognitive impairment	4.51 (2.02–10.08)	<0.01	3.12 (1.85–5.26)	<0.01	9.74% (19/195)	29.69% (19/64)	25.36% (107/422)
Lightheaded-ness on standing	3.77 (1.80–7.90)	<0.01	3.12 (1.87–5.20)	<0.01	10.26% (20/195)	35.94% (23/64)	26.3% (111/422)
Excessive daytime sleepiness	3.55 (1.88–6.71)	<0.01	1.82 (1.28–2.58)	<0.01	34.87% (68/195)	65.63% (42/64)	49.53% (209/422)
Apathy	3.45 (1.10–10.83)	0.03	4.20 (2.05–8.60)	<0.01	4.62% (9/195)	10.94% (7/64)	16.82% (71/422)
Speech difficulties	3.12 (0.76–12.73)	0.11	19.61 (7.88–48.81)	<0.01	2.56% (5/195)	7.81% (5/64)	33.89% (143/422)
Urinary problems	2.30 (1.22–4.35)	0.01	3.34 (2.26–4.92)	<0.01	24.10% (47/195)	53.13% (34/64)	50.95% (215/422)
Fatigue	1.96 (1.03–3.75)	0.04	3.06 (2.10–4.47)	<0.01	25.13% (49/195)	42.19% (27/64)	50.24% (212/422)
Pain	1.83 (0.98–3.42)	0.06	2.23 (1.56–3.18)	<0.01	33.85% (66/195)	48.44% (31/64)	52.37% (221/422)
Insomnia	1.80 (0.97–3.34)	0.06	1.46 (1.03–2.05)	0.03	43.59% (85/195)	60.94% (39/64)	53.08% (224/422)
Depressed mood	1.77 (0.77–4.06)	0.18	2.31 (1.42–3.77)	<0.01	12.31% (24/195)	18.75% (12/64)	23.70% (100/422)
Anxious mood	1.70 (0.82–3.54)	0.16	2.38 (1.58–3.59)	<0.01	19.49% (38/195)	26.56% (17/64)	35.78% (151/422)

OR, odds ratio; PD, Parkinson's disease; HC, healthy controls; C.I., confidence intervals; LR, logistic regression; Prev, prevalence.

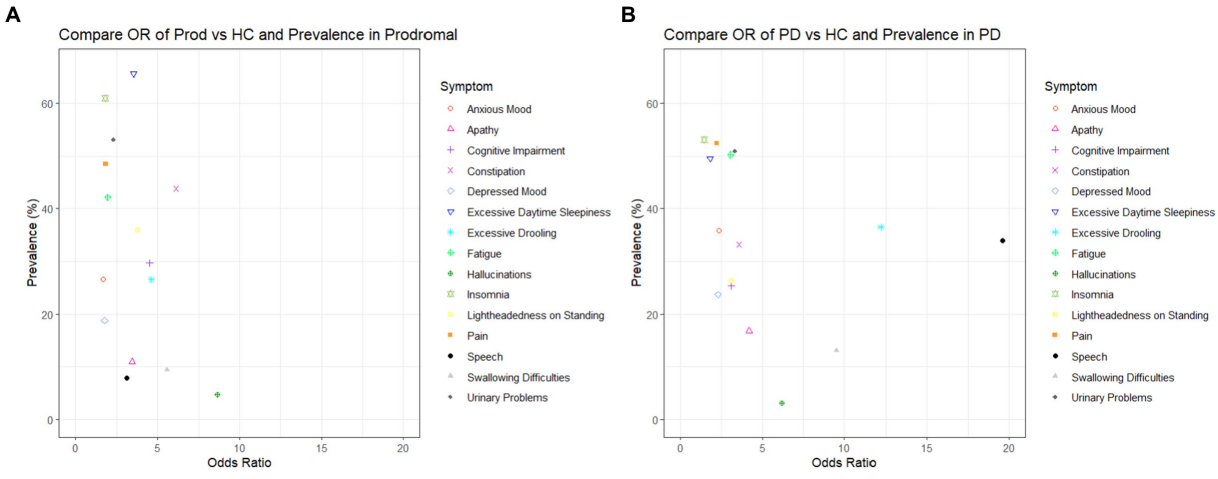

FIGURE 2
Plots to show the adjusted odds ratio and the prevalence of each symptom when: **(A)** healthy controls are compared to prodromal participants and **(B)** healthy controls are compared to PD patients.

urinary problems (50.95%). These symptoms were among the five most common in healthy controls, with insomnia having a prevalence of 43.59%, excessive daytime sleepiness, 34.87%, pain, 33.85%, and urinary problems, 24.10%. Therefore, these symptoms did not have large adjusted odds ratios for either comparison, as they were also common in healthy controls.

4. Discussion

In this study, we investigated the prevalence of symptoms in the prodromal PD population, PD population and in healthy controls. Furthermore, we assessed how specific these symptoms were to individuals with prodromal PD and PD compared to healthy controls, by classifying them as having either: low (adjusted odds ratio < 3), moderate (3 ≤ adjusted odds ratio < 6) or high (6 ≤ adjusted odds ratio) specificity. We observed that visual hallucinations and constipation were the symptoms which were highly specific to prodromal PD. However, of these symptoms, only constipation was prevalent in participants with prodromal PD. Additionally, the symptoms that were highly specific to PD were speech difficulties, excessive drooling, swallowing difficulties and visual hallucinations. Speech difficulties and excessive drooling were prevalent in individuals with PD, whereas swallowing difficulties and visual hallucinations were not.

Of the four most specific symptoms to prodromal PD (those symptoms with the largest odds ratios: visual hallucinations, 8.64, constipation, 6.14, swallowing difficulties, 5.57, excessive drooling 4.62), only constipation and excessive drooling were moderately prevalent in the prodromal PD population, 43.75% and 26.56%. Visual hallucinations and swallowing difficulties were among the least common in the prodromal PD population. Of the four most specific symptoms to PD (those symptoms with the largest odds ratios: speech difficulties, 19.61, excessive drooling, 12.18, swallowing difficulties, 9.51, visual hallucinations, 6.19), only excessive drooling and speech difficulties were moderately prevalent in the PD population, 36.49% and 33.89%. Visual hallucinations and swallowing difficulties were among the least common in the PD population. This indicates that the symptoms that are most specific to the disease (prodromal PD or PD), are not necessarily the symptoms which are most prevalent in each disease population, and vice versa (see Figure 2).

We further found that the clinical markers in prodromal PD and PD were different. This supports the hypothesis that symptoms may develop at different times over the course of the disease. The adjusted odds ratio for speech difficulties gave the largest increase from participants living with prodromal PD to PD, this could indicate that this clinical marker becomes more common as patients progress. Varanese et al. (2010), supports this idea. In contrast, the adjusted odds ratio for visual hallucinations decreased by the largest amount from prodromal PD to PD participants. One reason behind this decrease could be that this symptom becomes less common as patients progress. However, Varanese et al. (2010) suggests the opposite. They suggest that visual hallucinations become more common over the course of the disease. Therefore, an alternative reason may be behind this decrease in adjusted odds ratio. Prodromal PD is also prodromal of dementia with Lewy bodies. Therefore, individuals labeled as prodromal PD within PPMI might not actually develop PD in the future; they may develop dementia with Lewy bodies instead. As these prodromal individuals have a higher risk of developing dementia than the PD cohort, they might also have a larger adjusted odds ratio to suffer from visual hallucinations, which is a key cardinal symptom of dementia with Lewy bodies.

It is generally thought that visual hallucinations, constipation, swallowing difficulties and excessive drooling are symptoms which dominate late stages of PD (Rukavina et al., 2021). This is not in complete contrast to our findings, as we observed a low prevalence of visual hallucinations and swallowing difficulties in prodromal PD participants. However, whereas many previous studies and articles explore the prevalence of symptoms in the prodromal PD and PD population, they do not often compare the prevalence of these symptoms to the age-matched healthy controls. Even though visual hallucinations and swallowing difficulties are not common in participants living with prodromal PD, they may still be specific symptoms of prodromal PD as their prevalence was much higher in prodromal PD compared to the healthy control population.

In order for a symptom to aid in the early diagnosis of prodromal PD, it should be both highly specific and sufficiently prevalent in the prodromal PD population to detect enough participants. However, we have shown above that the symptoms that are most specific to the disease (prodromal PD or PD), are not necessarily the symptoms which are most prevalent in these disease populations, and vice versa. Unfortunately, there are not many symptoms which are both, so one must compromise to select symptoms which are either moderately specific and highly prevalent or highly specific and only moderately prevalent. Therefore, we suggest it is the symptoms, such as constipation and excessive drooling, which had large and moderate adjusted odds ratios (6.14 and 4.62), moderately high prevalence in prodromal participants (43.75% and 26.56%) and fairly low prevalence in healthy controls (12.31% and 4.62%), which would make robust predictors of prodromal PD. In addition, symptoms such as excessive drooling and speech difficulties, which had large adjusted odds ratios (12.81 and 19.61), moderately high prevalence in PD patients (36.49 and 33.89%) and low prevalence in healthy controls (4.62% and 2.56%), which would make robust predictors of PD (see Table 2).

The main strength of this study is the comparison of all three cohorts: healthy controls, prodromal PD participants, as well as individuals with PD. Today, prodromal PD is particularly difficult to detect (Berg et al., 2014). Therefore, these individuals are not included in many studies or even if they are, they are not deeply characterized with information with every item of the MDS-UPDRS. Due to the lack of treatment to delay PD progression, it is particularly important to try to diagnose PD earlier in patients and recruit these early PD patients into clinical trials of drugs designed to slow the progression of the disease. The comparison of healthy controls and prodromal PD participants in this work, allows us to detect which symptoms could be used in future to enable this earlier PD diagnosis. Furthermore, many studies look at the prevalence of symptoms in PD patients only and do not include a healthy control comparison. This comparison is particularly useful, as many symptoms, which are most common in PD

patients (such as insomnia, pain, and urinary problems) are also common in age-matched healthy controls. With these two comparisons, we can see which symptoms are most common in people suffering from prodromal PD compared to healthy controls and see how their prevalence develops as prodromal PD participants progress and develop clinical PD. Prior studies have demonstrated the high risk of PD onset in the prodromal PD population with hyposmia or RBD (Iranzo et al., 2017; Jennings et al., 2017). Pilot prodromal data from PPMI indicate that 35% of the prodromal PD participants with hyposmia or RBD with abnormal DAT developed PD within the first four years (PPMI, 2023b). We expect this number to increase as time continues.

There are potential limitations of this study. Firstly, in the PPMI study, the prodromal PD cohort was a pilot effort, as such, the sample size of this population is relatively small compared to the numbers of healthy controls and individuals with PD recruited. This causes some of the confidence intervals, especially for symptoms such as visual hallucinations, excessive drooling, swallowing difficulties and speech difficulties, to be particularly wide. Secondly, the prevalence of these symptoms in the healthy control population may not be generalizable to the healthy control population outside of PPMI (Jackson et al., 2022). Additionally, the prodromal PD and PD cohorts had different eligibility criteria (Mollenhauer et al., 2019). Only participants with isolated RBD or isolated hyposmia were recruited into the prodromal PD cohort investigated here. The PD participants needed to be older than 30, whereas the prodromal PD participants had to be at least 60 years old. In addition, the PD patients were required to have a DaT deficit in the putamen on 123-I Ioflupane DaT imaging, conversely, only 80% of the prodromal PD participants had a similar DaT deficit (Mollenhauer et al., 2019). Furthermore, the majority of the prodromal PD cohort suffered from isolated rapid eye movement sleep behavior disorder and as such, were likely to develop dementia with Lewy bodies with visual hallucinations. Due to the characteristics of the prodromal PD cohort within the PPMI database, the dementia with Lewy bodies phenoconversions are driving some important symptom differences. Therefore, one must be careful when making conclusions about the differences between the prodromal PD and PD populations. In addition, we only looked at the 15 symptoms available in the MDS-UPDRS, there are other tools available which track more symptoms (and in greater detail) in PD participants. These include the non-motor symptom questionnaire (Chaudhuri et al., 2006) and the non-motor symptom scale (Chaudhuri et al., 2007), which evaluate a further 15 symptoms, or the more recent MDS version of the non-motor symptom scale (Martinez-Martin et al., 2019). These scales would have been useful if they had been included in the PPMI database. As this is an exploratory study by nature, we make no corrections for multiplicity.

Further work includes correlating clinical markers with DaT binding and performing subgroup analysis with clustering of prodromal markers (RBD, hyposmia and DaT deficit). Unfortunately, this is not possible yet within PPMI for external investigators (PPMI, 2023c). In addition, these results must be validated in another dataset or multiple datasets, which have a larger and more generalizable prodromal PD and healthy control cohort. Next steps would be performing a meta-analysis of all published studies including motor and non-motor features of PD to confirm our hypothesis in a much larger sample size. In addition, when the most useful symptoms, which could aid in the early diagnosis of prodromal PD have been identified, the next step would be to link these symptoms to biomarkers. If these useful symptoms can be anchored to a certain biomarker (or biomarkers), then these biomarkers could be used to aid in the diagnosis of prodromal PD even earlier.

Data availability statement

Publicly available datasets were analyzed in this study. This data can be found here: https://ida.loni.usc.edu/login.jsp. This PPMI dataset was obtained from the LONI Image data archive in January 2021.

Ethics statement

Ethical review and approval was not required for the study of human participants in accordance with the local legislation and institutional requirements.

Author contributions

GP and JA-C designed the study. HJ and JA-C were involved in data collection and analyzing the data. GP, JA-C, and HJ contributed to data interpretation. All authors contributed to the article and approved the submitted version.

Funding

This study received funding from F. Hoffmann-La Roche Ltd. The funder was not involved in the study design, collection, analysis, interpretation of data, the writing of this article or the decision to submit it for publication. All authors declare no other competing interests.

Acknowledgments

We thank the Michael J. Fox Foundation, their PPMI colleagues, and the individuals who participated in the PPMI study. PPMI, a public-private partnership, was sponsored by the Michael J. Fox Foundation (MJFF) for Parkinson's Research and is co-funded by MJFF, AbbVie, Allergan, Amathus Therapeutics, Avid Radiopharmaceuticals, Bial Biotech, Biogen Idec, BioLegend, Bristol-Myers Squibb, Calico, Celgene, Denali Therapeutics Inc., 4D Pharma Plc, Eli Lilly and Company, F. Hoffmann-La Roche Ltd., GE Healthcare, Genentech Inc., GlaxoSmithKline, Golub Capital BDC, Handl Therapeutics, Insitro, Janssen Neuroscience, Lundbeck, Merck, Meso Scale, Neurocrine Biosciences, Pfizer, Piramal, Prevail Therapeutics, Sanofi Genzyme, Servier, Takeda, Teva Pharmaceutical Industries Ltd., UCB, Verily Life Sciences and Voyager Therapeutics. Industry partners contribute to PPMI through financial and in-kind donations and have a lead role in providing feedback on study parameters through the Partners Scientific Advisory Board (PSAB). Through close interaction with the study, the PSAB is positioned to

inform the selection and review of potential progression markers that could be used in clinical testing.

Conflict of interest

HJ was a paid intern employed through The Roche Internships for Scientific Exchange (RiSE) Programme within F. Hoffmann-La Roche Ltd. JA-C is a full-time employee of Roche Products Ltd and a shareholder of F. Hoffmann-La Roche Ltd. GP is a full-time employee of Roche Pharma Research and Early Development and a shareholder of F. Hoffmann-La Roche Ltd.

The remaining authors declare that the research was conducted in the absence of any commercial or financial relationships that could be construed as a potential conflict of interest.

Publisher's note

Supplementary material

The Supplementary material for this article can be found online at: https://www.frontiersin.org/articles/10.3389/fnagi.2023.1232387/full#supplementary-material

References

Berg, D., Postuma, R. B., Adler, C. H., Bloem, B. R., Chan, P., Dubois, B., et al. (2015). MDS research criteria for prodromal Parkinson's disease. *Mov. Disord.* 30, 1600–1611. doi: 10.1002/mds.26431

Berg, D., Postuma, R. B., Bloem, B., Chan, P., Dubois, B., Gasser, T., et al. (2014). Time to redefine PD? Introductory statement of the MDS task force on the definition of Parkinson's disease. *Mov. Disord.* 29, 454–462. doi: 10.1002/mds.25844

Chaudhuri, K. R., Martinez-Martin, P., Brown, R. G., Sethi, K., Stocchi, F., Odin, P., et al. (2007). The metric properties of a novel non-motor symptoms scale for Parkinson's disease: results from an international pilot study. *Mov. Disord.* 22, 1901–1911. doi: 10.1002/mds.21596

Chaudhuri, K. R., Martinez-Martin, P., Schapira, A. H., Stocchi, F., Sethi, K., Odin, P., et al. (2006). International multicenter pilot study of the first comprehensive self-completed nonmotor symptoms questionnaire for Parkinson's disease: the NMSQuest study. *Mov. Disord.* 21, 916–923. doi: 10.1002/mds.20844

Chen, Y., Gao, Y., Sun, X., Liu, Z., Zhang, Z., Qin, L., et al. (2023). Predictive models for the incidence of Parkinson's disease: systematic review and critical appraisal. *Rev. Neurosci.* 34, 63–74. doi: 10.1515/revneuro-2022-0012

de Lau, L. M., and Breteler, M. M. (2006). Epidemiology of Parkinson's disease. *Lancet Neurol.* 5, 525–535. doi: 10.1016/S1474-4422(06)70471-9

Faust, I. M., Racette, B. A., and Searles Nielsen, S. (2020). Validation of a Parkinson disease predictive model in a population-based study. *Parkinsons Dis.* 2020, 1–7. doi: 10.1155/2020/2857608

Goetz, C. G., Tilley, B. C., Shaftman, S. R., Stebbins, G. T., Fahn, S., Martinez-Martin, P., et al. (2008). Movement Disorder Society-sponsored revision of the unified Parkinson's disease rating scale (MDS-UPDRS): scale presentation and clinimetric testing results. *Mov. Disord.* 23, 2129–2170. doi: 10.1002/mds.22340

Iranzo, A., Santamaría, J., Valldeoriola, F., Serradell, M., Salamero, M., Gaig, C., et al. (2017). Dopamine transporter imaging deficit predicts early transition to synucleinopathy in idiopathic rapid eye movement sleep behavior disorder. *Ann. Neurol.* 82, 419–428. doi: 10.1002/ana.25026

Jackson, H., Anzures Cabrera, J., and Pagano, G. (2022) The 16th international AD/PD 2022: advances in science and therapy conference non-motor symptoms in Parkinson's disease: a systematic review and meta-analysis of prevalence.

Jennings, D., Siderowf, A., Stern, M., Seibyl, J., Eberly, S., Oakes, D., et al. (2017). Conversion to Parkinson disease in the PARS Hyposmic and dopamine transporter-deficit prodromal cohort. *JAMA Neurol.* 74, 933–940. doi: 10.1001/jamaneurol.2017.0985

Karabayir, I., Butler, L., Goldman, S. M., Kamaleswaran, R., Gunturkun, F., Davis, R. L., et al. (2022). Predicting Parkinson's disease and its pathology via simple clinical variables. *J. Parkinsons Dis.* 12, 341–351. doi: 10.3233/JPD-212876

Mahlknecht, P., Gasperi, A., Willeit, P., Kiechl, S., Stockner, H., Willeit, J., et al. (2016). Prodromal Parkinson's disease as defined per MDS research criteria in the general elderly community. *Mov. Disord.* 31, 1405–1408. doi: 10.1002/mds.26674

Marek, K., Jennings, D., Lasch, S., Siderowf, A., Tanner, C., Simuni, T., et al. (2011). The Parkinson progression marker initiative (PPMI). *Prog. Neurobiol.* 95, 629–635. doi: 10.1016/j.pneurobio.2011.09.005

Martinez-Martin, P., Schrag, A., Weintraub, D., Rizos, A., Rodriguez-Blazquez, C., Chaudhuri, K. R., et al. (2019). Pilot study of the International Parkinson and Movement Disorder Society-sponsored non-motor rating scale (MDS-NMS). *Mov. Disord. Clin. Pract.* 6, 227–234. doi: 10.1002/mdc3.12728

Mollenhauer, B., Caspell-Garcia, C. J., Coffey, C. S., Taylor, P., Singleton, A., Shaw, L. M., et al. (2019). Longitudinal analyses of cerebrospinal fluid alpha-Synuclein in prodromal and early Parkinson's disease. *Mov. Disord.* 34, 1354–1364. doi: 10.1002/mds.27806

Pagano, G., Boess, F. G., Taylor, K. I., Ricci, B., Mollenhauer, B., Poewe, W., et al. (2021). A phase II study to evaluate the safety and efficacy of prasinezumab in early Parkinson's disease (PASADENA): rationale, design and baseline data. *Front. Neurol.* 12:705407. doi: 10.3389/fneur.2021.705407

Pellicano, C., Benincasa, D., Pisani, V., Buttarelli, F. R., Giovannelli, M., and Pontieri, F. E. (2007). Prodromal non-motor symptoms of Parkinson's disease. *Neuropsychiatr. Dis. Treat.* 3, 145–151. doi: 10.2147/nedt.2007.3.1.145

Pfeiffer, R. F. (2016). Non-motor symptoms in Parkinson's disease. *Parkinsonism Relat. Disord.* 22, S119–S122. doi: 10.1016/j.parkreldis.2015.09.004

Postuma, R. B., Aarsland, D., Barone, P., Burn, D. J., Hawkes, C. H., Oertel, W., et al. (2012). Identifying prodromal Parkinson's disease: pre-motor disorders in Parkinson's disease. *Mov. Disord.* 27, 617–626. doi: 10.1002/mds.24996

Postuma, R. B., and Berg, D. (2019). Prodromal Parkinson's disease: the decade past, the decade to come. *Mov. Disord.* 34, 665–675. doi: 10.1002/mds.27670

Postuma, R. B., Pelletier, A., Berg, D., Gagnon, J. F., Escudier, F., and Montplaisir, J. (2016). Screening for prodromal Parkinson's disease in the general community: a sleep-based approach. *Sleep Med.* 21, 101–105. doi: 10.1016/j.sleep.2015.12.016

PPMI, (2023a). *Study cohorts*, Available at: https://www.ppmi-info.org/study-design/study-cohorts#pd/, (Accessed 02 May, 2023).

PPMI, (2023b) Research documents and SOPS, Available at: https://www.ppmi-info.org/study-design/research-documents-and-sops, Accessed August 06, 2023.

PPMI, (2023c). Publication policy, Available at: https://www.ppmi-info.org/sites/default/files/docs/ppmi-publication-policy.pdf, (Accessed August 10, 2023).

Rukavina, K., Batzu, L., Boogers, A., Abundes-Corona, A., Bruno, V., and Chaudhuri, K. R. (2021). Non-motor complications in late stage Parkinson's disease: recognition, management and unmet needs. *Expert. Rev. Neurother.* 21, 335–352. doi: 10.1080/14737175.2021.1883428

Sperandei, S. (2014). Understanding logistic regression analysis. *Biochem. Med.* 24, 12–18. doi: 10.11613/BM.2014.003

Stuart, E. A., Lee, B. K., and Leacy, F. P. (2013). Prognostic score-based balance measures can be a useful diagnostic for propensity score methods in comparative effectiveness research. *J. Clin. Epidemiol.* 66, S84–90.e1. doi: 10.1016/j.jclinepi.2013.01.013

Varanese, S., Birnbaum, Z., Rossi, R., and Di Rocco, A. (2010). Treatment of advanced Parkinson's disease. *Parkinsons Dis.* 2010:480260. doi: 10.4061/2010/480260

frontiers | Frontiers in Aging Neuroscience

TYPE Original Research
PUBLISHED 27 November 2023
DOI 10.3389/fnagi.2023.1287917

OPEN ACCESS

EDITED BY
Robert Petersen,
Central Michigan University, United States

REVIEWED BY
Wooyoung Jang,
Gangneung Asan Hospital, Republic of Korea
Yutaka Oji,
Juntendo University, Japan

*CORRESPONDENCE
Ling Ling Chan
✉ ling2chanSGH@gmail.com

RECEIVED 03 September 2023
ACCEPTED 26 October 2023
PUBLISHED 27 November 2023

CITATION
Hartono S, Chen RC, Welton T, Tan AS, Lee W, Teh PY, Chen C, Hou W, Tham WP, Lim EW, Prakash KM, Shih Y-C, Lee KJ, Tan LCS, Tan EK and Chan LL (2023) Quantitative iron–neuromelanin MRI associates with motor severity in Parkinson's disease and matches radiological disease classification. *Front. Aging Neurosci.* 15:1287917. doi: 10.3389/fnagi.2023.1287917

Quantitative iron–neuromelanin MRI associates with motor severity in Parkinson's disease and matches radiological disease classification

Septian Hartono[1,2], Robert Chun Chen[2,3], Thomas Welton[1,2], An Sen Tan[3], Weiling Lee[3], Peik Yen Teh[3], Celeste Chen[1], Wenlu Hou[3], Wei Ping Tham[3], Ee Wei Lim[1], Kumar M. Prakash[1], Yao-Chia Shih[3,4], Kuan Jin Lee[5], Louis C. S. Tan[1,2], Eng King Tan[1,2] and Ling Ling Chan[2,3]*

[1]Department of Neurology, National Neuroscience Institute, Singapore, Singapore, [2]Duke-NUS Graduate Medical School, Singapore, Singapore, [3]Department of Diagnostic Radiology, Singapore General Hospital, Singapore, Singapore, [4]Yuan Ze University, Taoyuan, Taiwan, [5]Singapore BioImaging Consortium (SBIC), Agency for Science, Technology and Research (A*STAR), Singapore, Singapore

Background: Neuromelanin- and iron-sensitive MRI studies in Parkinson's disease (PD) are limited by small sample sizes and lack detailed clinical correlation. In a large case–control PD cohort, we evaluated the diagnostic accuracy of quantitative iron–neuromelanin MRI parameters from the substantia nigra (SN), their radiological utility, and clinical association.

Methods: PD patients and age-matched controls were prospectively recruited for motor assessment and midbrain neuromelanin- and iron-sensitive [quantitative susceptibility mapping (QSM) and susceptibility map-weighted imaging (SMWI)] MRI. Quantitative neuromelanin–iron parameters from the SN were assessed for their discriminatory performance in PD classification using ROC analysis compared to those of qualitative visual classification by radiological readers of differential experience and used to predict motor severity.

Results: In total, 191 subjects (80 PD, mean age 65.0 years; 111 controls, 65.6) were included. SN masks showed (a) higher mean susceptibility ($p < 0.0001$) and smaller sizes after thresholding for low susceptibility ($p < 0.0001$) on QSM and (b) lower contrast range ($p < 0.0001$) and smaller sizes after thresholding for high-signal voxels ($p < 0.0001$) on neuromelanin-sensitive MRI in patients than in controls. Quantitative iron and neuromelanin parameters showed a moderate correlation with motor dysfunction (87.5%: $0.4 < |r| < 0.6$, $p < 0.0001$), respectively. A composite quantitative neuromelanin–iron marker differentiated the groups with excellent performance (AUC 0.94), matching the diagnostic accuracy of the best-performing reader (accuracy 97%) using SMWI.

Conclusion: Quantitative neuromelanin–iron MRI is associated with PD motor severity and matched best-performing radiological PD classification using SMWI, with the potential to improve diagnostic confidence in the clinics and track disease progression and response to neuroprotective therapies.

KEYWORDS

Parkinson's disease, MRI, substantia nigra, classification, comparative study, correlation analysis, iron, neuromelanin

Introduction

Parkinson's disease (PD) is a common neurodegenerative disease characterized clinically by rest tremor, bradykinesia, rigidity, and postural instability. Clinical features are only apparent after a significant (50–70%) loss of dopaminergic neurons in the substantia nigra (SN) (Sulzer et al., 2018). The clinical diagnosis of PD may be difficult (Rizzo et al., 2016; Beach and Adler, 2018), and a recent poll of PD patients reported misdiagnosis in 26%, and a further 21% saw a general practitioner three times before a specialist referral was made (Parkinson's UK, 2020). Non-invasive neuroimaging holds promise in improving confidence in the clinical diagnosis and management of PD. High-resolution neuromelanin- and iron-sensitive MRI of the midbrain are useful sequences in delineating radiological biomarkers in the SN in PD patients (Pavese and Tai, 2018; Pyatigorskaya et al., 2020; Cho et al., 2021a,b). However, the value of their quantitative markers is moot.

Human cadaveric studies have shown that neurons rich in the dark-brown cytoplasmic neuromelanin pigment in the midbrain are susceptible to degeneration in PD (Sasaki et al., 2006; Sulzer and Surmeier, 2013). The loss of dopaminergic neurons in these vulnerable neuromelanin-rich brain regions in the SN underlies the characteristic motor symptoms of the disease (Sasaki et al., 2006; Sulzer et al., 2018). *In vivo* neuromelanin-sensitive MRI reliably quantified nigral damage and distinguished PD from healthy subjects (Wang et al., 2019). Iron also plays an important role in the neurodegenerative process in PD; free iron promotes the production of toxic-free radicals leading to dopaminergic cell death (Dexter et al., 1989). Iron-sensitive MRI such as quantitative susceptibility mapping (QSM) has consistently found increased susceptibility in the SN of PD patients (Pyatigorskaya et al., 2020; Tan et al., 2021). Pathological correlates on ultrahigh field MRI support preferential dopaminergic cell loss in nigrosome-1, a main sub-component of the SN, as an accurate MRI biomarker in PD (Blazejewska et al., 2013; Sung et al., 2018; Bae et al., 2021a).

Although the literature suggests good results for differentiating PD patients from healthy controls using neuromelanin- and iron-sensitive MRI techniques, these studies are limited by small sample sizes, non-comparative single modal evaluations, inadequate discriminant reliability for clinical adoption, or lack of evaluation by readers of differential training and systematic or detailed clinical characteristics for robust correlation with imaging markers. To address these gaps, we conducted a large prospective case–control study to evaluate the diagnostic accuracy and clinical association of quantitative iron–neuromelanin parameters and compared these against a qualitative visual evaluation of nigrosome-1 and neuromelanin hyperintensity as proxies of nigral dopaminergic neurodegeneration across radiological readers of differential training. We hypothesized that quantitative iron–neuromelanin parameters can add value to the radiological workflow in the clinical evaluation and management of Parkinsonism, beyond a role in research settings.

Materials and methods

Subjects

This study was approved by the local ethics board, and informed consent was obtained from all participants. Patients were clinically diagnosed with PD by four movement disorders neurologists (two with 24, one with 15, and the last with

TABLE 1 Subject clinical demographics.

	Healthy controls	PD patients	*p*-value
Number	111	80	
Age	65.6 ± 6.5	65.0 ± 9.3	0.66
Sex (M/F)	52/59	55/25	**0.003**
Motor			
Disease duration (years)	N.A.	6. 7 ± 5.5	N.A.
Age of onset	N.A.	58.1 ± 11.4	N.A.
PD subtype	N.A.	44 Tremor 14 Bradykinesia 12 Rigidity 10 Mixed	N.A.
UPDRS-II	0.5 ± 1.7	7.8 ± 6.2	**<0.0001**
UPDRS-III	3.4 ± 4.4	29.4 ± 13.3	**<0.0001**
H&Y	0	2.0 ± 0.5	**<0.0001**
LEDD	N.A.	452.9 ± 280.5	N.A.
Non-motor			
UPDRS-I	1.6 ± 2.9	5.6 ± 5.8	**<0.0001**
MMSE	27.3 ± 2.1	25.9 ± 3.0	**0.0002**

Statistical significance is defined at $p < 0.05$ (bold). F, Female; H&Y, Hoehn and Yahr staging; LEDD, Levodopa equivalent daily dose; M, Male; MMSE, Mini-Mental State Examination; N.A., Not applicable; PD, Parkinson's Disease; UPDRS, Unified Parkinson's Disease Rating Scale.

8 years of experience) using the Movement Disorder Society Clinical Diagnostic Criteria for Parkinson's disease (Postuma et al., 2015), and prospectively recruited from the clinics at our tertiary referral center. Only patients with clinically established PD were recruited. Age-matched healthy controls without neurological conditions were recruited from the community, health screening clinics and among the spouses of patients in the hospital clinics. Subjects with MRI contraindications, claustrophobia, known neurological/psychiatric diagnosis other than PD, chronic debilitating medical conditions, or poor cognitive function that would hinder patients' understanding of the study were excluded. All participants underwent clinical motor and non-motor assessments, including the Unified Parkinson's Disease Rating Scale motor sub-score (UPDRS-III), motor (UPDRS-II), and non-motor (UPDRS-I) aspects of experiences of daily living, and the Mini-Mental State Examination (MMSE). Demographic and clinical information were recorded in Table 1.

Image acquisition and processing

All subjects underwent brain MRI on a 3T scanner (Siemens Skyra, Erlangen, Germany). High-resolution midbrain sequences used the following MRI parameters: (1) 3D T2* susceptibility weighted imaging (SWI) multi-echo gradient echo sequence (TR 48 ms, TE 13.77/26.39/39 ms, FA 20°, voxel size 0.5 × 0.5 × 1 mm^3, slices 32, duration 4.15 min); (2) neuromelanin-sensitive T1 TSE sequence (TR/TE 938/15 ms, voxel size 0.5 × 0.5 × 3 mm^3, slices 13, duration 10.42 min). The details of the standardized MRI scan planning protocol are found in Supplementary material and shown in Supplementary Figure S1. QSM and susceptibility map-weighted imaging (SMWI) images were reconstructed from the multi-echo GRE images using proprietary SMWI software (Seoul National University, Seoul, South Korea) (Nam et al., 2017). Quantitative susceptibility in parts per billion (ppb) was computed from QSM based on the STI Suite embedded in SMWI software (Li et al., 2014). Representative QSM, SMWI, and neuromelanin-sensitive MRI images in control and PD subjects illustrating the presence and absence of nigrosome-1 and substantia nigra hyperintensity, respectively, are shown in Supplementary Figure S1.

Qualitative visual evaluation

SMWI and neuromelanin-sensitive anonymized MRI images of the first 80 study participants (47 PD patients and 33 healthy controls) were separately and independently reviewed by four radiologist readers of different training and experience (Table 2) using syngo.via (Siemens, Germany) on a clinical reporting workstation, blinded to the subject status. Readers 1, 2, and 3 had more than 2 decades, 1 decade, and only a year of neuroradiology practice, respectively, and Reader 4 had 6 years of non-neuroradiology practice. Reader 1 also completed a visual evaluation for the full cohort. Standardized slice selection (Figure 1) and the rating protocol were employed for PD classification, based on the

TABLE 2 Classification performance of qualitative visual nigral evaluation by four radiologists using neuromelanin- and iron-sensitive (SMWI) MRI.

MR	Reader	Reader 1—senior neuroradiologist (>20 years)	Reader 2—senior neuroradiologist (>10 years)	Average of Readers 1–2	Reader 3—junior neuroradiologist (1 year)	Reader 4—non-neuroradiologist (6 years)	Average of Readers 3-4	*p*-value (Readers 1–2 vs. 3–4)	Average of all Readers
Neuromelanin	Sensitivity	81%	68%	74.5%	100%	58%	79%	0.767	77%
	Specificity	93%	93%	93%	63%	59%	61%	**0.0002**	77%
	Accuracy	88%	83%	85.5%	78%	58%	68%	**0.008**	77%
SMWI (iron)	Sensitivity	100%	99%	99.5%	94%	74%	84%	0.086	92%
	Specificity	98%	96%	97%	89%	80%	84.5%	**0.026**	91%
	Accuracy	99%	97%	98%	91%	78%	84.5%	**0.005**	91%

Statistical significance is defined at a *p*-value of <0.05 (bold).

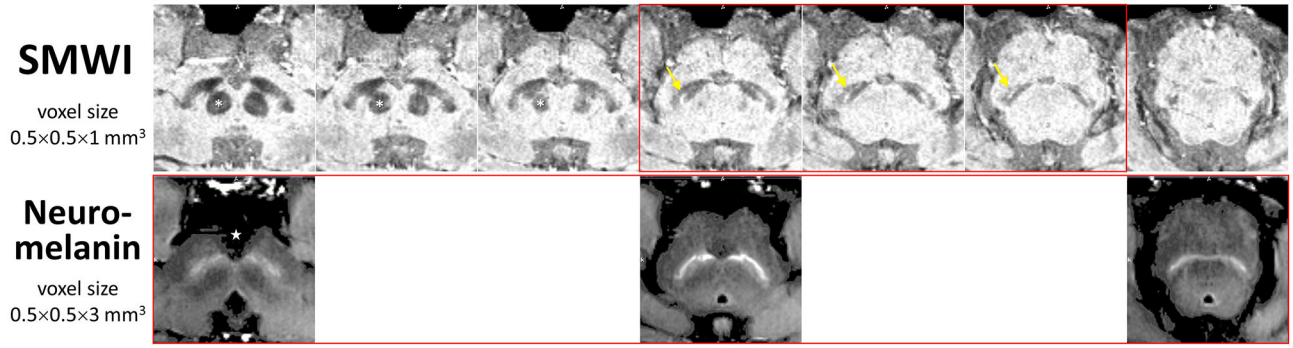

FIGURE 1
Anatomical landmarks for slice selection for qualitative visual evaluation and segmentation of the substantia nigra for quantitative image analysis. Corresponding consecutive (cranio-caudal—left-to-right) midbrain iron- (SMWI) and neuromelanin-sensitive MRI slices demonstrate the relations of the three slices (boxed in red) used between modalities. Loss of the normal hyperintense nigrosome-1 within the hypointense substantia nigra (yellow arrow) was assessed on SMWI slices just below the inferior pole of the red nucleus (asterisk). Loss of normal hyperintensity in the substantia nigra was assessed on neuromelanin-sensitive slices from the last slice through the interpeduncular fossa (star). Permission had been granted by the participating control subject for the publishing of these images.

visual assessment of a hyperintense nigrosome-1 substructure within the hypointense SN on SMWI images, and SN hyperintensity on neuromelanin-sensitive images, as detailed in Supplementary material.

Quantitative analysis

SN masks (Supplementary Figure S2) and background regions of interest were manually drawn using MRIcroGL (University of South Carolina, USA) independently and separately by Readers 1 and 5 (postdoctoral researcher), blinded to subject status and using a standardized protocol (Figure 1), as detailed in Supplementary material. Quantitative MRI parameters from these, viz. susceptibility (QSM) or signal intensity (SMWI, neuromelanin-sensitive) values, and mask sizes, were extracted. The entire operational workflow from bilateral SN segmentation to quantitative parameter extraction was completed within 10 min on average per subject.

Statistical analysis

Statistical analysis was performed using RStudio. Group comparisons were performed using chi-squared tests for categorical variables and two-tailed *t*-tests, or Kruskal–Wallis rank sum tests for continuous variables. Inter-rater agreement for qualitative visual evaluation was assessed using Fleiss' and Cohen's kappa. Inter-rater reliability of quantitative measures extracted from SN masks was assessed by intraclass correlation coefficient (ICC). Qualitative visual evaluation and quantitative SN parameters from Reader 1 were used for full cohort analysis. Receiver operating characteristic (ROC) analysis was performed to evaluate (a) the discriminative reliability of SMWI and neuromelanin-sensitive MRI in qualitative visual evaluation across readers and (b) the sensitivity and specificity of quantitative parameters as screening diagnostic discriminant tools between groups. Bivariate association between quantitative MRI parameters which were highly discriminant (AUC $>$ 80%), and clinical parameters was performed using Spearman's correlation. A default statistical significance level was set at a p-value of < 0.05, and Bonferroni correction was performed for multiple comparisons.

Results

Clinical characteristics

Four subjects were excluded because of incomplete scans due to claustrophobia or poor image quality due to motion. A total of 191 subjects, comprising 80 PD patients and 111 age-matched healthy controls were finally included. Table 1 details the full clinico-demographics, and motor and non-motor characteristics of the study subjects. The patients had mild bilateral disease (mean UPDRS-III scores <33) without impaired balance, and the majority were of the tremor-dominant subtype (Table 1).

Qualitative visual evaluation

Image quality was good or acceptable for all included subjects. Inter-rater agreement was substantial for SMWI (Fleiss' $\kappa = 0.743$) and fair for neuromelanin-sensitive MRI ($\kappa = 0.366$) across all Readers 1–4. For senior Readers 1–2, this was excellent for SMWI (Cohen's $\kappa = 0.922$) and substantial for neuromelanin-sensitive MRI ($\kappa = 0.634$).

PD classification performance was variable across Readers 1–4 for SMWI (sensitivity 74–100%, specificity 80–98%, and accuracy 78–99%) and neuromelanin-sensitive (58–100%, 59–93%, and 58–88%) MRI but superior among senior Readers 1-2 (Table 2).

10.3389/fnagi.2023.1287917

Quantitative analysis

The quantitative neuromelanin, QSM, and SMWI parameters extracted from SN masks segmented by Readers 1 and 5 showed excellent ICC (0.88, 0.95, and 0.97). ICC was also excellent (0.95) for area of SN masks segmented on SMWI and QSM. Group differences, effect sizes, and classification performance for quantitative parameters are detailed in Table 3.

SN masks on neuromelanin-sensitive MRI were more hyperintense ($p = 0.091$) and contained a higher ($p < 0.0001$) contrast range (ratio of 90th to 10th percentile signal intensity) in controls than in patients. These masks were three times smaller ($p < 0.0001$) in patients after optimized thresholding for high signal voxels (Supplementary Figure S2). Good PD classification performance was seen with both contrast range (sensitivity 80.2%, specificity 84.1%, and AUC 0.86) and smaller SN mask size after optimized thresholding for high signal voxels (79.3%, 74.4%, and 0.83).

QSM masks contained a higher ($p < 0.0001$) mean susceptibility (iron) in patients than in controls. These were 13% smaller ($p < 0.0001$) in patients, and the difference was magnified 4.6 times ($p < 0.0001$) after thresholding for voxels with low susceptibility (<70 ppb). The latter yielded good classification performance (sensitivity 76.6%, specificity 81.7%, and AUC 0.84). SMWI masks were darker and smaller ($p < 0.0001$) in patients than controls but were 1.8 times larger ($p = 0.0006$) in patients upon optimized thresholding for low-signal voxels. The latter showed decent PD classification performance (sensitivity 65.6%, specificity 78.7%, and AUC 0.79).

Based on the above findings, we derived a composite neuromelanin–iron marker using the product of the best-performing quantitative SN mask parameters (Supplementary Figure S3), viz. (i) neuromelanin contrast range, and mask sizes after optimized thresholding for voxels with (ii) high neuromelanin signal, and (iii) low susceptibility on QSM:

$$Composite\ Marker\ = \frac{Neuromelanin_{90th}}{Neuromelanin_{10th}} * Size\ Neuromelanin_{high} * Size\ QSM_{low}$$

ROC analyses, as detailed in Table 4, showed the composite marker as the best-performing among quantitative parameters (Figure 2). Its AUC of 0.94 (at cut-offs: sensitivity 85%, specificity 94%, and accuracy 90%) compared favorably to qualitative PD classification (Reader 1) using SMWI (sensitivity 99%, specificity 95%, and accuracy 97%) and neuromelanin-sensitive MRI (79, 93, and 87%).

Association between clinical and quantitative MRI parameters from SN masks

On neuromelanin-sensitive MRI, segmented SN mask size negatively correlated with age ($r = -0.22$, $p = 0.002$). Multiple significant correlations were found between clinical motor and non-motor scores and quantitative neuromelanin and QSM parameters, which survived correction for multiple comparisons (Table 5). Specifically, there were moderate associations (87.5%: $0.4 < |r| < 0.6$) between motor scores (UPDRS-II and UPDRS-III) and various neuromelanin and QSM parameters. There were

TABLE 3 Group differences in quantitative neuromelanin- and iron-sensitive (QSM and SMWI) MRI from substantia nigra masks.

MRI	Substantia nigra mask parameter	Healthy controls (mean ± sd)	PD Patients (mean ± sd)	*p*-value	Hedges' g	AUC (95% CI)
Neuromelanin	Signal intensity (a.u.)	226.8 ± 36.6	211.2 ± 54.2	0.091	0.348	0.58 (0.50–0.68)
	Contrast range (ratio of 90 to 10% signal intensity)	1.18 ± 0.12	1.10 ± 0.25	**<0.0001**	0.431	0.86 (0.80–0.92)
	Size (mm^2)	556.8 ± 108.1	580.34 ± 184.4	0.006	0.162	0.60 (0.52–0.68)
	Size after thresholding for high signal voxels (mm^2)	92.3 ± 65.6	29.1 ± 30.6	**<0.0001**	1.174	0.83 (0.77–0.89)
QSM (iron)	Mean susceptibility, χ (ppb)	84.5 ± 27.5	119.2 ± 33.5	**<0.0001**	1.151	0.80 (0.74–0.86)
	Size (mm^2)	277.7 ± 45.9	240.6 ± 56.7	**<0.0001**	0.731	0.70 (0.63–0.78)
	Size after thresholding for voxels χ < 70 ppb (mm^2)	102.3 ± 55.9	40.1 ± 42.1	**<0.0001**	1.229	0.84 (0.78–0.90)
SMWI (iron)	Signal intensity (a.u.)	171.2 ± 49.7	145.9 ± 35.7	**<0.0001**	0.570	0.67 (0.61–0.76)
	Size (mm^2)	277.7 ± 45.9	240.6 ± 56.7	**<0.0001**	0.731	0.70 (0.64–0.78)
	Size after thresholding for low signal voxels (mm^2)	46.2 ± 70.4	83.2 ± 76.6	**0.0006**	0.506	0.79 (0.70–0.88)

Statistical significance is defined at a *p*-value of <0.005 (bold) after Bonferroni correction. a.u., arbitrary units; AUC, area under the ROC curve; CI, confidence interval; ppb, parts per billion; sd, standard deviation.

TABLE 4 Comparison of classification performance between qualitative visual and quantitative substantia nigra (SN) parameters using iron- and neuromelanin-sensitive MRI.

MRI	MRI	SN feature	Accuracy	AUC (95% CI)
Qualitative visual categoric	SMWI (iron)	Nigrosome-1	97%	N.A.
	Neuromelanin	Signal intensity and size	87%	N.A.
Quantitative from substantia nigral masks	Neuromelanin	Contrast range (ratio of 90 to 10% signal intensity)	82%	0.86 (0.80–0.91)
		SN mask size after thresholding for high signal voxels (mm^2)	76%	0.83 (0.76–0.88)
	QSM (iron)	SN mask size after thresholding for voxels $\chi < 70$ ppb (mm^2)	80%	0.84 (0.79–0.90)
	Composite marker product of neuromelanin and iron parameters	$\frac{Neuromelanin_{90th}}{Neuromelanin_{10th}} * Size\ Neuromelanin_{high} * Size\ QSM_{low}$	90%	0.94 (0.90–0.97)

AUC, area under the ROC curve; CI, confidence interval; N.A., Not applicable.

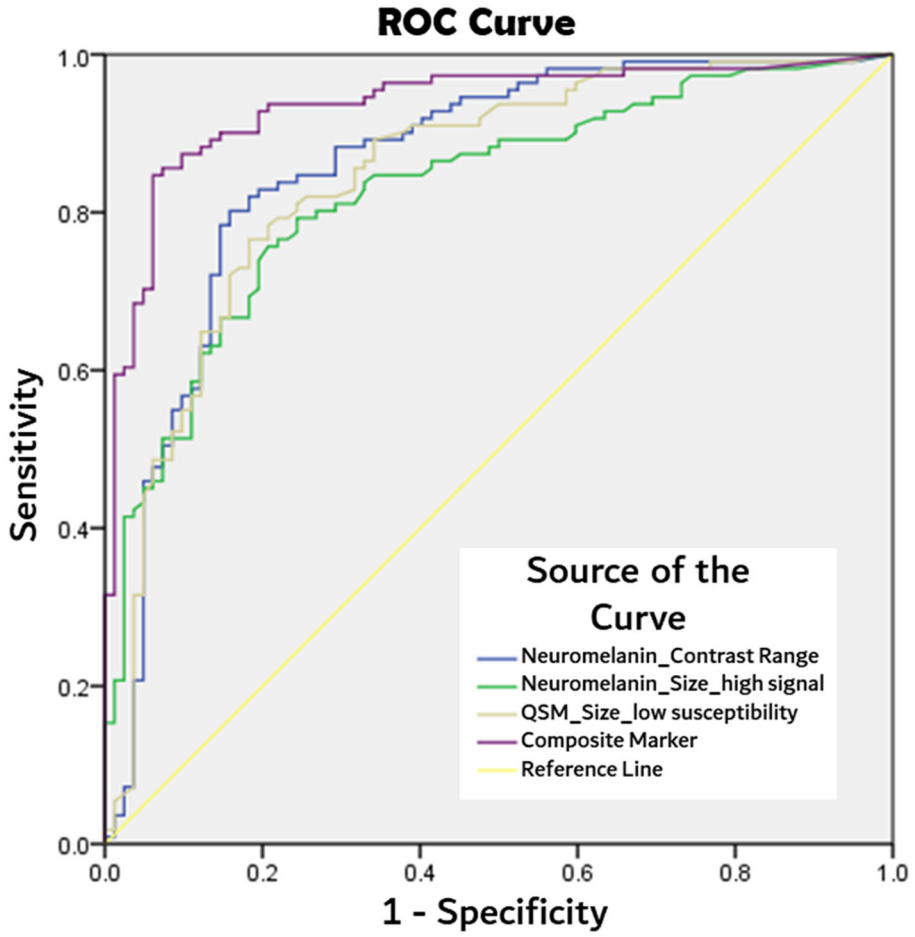

FIGURE 2
Comparison of receiver operating characteristics (ROC) curves from best performing quantitative MRI parameters of: neuromelanin signal contrast range within segmented substantia nigral mask, substantia nigra mask size after thresholding for high neuromelanin signal voxels, and low susceptibility (<70 ppb) voxels on QSM, and composite marker (product of three aforesaid parameters) in PD classification.

also significant but weaker correlations between worse non-motor (higher UPDRS-I) scores and narrower neuromelanin contrast range and higher iron and smaller SN masks on QSM after thresholding. Additionally, cognitive impairment (low MMSE) was also associated with higher iron and smaller SN masks on QSM after thresholding. In the subset correlation analysis of PD

TABLE 5 Association between clinical and quantitative MRI parameters from SN masks.

MRI	Substantia Nigra Mask Parameter	Age	MMSE	UPDRS-I	UPDRS-II	UPDRS-III
		Coefficient r (*p*-value)				
Neuromelanin	Contrast range (ratio of 90% to 10% signal intensity)	−0.051 (0.487)	0.196 (0.008)	**−0.274 (<0.001)**	**−0.466 (<0.001)**	**−0.532 (<0.001)**
	Size after thresholding for high signal voxels (mm^2)	**−0.220 (0.002)**	0.126 (0.087)	−0.173 (0.018)	**−0.372 (<0.001)**	**−0.417 (<0.001)**
QSM (iron)	Mean susceptibility, χ (ppb)	0.027 (0.713)	**−0.273 (<0.001)**	**0.298 (<0.001)**	**0.453 (<0.001)**	**0.443 (<0.001)**
	Size after thresholding for voxels $\chi < 70$ ppb (mm^2)	0.012 (0.865)	**0.272 (<0.001)**	**−0.360 (<0.001)**	**−0.479 (<0.001)**	**−0.445 (<0.001)**

Statistical significance is defined at a *p*-value of < 0.0025 (marked in bold) after Bonferroni correction (0.05/20). a.u., arbitrary units; MMSE, Mini-Mental State Examination; PD, Parkinson's Disease; UPDRS, Unified Parkinson's Disease Rating Scale.

patients alone, only QSM mask size after thresholding for low susceptibility correlated with MMSE ($r = 0.306$, $p = 0.006$) after Bonferroni correction.

Discussion

This is a large case–control PD cohort study with complete clinico-imaging data, assessing the value add of quantitative multimodal neuromelanin–iron MRI parameters of the midbrain for screening and diagnosis, their clinical associations, and comparative performance against radiological qualitative evaluation across readers of varied experience and training. Our senior neuroradiology readers excelled in visual PD classification using SMWI, and this was superior to using unprocessed neuromelanin-sensitive MRI for both accuracy and inter-rater agreement. Reader experience affected visual classification performance whether SMWI or neuromelanin-sensitive MRI was used. Unique information from quantitative neuromelanin and iron (QSM) parameters in the segmented SN masks discriminated the groups with excellent performance (AUC 0.94) when harnessed in composite neuromelanin–iron marker and showed robust association with age, motor, and non-motor severity. Its disease classification performance also matched with that of senior neuroradiologists using SMWI in qualitative visual evaluation. Quantitative neuromelanin–iron MRIs are complementary techniques that provide high diagnostic accuracy and hold promise to more objectively aid PD diagnoses that are accurate, timely, and cost effective on a wide scale in the clinic.

Qualitative visual evaluation of nigrosome-1 on SMWI by senior neuroradiologists (Readers 1 and 2) showed excellent diagnostic accuracy (98%) for PD classification (Sung et al., 2019, 2022) and fared better than that in the literature using other iron-sensitive methodologies or quantitative analysis (Cho et al., 2021b). Diagnostic accuracy using unprocessed neuromelanin-sensitive MRI by our senior neuroradiology readers (85.5%) also compared favorably to that reported by small studies using qualitative visual evaluation, with or without thresholding for voxels with high signal (Pyatigorskaya et al., 2018; Cho et al., 2021a). Overall, our results and the literature suggest that visual evaluation of the midbrain for PD classification by radiologists using SMWI yielded the best performance. Between techniques, qualitative evaluation for loss of nigrosome-1 using iron-sensitive techniques provided better results than evaluation for loss of hyperintensity on neuromelanin-sensitive MRI as was also reported by the few small studies with cross-modal evaluation (Pyatigorskaya et al., 2018; He et al., 2021).

The superior sensitivity of SMWI is related to the ease of identification of the hyperintense nigrosome-1 within the iron-rich hypointense SN, making it an ideal visual tool for quick radiological reading. SMWI are multi-echo iron-sensitive post-processed images that combine local susceptibility from phase information and SWI magnitude images to improve the delineation of nigrosome-1 on clinical 3T scanners (Nam et al., 2017). SMWI heightens the contrast between voxels containing high and low susceptibility, sharply demarcating the SN margins and depicting the small nigrosome-1 substructure precisely within. The lower specificity of SMWI, and other iron-sensitive methodologies in the literature, compared to its supreme sensitivity in qualitative nigrosome-1 evaluation (Pyatigorskaya et al., 2018; Zorzenon et al., 2021; Sung et al., 2022), could be related to the occasional instance of an intact but tiny nigrosome-1 substructure, which was read as partially lost. In contrast, the posterolateral to the anteromedial gradient of depigmentation in the SN from neurodegeneration related to aging and PD (Supplementary Figure S2) is visually problematic on neuromelanin-sensitive MRI (Table 2) when incomplete. Image postprocessing through thresholding for high-signal voxels within the SN mask could assist in qualitative visual evaluation (Supplementary Figure S2).

Our quantitative analysis showed SN atrophy in PD patients compared to controls on iron-sensitive images ($p < 0.0001$, Table 3). On neuromelanin-sensitive MRI, the hyperintense SN margins were less distinct for patients (Supplementary Figure S2) and manifested as counter-intuitively larger SN masks (insignificant after Bonferroni correction, Table 3). Table 3 also shows how optimized thresholding for voxels with high-signal intensity (neuromelanin surrogate) or low susceptibility and SMWI signal (iron surrogate) helped accentuate volumetric differences in the dopaminergic midbrain neurodegeneration between groups (Kim et al., 2018; Cho et al., 2021a). Even though neuromelanin has a high binding affinity for iron, no significant correlation between NM and iron content in the SN has been reported (Reimão et al., 2016). This could account for the additive value of combined quantitative neuromelanin–iron MRI in a high-resolution protocol for midbrain evaluation in PD (He et al., 2021).

The composite quantitative neuromelanin–iron MRI marker achieved excellent classification performance (AUC 0.94) akin to the best qualitative visual evaluation using SMWI (97% accuracy, Table 4). This is important as SMWI is not widely available even though its diagnostic performance has been exceptional. Other image acquisition and post-processing techniques generating images with similar contrasts to SMWI (He et al., 2021; Liu et al., 2021) have reported lower classification performances (AUC 0.891–0.91) as spatial resolution (SMWI 0.5 × 0.5 × 1 mm^3) affects the classification performance of the tiny nigrosome-1 as a radiological marker (Cho et al., 2021b; He et al., 2021; Liu et al., 2021). QSM images are readily reconstructed from multi-echo gradient echo sequences using open-source software (https://github.com/mathieuboudreau/qsm-tools). Adding a second neuromelanin-sensitive sequence to the MRI protocol prolongs total scan time and requires patient cooperation. Fortunately, recent multiband technology incorporated into neuromelanin-sensitive (standard T1 true spin echo) MRI acquisitions significantly reduces scan times (from 10 to 3 min).

The composite quantitative neuromelanin–iron marker has the potential for objective wide-scale diagnostic evaluation of Parkinson's disease through ease of accessibility and implementation in the clinical workflow. In our workflow, quantitative parameters from SN masks drawn by non-radiologist assistants were efficiently extracted in our image post-processing pipeline, with results made available in <10 min. While this could benefit non-expert readers the most, experienced readers could also use the additional data point to assist in the evaluation of borderline cases, with potential impact on clinical management (e.g., when to commence levodopa treatment; titrating levodopa dose). Clinical evaluation and MRI qualitative visual evaluation of the SN are not always straightforward, particularly in the presence of vascular co-morbidities or early PD, respectively (Reimão et al., 2016; Beach and Adler, 2018; He et al., 2021). More confident diagnoses could reduce costs by screening and triaging only clinico-radiologically borderline or atypical cases of parkinsonism for further radionuclide dopamine transporter imaging evaluation. The latter is more expensive, invasive, less available in some parts of the world, and incurs a radiation dose penalty. This is relevant to growing numbers of patients with parkinsonian syndrome in rapidly aging populations.

Our large case–control cohort demonstrated multiple moderate correlations between motor dysfunction (higher UPDRS-II and III scores) and SN iron (QSM mean susceptibility), narrower neuromelanin contrast range, and smaller SN masks after optimized thresholding on both QSM and neuromelanin-sensitive MRI (Table 5). Physiological neurodegeneration and nigral pathology increase with age, and mild parkinsonian signs are also common in elders without PD (Louis and Bennett, 2007; Buchman et al., 2012; Aye et al., 2020). The inclusion of a considerable number of control subjects who also underwent full clinical assessments in our cohort could explain our robust findings on correlation analyses. In contrast, individual small studies have reported limited, weak, or lateralized correlation of contralateral motor score in PD using either iron-sensitive or optimized neuromelanin-sensitive MRI methodologies (Schwarz et al., 2011, 2017; Miyoshi et al., 2013; Wang et al., 2018; He et al., 2021) or pooled meta-analysis for improved correlations (Pyatigorskaya et al., 2020). Older subjects in our cohort had smaller SN masks on neuromelanin-sensitive MRI ($r = -0.22$, $p = 0.002$), suggesting a trajectory of depigmentation in the SN with advancing age. This negative association of SN neuromelanin-related hyperintensity with age agrees with a lifespan study that included a small cohort ($n = 30$) of elderly aged >60 years, using a suprathreshold volume based on neuromelanin-sensitive MRI signal (Xing et al., 2018). Postmortem histological studies (Ma et al., 1999) also observed volume reductions of the pigmented SN from middle age. In addition to concordance with dopamine transporter imaging, quantitative neuromelanin-sensitive MRI has been reported to be more effective as a predictor of motor fluctuations in advanced PD (Okuzumi et al., 2019).

We found fewer and weaker associations between non-motor (MMSE and UPDRS-I) scores and midbrain MRI parameters. This is not surprising as non-motor features in PD are also known to be related to extranigral multisystem neuropathology involving neurotransmitter pathways beyond dopamine deficiency (Sulzer and Surmeier, 2013). Taken together, the observed quantitative MRI correlations with clinical scores, as measures of parkinsonian motor and non-motor dysfunction across a continuum of nigral and related extranigral neurodegeneration, from normal aging to PD, indicate the potential of quantitative iron–neuromelanin MRI as objective tools to track dopaminergic denervation, iron toxicity, and PD progression. Neuromelanin is thought to protect neurons against oxidative damage by inactivating free radicals or chelating transition metals (Pyatigorskaya et al., 2020). The degeneration of dopaminergic neurons in the SN (Cassidy et al., 2019) and breakdown of neuromelanin is thus accompanied by an increase in iron content, leading to further oxidative damage which manifests as the progression of the disease. Therefore, it is expected that excess iron deposition within the SN also serves as a specific imaging biomarker for PD progression.

Our study has its limitations. First, our manual SN segmentation is limited to three representative slices, while fully or semi-automated segmentation may enable interrogation of the entire SN volume and be less prone to variability, particularly for neuromelanin-sensitive MRI images (Cho et al., 2021a). Nonetheless, our inter-rater agreement for quantitative neuromelanin-sensitive MRI, QSM, and SMWI measures extracted from the manually segmented SN masks by radiology and non-radiology readers was excellent and yielded positive correlation results. These indicate that our technique can be practicably performed in the real-world clinical setting, with confidence that the manual segmentations are reliable. Second, we used SMWI for qualitative visual evaluation when it is not widely available as an open-source post-processing software. However, SMWI has produced superior results in visual analyses and has been extensively validated against dopamine transporter imaging evaluation for concordance (Sung et al., 2019, 2022; Bae et al., 2021b). Third, we did not perform deep learning analysis to further improve the diagnostic performance of our quantitative analysis (Jung et al., 2022). This could be the work of a future large cohort study. Fourth, our non-motor clinical assessments were limited and inadequately framed for the wide scoping non-motor symptomatology that exists in PD, including rapid eye movement

sleep behavior disorder, which would be relevant for future study in prodromal PD in relation to composite midbrain quantitative neuromelanin–iron parameters.

Conclusion

Our large, cross-modal, case–control study in PD showed (i) moderate associations between quantitative iron–neuromelanin MRI and motor and non-motor dysfunction, (ii) composite quantitative neuromelanin–iron marker matching best-performing qualitative radiological PD classification using SMWI, and (iii) potential for these techniques to be adopted to improve diagnostic confidence, tracking of disease progression and response to neuroprotective therapies in both clinical and research settings.

Data availability statement

The original contributions presented in this study are included in the article/Supplementary material, further inquiries can be directed to the corresponding author.

Ethics statement

The studies involving humans were approved by SingHealth Centralised Institutional Review Board (CIRB). The studies were conducted in accordance with the local legislation and institutional requirements. The participants provided their written informed consent to participate in this study.

Author contributions

SH: Data curation, Formal analysis, Investigation, Software, Writing—original draft. RC: Investigation, Validation, Writing—review & editing. TW: Investigation, Writing—review & editing, Validation. AT: Investigation, Software, Writing—review & editing. WL: Investigation, Supervision, Visualization, Writing—review & editing. PT: Investigation, Software, Writing—review & editing. CC: Investigation, Writing—review & editing. WH: Investigation, Writing—review & editing. WT: Investigation, Writing—review & editing. EL: Investigation, Writing—review & editing. KP: Investigation, Writing—review & editing. Y-CS: Investigation, Supervision, Writing—review & editing. KL: Methodology, Software, Supervision, Writing—review & editing. LT: Investigation, Writing—review & editing. ET: Conceptualization, Investigation, Methodology, Resources, Supervision, Writing—review & editing. LC: Conceptualization, Data curation, Formal analysis, Funding acquisition, Investigation, Methodology, Project administration, Resources, Software, Supervision, Validation, Visualization, Writing—review & editing.

Funding

The author(s) declare financial support was received for the research, authorship, and/or publication of this article. This work was supported by grants from the Singapore National Medical Research Council (NMRC/CSA/INV2017 and NMRC/CSASI/20nov-0008).

Acknowledgments

The authors would like to thank Professor Jongho Lee of Seoul National University who kindly shared his SMWI toolbox for this study.

Conflict of interest

The authors declare that the research was conducted in the absence of any commercial or financial relationships that could be construed as a potential conflict of interest.

Publisher's note

Supplementary material

The Supplementary Material for this article can be found online at: https://www.frontiersin.org/articles/10.3389/fnagi.2023.1287917/full#supplementary-material

References

Aye, Y. M., Liew, G. M., Ng, S. Y. E., Wen, M. C., Lim, L. L. H., Chua, S. T., et al. (2020). Mild parkinsonian signs in a community ambulant population. *J. Parkinsons Dis.* 10, 1231–1237. doi: 10.3233/JPD-191849

Bae, Y. J., Kim, J. M., Sohn, C. H., Choi, J. H., Choi, B. S., Song, Y. S., et al. (2021a). Imaging the substantia nigra in Parkinson disease and other parkinsonian syndromes. *Radiology* 300, 260–278. doi: 10.1148/radiol.2021203341

Bae, Y. J., Song, Y. S., Kim, J. M., Choi, B. S., Nam, Y., Choi, J. H., et al. (2021b). Determining the degree of dopaminergic denervation based on the loss of nigral hyperintensity on SMWI in parkinsonism. *AJNR* 42, 681–687. doi: 10.3174/ajnr.A6960

Beach, T. G., and Adler, C. H. (2018). Importance of low diagnostic accuracy for early Parkinson's disease. *Mov. Disord.* 33, 1551–1554. doi: 10.1002/mds.27485

Blazejewska, A. I., Schwarz, S. T., Pitiot, A., Stephenson, M. C., Lowe, J., Bajaj, N., et al. (2013). Visualization of nigrosome 1 and its loss in PD: pathoanatomical correlation and *in vivo* 7 T MRI. *Neurology* 81, 534–540. doi: 10.1212/WNL.0b013e31829e6fd2

Buchman, A. S., Shulman, J. M., Nag, S., Leurgans, S. E., Arnold, S. E., Morris, M. C., et al. (2012). Nigral pathology and parkinsonian signs in elders without Parkinson disease. *Ann. Neurol.* 71, 258–266. doi: 10.1002/ana.22588

Cassidy, C. M., Zucca, F. A., Girgis, R. R., Baker, S. C., Weinstein, J. J., Sharp, M. E., et al. (2019). Neuromelanin-sensitive MRI as a noninvasive proxy measure of dopamine function in the human brain. *Proc. Natl. Acad. Sci. USA* 116, 5108–5117. doi: 10.1073/pnas.1807983116

Cho, S. J., Bae, Y. J., Kim, J.-M., Kim, H. J., Baik, S. H., Sunwoo, L., et al. (2021b). Iron-sensitive magnetic resonance imaging in Parkinson's disease: a systematic review and meta-analysis. *J. Neurol.* 268, 4721–4736. doi: 10.1007/s00415-021-10582-x

Cho, S. J., Bae, Y. J., Kim, J. M., Kim, D., Baik, S. H., Sunwoo, L., et al. (2021a). Diagnostic performance of neuromelanin-sensitive magnetic resonance imaging for patients with Parkinson's disease and factor analysis for its heterogeneity: a systematic review and meta-analysis. *Eur. Radiol.* 31, 1268–1280. doi: 10.1007/s00330-020-07240-7

Dexter, D. T., Wells, F. R., Lees, A. J., Agid, F., Agid, Y., Jenner, P., et al. (1989). Increased nigral iron content and alterations in other metal ions occurring in brain in Parkinson's disease. *J. Neurochem.* 52, 1830–1836. doi: 10.1111/j.1471-4159.1989.tb07264.x

He, N., Ghassaban, K., Huang, P., Jokar, M., Wang, Y., Cheng, Z., et al. (2021). Imaging iron and neuromelanin simultaneously using a single 3D gradient echo magnetization transfer sequence: Combining neuromelanin, iron and the nigrosome-1 sign as complementary imaging biomarkers in early stage Parkinson's disease. *Neuroimage* 230, 117810. doi: 10.1016/j.neuroimage.2021.117810

Jung, W., Bollmann, S., and Lee, J. (2022). Overview of quantitative susceptibility mapping using deep learning: current status, challenges and opportunities. *NMR Biomed.* 35, e4292. doi: 10.1002/nbm.4292

Kim, E. Y., Sung, Y. H., Shin, H. G., Noh, Y., Nam, Y., Lee, J., et al. (2018). Diagnosis of early-stage idiopathic parkinson's disease using high-resolution quantitative susceptibility mapping combined with histogram analysis in the substantia nigra at 3 T. *J. Clin. Neurol.* 14, 90–97. doi: 10.3988/jcn.2018.14.1.90

Li, W., Avram, A. V., Wu, B., Xiao, X., and Liu, C. (2014). Integrated Laplacian-based phase unwrapping and background phase removal for quantitative susceptibility mapping. *NMR Biomed.* 27, 219–227. doi: 10.1002/nbm.3056

Liu, X., Wang, N., Chen, C., Wu, P. Y., Piao, S., Geng, D., et al. (2021). Swallow tail sign on susceptibility map-weighted imaging (SMWI) for disease diagnosing and severity evaluating in parkinsonism. *Acta Radiol.* 62, 234–242. doi: 10.1177/0284185120920793

Louis, E. D., and Bennett, D. A. (2007). Mild Parkinsonian signs: an overview of an emerging concept. *Mov. Disord.* 22, 1681–1688. doi: 10.1002/mds.21433

Ma, S. Y., Roytt, M., Collan, Y., and Rinne, J. O. (1999). Unbiased morphometrical measurements show loss of pigmented nigral neurones with ageing. *Neuropathol. Appl. Neurobiol.* 25, 394–399. doi: 10.1046/j.1365-2990.1999.00202.x

Miyoshi, F., Ogawa, T., Kitao, S. I., Kitayama, M., Shinohara, Y., Takasugi, M., et al. (2013). Evaluation of Parkinson disease and Alzheimer disease with the use of neuromelanin MR imaging and (123)I-metaiodobenzylguanidine scintigraphy. *AJNR* 34, 2113–2118. doi: 10.3174/ajnr.A3567

Nam, Y., Gho, S. M., Kim, D. H., Kim, E. Y., and Lee, J. (2017). Imaging of nigrosome 1 in substantia nigra at 3T using multiecho susceptibility map-weighted imaging (SMWI). *J. Magn. Reson. Imaging* 46, 528–536. doi: 10.1002/jmri.25553

Okuzumi, A., Hatano, T., Kamagata, K., Hori, M., Mori, A., Oji, Y., et al. (2019). Neuromelanin or DaT-SPECT: which is the better marker for discriminating advanced Parkinson's disease? *Eur. J. Neurol.* 26, 1408–1416. doi: 10.1111/ene.14009

Parkinson's UK (2020). Available online at: https://www.parkinsons.org.uk/news/poll-finds-quarter-people-parkinsons-are-wrongly-diagnosed (accessed November 10, 2023).

Pavese, N., and Tai, Y. F. (2018). Nigrosome imaging and neuromelanin sensitive MRI in diagnostic evaluation of parkinsonism. *Mov. Disord. Clin. Pract.* 5, 131–140. doi: 10.1002/mdc3.12590

Postuma, R. B., Berg, D., Stern, M., Poewe, W., Olanow, C. W., Oertel, W., et al. (2015). MDS clinical diagnostic criteria for Parkinson's disease. *Mov. Disord.* 30, 1591–1601. doi: 10.1002/mds.26424

Pyatigorskaya, N., Magnin, B., Mongin, M., Yahia-Cherif, L., Valabregue, R., Arnaldi, D., et al. (2018). Comparative study of MRI biomarkers in the substantia nigra to discriminate idiopathic Parkinson disease. *AJNR* 39, 1460–1467. doi: 10.3174/ajnr.A5702

Pyatigorskaya, N., Sanz-Morère, C. B., Gaurav, R., Biondetti, E., Valabregue, R., Santin, M., et al. (2020). Iron imaging as a diagnostic tool for Parkinson's disease: a systematic review and meta-analysis. *Front. Neurol.* 11, 366. doi: 10.3389/fneur.2020.00366

Reimão, S., Ferreira, S., Nunes, R. G., Pita Lobo, P., Neutel, D., Abreu, D., et al. (2016). Magnetic resonance correlation of iron content with neuromelanin in the substantia nigra of early-stage Parkinson's disease. *Eur. J. Neurol.* 23, 368–374. doi: 10.1111/ene.12838

Rizzo, G., Copetti, M., Arcuti, S., Martino, D., Fontana, A., and Logroscino, G. (2016). Accuracy of clinical diagnosis of Parkinson disease: a systematic review and meta-analysis. *Neurology* 86, 566–576. doi: 10.1212/WNL.0000000000002350

Sasaki, M., Shibata, E., Tohyama, K., Takahashi, J., Otsuka, K., Tsuchiya, K., et al. (2006). Neuromelanin magnetic resonance imaging of locus ceruleus and substantia nigra in Parkinson's disease. *Neuroreport* 17, 1215–1218. doi: 10.1097/01.wnr.0000227984.84927.a7

Schwarz, S. T., Rittman, T., Gontu, V., Morgan, P. S., Bajaj, N., and Auer, D. P. (2011). T1-weighted MRI shows stage-dependent substantia nigra signal loss in Parkinson's disease. *Mov. Disord.* 26, 1633–1638. doi: 10.1002/mds.23722

Schwarz, S. T., Xing, Y., Tomar, P., Bajaj, N., and Auer, D. P. (2017). In vivo assessment of brainstem depigmentation in Parkinson disease: potential as a severity marker for multicenter studies. *Radiology* 283, 789–798. doi: 10.1148/radiol.2016160662

Sulzer, D., Cassidy, C., Horga, G., Kang, U. J., Fahn, S., Casella, L., et al. (2018). Neuromelanin detection by magnetic resonance imaging (MRI) and its promise as a biomarker for Parkinson's disease. *NPJ Parkinsons Dis.* 4, 11. doi: 10.1038/s41531-018-0047-3

Sulzer, D., and Surmeier, D. J. (2013). Neuronal vulnerability, pathogenesis, and Parkinson's disease. *Mov. Disord.* 28, 715–724. doi: 10.1002/mds.25187

Sung, Y. H., Kim, J. S., Yoo, S. W., Shin, N. Y., Nam, Y., Ahn, T. B., et al. (2022). A prospective multi-centre study of susceptibility map-weighted MRI for the diagnosis of neurodegenerative parkinsonism. *Eur. Radiol.* 32, 3597–3608. doi: 10.1007/s00330-021-08454-z

Sung, Y. H., Lee, J., Nam, Y., Shin, H. G., Noh, Y., Hwang, K. H., et al. (2019). Initial diagnostic workup of parkinsonism: Dopamine transporter positron emission tomography versus susceptibility map-weighted imaging at 3T. *Parkinsonism Relat. Disord.* 62, 171–178. doi: 10.1016/j.parkreldis.2018.12.019

Sung, Y. H., Lee, J., Nam, Y., Shin, H. G., Noh, Y., Shin, D. H., et al. (2018). Differential involvement of nigral subregions in idiopathic parkinson's disease. *Hum. Brain Mapp.* 39, 542–553. doi: 10.1002/hbm.23863

Tan, S., Hartono, S., Welton, T., Ann, C. N., Lim, S. L., Koh, T. S., et al. (2021). Utility of quantitative susceptibility mapping and diffusion kurtosis imaging in the diagnosis of early Parkinson's disease. *Neuroimage Clin.* 32, 102831. doi: 10.1016/j.nicl.2021.102831

Wang, J., Li, Y., Huang, Z., Wan, W., Zhang, Y., Wang, C., et al. (2018). Neuromelanin-sensitive magnetic resonance imaging features of the substantia nigra and locus coeruleus in de novo Parkinson's disease and its phenotypes. *Eur. J. Neurol.* 25, 949–e73. doi: 10.1111/ene.13628

Wang, X., Zhang, Y., Zhu, C., Li, G., Kang, J., Chen, F., et al. (2019). The diagnostic value of SNpc using NM-MRI in Parkinson's disease: meta-analysis. *Neurol. Sci.* 40, 2479–2489. doi: 10.1007/s10072-019-04014-y

Xing, Y., Sapuan, A., Dineen, R. A., and Auer, D. P. (2018). Life span pigmentation changes of the substantia nigra detected by neuromelanin-sensitive MRI. *Mov. Disord.* 33, 1792–1799. doi: 10.1002/mds.27502

Zorzenon, C. D. F., Bienes, G. H. A. A., Alves, E. D., Tibana, L. A. T., Júnior, H. C., Ferraz, H. B., et al. (2021). Magnetic resonance imaging evaluation of nigrosome 1 and neuromelanin can assist Parkinson's disease diagnosis, but requires an expert neuroradiologist. *Parkinsonism Relat. Disord.* 83, 8–12. doi: 10.1016/j.parkreldis.2020.12.006

frontiers | Frontiers in Aging Neuroscience

TYPE Original Research
PUBLISHED 06 December 2023
DOI 10.3389/fnagi.2023.1282962

OPEN ACCESS

EDITED BY
Robert Petersen,
Central Michigan University, United States

REVIEWED BY
Ane Murueta-Goyena,
University of the Basque Country, Spain
Keisuke Suzuki,
Dokkyo Medical University, Japan

*CORRESPONDENCE
Zhijian Lin
✉ linzjpush@139.com
Guanxun Cheng
✉ chengguanxun@outlook.com

†These authors have contributed equally to this work

RECEIVED 25 August 2023
ACCEPTED 23 November 2023
PUBLISHED 06 December 2023

CITATION
Tan Z, Zeng Q, Hu X, Di D, Chen L, Lin Z and Cheng G (2023) Altered dynamic functional network connectivity in drug-naïve Parkinson's disease patients with excessive daytime sleepiness.
Front. Aging Neurosci. 15:1282962.
doi: 10.3389/fnagi.2023.1282962

Altered dynamic functional network connectivity in drug-naïve Parkinson's disease patients with excessive daytime sleepiness

Zhiyi Tan[1†], Qiaoling Zeng[1†], Xuehan Hu[1], Duoduo Di[1], Lele Chen[1], Zhijian Lin[2*] and Guanxun Cheng[1*]

[1]Department of Medical Imaging, Peking University Shenzhen Hospital, Shenzhen, Guangdong, China, [2]Department of Neurology, Peking University Shenzhen Hospital, Shenzhen, Guangdong, China

Background: Excessive daytime sleepiness (EDS) is a frequent nonmotor symptoms of Parkinson's disease (PD), which seriously affects the quality of life of PD patients and exacerbates other nonmotor symptoms. Previous studies have used static analyses of these resting-state functional magnetic resonance imaging (rs-fMRI) data were measured under the assumption that the intrinsic fluctuations during MRI scans are stationary. However, dynamic functional network connectivity (dFNC) analysis captures time-varying connectivity over short time scales and may reveal complex functional tissues in the brain.

Purpose: To identify dynamic functional connectivity characteristics in PD-EDS patients in order to explain the underlying neuropathological mechanisms.

Methods: Based on rs-fMRI data from 16 PD patients with EDS and 41 PD patients without EDS, we applied the sliding window approach, k-means clustering and independent component analysis to estimate the inherent dynamic connectivity states associated with EDS in PD patients and investigated the differences between groups. Furthermore, to assess the correlations between the altered temporal properties and the Epworth sleepiness scale (ESS) scores.

Results: We found four distinct functional connectivity states in PD patients. The patients in the PD-EDS group showed increased fractional time and mean dwell time in state IV, which was characterized by strong connectivity in the sensorimotor (SMN) and visual (VIS) networks, and reduced fractional time in state I, which was characterized by strong positive connectivity intranetwork of the default mode network (DMN) and VIS, while negative connectivity internetwork between the DMN and VIS. Moreover, the ESS scores were positively correlated with fraction time in state IV.

Conclusion: Our results indicated that the strong connectivity within and between the SMN and VIS was characteristic of EDS in PD patients, which may be a potential marker of pathophysiological features related to EDS in PD patients.

KEYWORDS

Parkinson's disease, excessive daytime sleepiness, resting-state functional magnetic resonance imaging, dynamic functional brain connectivity, neural network

Introduction

Parkinson's disease (PD) is the second most common neurodegenerative disease, with more than 8.5 million individuals suffering from PD worldwide (Grover et al., 2022). Excessive daytime sleepiness (EDS) is a frequent nonmotor symptoms in PD patients, affecting up to 20–60% of PD patients (Liu et al., 2022). EDS mainly manifests as the inability to stay awake and alert during typical waking periods, leading to unintended lapses into drowsiness or sleep states (Liu et al., 2022). EDS in PD patients not only has a negative impact on the patients' quality of life (Bloem et al., 2021), including occupational, psychological, and social abilities, but may also worsen nonmotor symptoms such as mood, apathy, anxiety, and cognitive function (Chan et al., 2020). Therefore, there is a strong interest in identifying the neurobiological abnormalities underlying EDS in PD patients. A better understanding of the pathogenesis of EDS and the identification of its biomarkers are essential for PD patients.

Resting-state functional magnetic resonance imaging (rs-fMRI) is a novel noninvasive neuroimaging method with high temporal and spatial resolution that has been widely used to explore the pathogenesis of EDS in PD patients. The amplitude of low-frequency fluctuation (ALFF), fractional ALFF and regional homogeneity methods reflect the intensity and consistency of spontaneous activities among brain regions. Previous studies have displayed increases in spontaneous neural activity in the medial prefrontal cortex, paracentral lobule, thalamus, putamen and pons and decreases in the inferior frontal gyrus, angular gyrus, cingulate cortex and cerebellum in patients of PD with EDS (PD-EDS) (Wen et al., 2016; Wang et al., 2020; Zi et al., 2022; Zheng et al., 2023). Functional connectivity analysis can be used to evaluate correlations and synchronization at brain regions and the whole brain network levels. Multiple studies have demonstrated that EDS in PD patients may be associated with abnormal functional connectivity among various brain regions, including the default mode network (DMN), cognitive executive network (CEN), salience network (SN) and cerebellum (CB) (Wen et al., 2016; Ooi et al., 2019; Wang et al., 2020; Zi et al., 2022; Zheng et al., 2023). However, these static rs-fMRI data were measured under the assumption that the intrinsic fluctuations during MRI scans are stationary, ignoring the temporal dynamic properties of functional connectivity.

In fact, the functional connectivity of brain networks changes during rs-fMRI scanning sequences (Hutchison et al., 2013). Dynamic functional connectivity analysis can capture variability in connectivity among brain regions over short periods (Hutchison et al., 2013), providing greater insights from a time-varying perspective. In recent years, emerging evidence based on dynamic functional connectivity analyses has shown that abnormal dynamic properties are associated with motor and nonmotor symptoms in patients with PD. For example, the mean dwell time of the functional separation state was negatively correlated with the severity of motor symptoms (Kim et al., 2017) and positively correlated with the severity of cognitive impairment (Fiorenzato et al., 2019) in patients with PD. In addition, PD patients with the tremor-dominant subtype and PD patients with rapid eye movement sleep behavior disorder both had longer dwell times and sparser network connectivity than other PD patients without these symptoms (Gan et al., 2021; Zhu et al., 2021). Additionally, PD patients with depression preferred to remain in states characterized by DMN-dominated and CEN-disconnected patterns (Xu et al., 2021). A recent study demonstrated that PD patients with levodopa-induced dyskinesia were more frequently in and dwelled longer in strongly connected states, characterized by strong positive connectivity between the visual network (VIS) and sensorimotor network (SMN) (Si et al., 2023). Another study showed that PD patients with impulse control disorders preferred to be in states with brain configuration patterns characterized by sparse internetwork connectivity and strong intranetwork connectivity involving the limbic circuit (Navalpotro-Gomez et al., 2020). However, to date, the dynamic functional network connectivity (dFNC) characteristics and underlying neuropathological features of PD-EDS have remained unclear.

The purpose of this study was to identify dFNC characteristics in patients with PD-EDS to explain the potential neuropathological mechanisms underlying this condition. Considering the possible effect of drugs on the dynamic functional measures of patients with PD-EDS, we focused on drug-naïve PD patients in this study (Arnone et al., 2018; Si et al., 2023).

Materials and methods

Participants

The data used in this study were obtained from the Parkinson's Progression Marker Initiative (PPMI) database, an ongoing, multicenter, international study aimed at identifying biomarkers related to PD progression. The inclusion and exclusion criteria have been published in PPMI (Marek et al., 2011).

A total of 152 PD patients with functional magnetic resonance imaging (fMRI) scans acquired between December 2020 and March 2023 were recruited from the PPMI dataset. The inclusion criteria for our research were as follows: (1) patients had never taken anti-Parkinson's medications or sleep-disrupting drugs before data collection; and (2) patients completed all clinical assessment scales and fMRI sequence scans. The exclusion criteria were as follows: (1) intracranial organic lesions, such as tumors, hematomas, and cerebral infarction; (2) patients with Parkinson's syndrome or Parkinson's superposition syndrome caused by other definite diseases; and (3) previous traumatic brain injury. The Epworth sleepiness scale (ESS) contains 8 items with scores ranging from 0 to 24 and is used to measure the subject's expectation of drowsiness in 8 daily situations during the past 1 week. Based on the ESS scores, PD patients were divided into two groups. Patients with ESS scores of 10 or greater were classified as the PD-EDS group ($n = 23$), while those with ESS scores of 3 or less were classified as the PD patients without EDS (PD-noEDS) group ($n = 42$). Patients with ESS scores of 4 to 9 were excluded ($n = 87$) (Wang et al., 2020). In addition, seven patients with ESS scores ≤ 3 or ≥ 10 who had already been treated were excluded. Then, one PD-EDS patient was excluded due to its head movement exceeding translation of 3 mm or rotation of 3°in the later MRI data preprocessing. Finally, our study included 57 drug-naïve PD patients, including 16 PD-EDS patients and 41 PD-noEDS patients. A flowchart of the patient inclusion was provided in Figure 1.

Clinical assessment

All patients were diagnosed by experienced neurologists. The patients' age, sex, years of education, age at onset and duration of

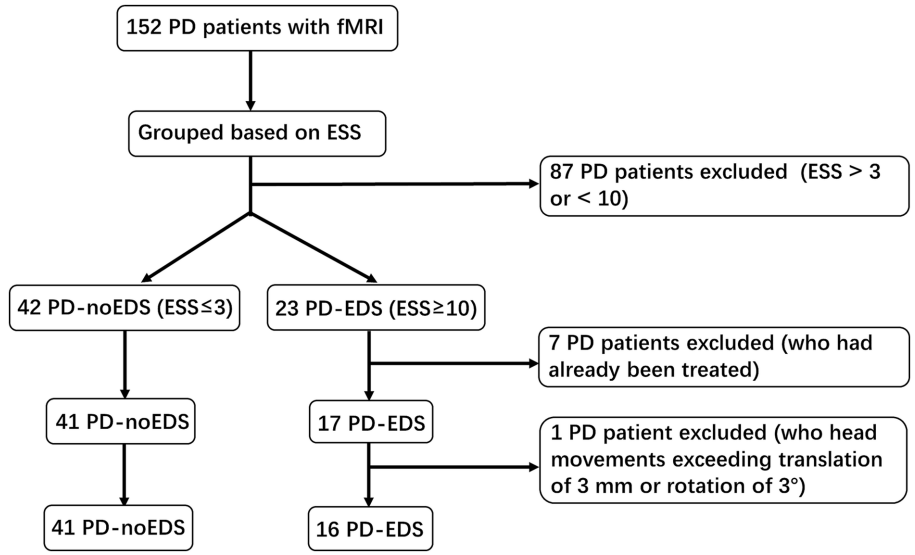

FIGURE 1
A flowchart of the selection of patients.

disease were recorded. All patients were evaluated with comprehensive clinical neuropsychological assessments including motor and nonmotor symptom-related scales, including the Unified Parkinson's Disease Rating Scale III (UPDRS III), Hoehn and Yahr (H&Y) staging scale, Montreal Cognitive Assessment (MoCA), State–trait Anxiety Inventory (STAI), Geriatric Depression Scale (GDS), rapid eye movement sleep behavior disorder questionnaire (RBDSQ) and ESS.

MRI data acquisition and preprocessing

All participants underwent rs-fMRI scans on 3.0 T MRI scanners (Siemens, Germany). Gradient-echo T2*-weighted echo-planar imaging sequences (GE-EPI) were applied for functional brain activity imaging, and 240 time points were acquired during the scan. The rs-fMRI acquisition parameters were as follows: repetition time = 2,500 ms, echo time = 30 ms, flip angle = 80 degrees, thickness = 3.5 mm, voxel size = 3.5 mm^3 and number of axial slices = 44.

The fMRI data were preprocessed using GRETNA software.[1] To equilibrate the MRI signals and ensure subjects were adapted to the scanning environment, the first 10 time points were removed. The fMRI images acquired at the remaining 230 time points were then slice-time corrected and realigned to the mean echo-planar image. In addition, all corrected fMRI images were spatially normalized into the Montreal Neurological Institute (MNI) standard space using EPI templates, resampled with a 3 mm isotropic voxel, and spatially smoothed with a 6 mm 3D-Gaussian filter. To reduce the potential effects of head movements, we excluded patients with mean frame displacement (FD) > 0.5 mm or head movements exceeding a maximum translation of 3 mm or rotation of 3° (excluding one PD-EDS patient) from further analysis, referring to two previous studies (Navalpotro-Gomez et al., 2020; Xu et al., 2021). There were no significant group differences in head movements among the patients in the PD-EDS group (mean FD = 0.09 ± 0.06 mm) and the PD-noEDS group (mean FD = 0.11 ± 0.07 mm) (Mann–Whitney U test, $p = 0.40$).

Group independent component analysis

Independent component analysis (ICA) was performed based on the preprocessed data using the group ICA in the functional MRI toolbox (GIFTv4.0b, http://mialab.mrn.org/software/gift/) to obtain specific data components. First, voxel-level variance normalization was performed based on all subject data. Next, the number of independent components (ICs) was estimated to be 36 on average using the minimum description length method. To improve accuracy, the subject data were reduced to 120 ICs using principal component analysis (PCA) and further decomposed into 50 components, as performed in previous studies (Si et al., 2023). Finally, the Infomax ICA algorithm in ICASSO was repeated 20 times to ensure stability and validity (Himberg et al., 2004). The spatial functional networks for each subject and corresponding time courses were created using the ICA back reconstruction method.

Among the 50 ICs, 27 ICs were identified as meaningful according to the following criteria by Allen et al. (2014), (1) peak coordinates of spatial maps located primarily in the gray matter; (2) low spatial overlap with known vascular, motion, and susceptibility artifacts; (3) time courses dominated by low-frequency signals (ratio of the integral of spectral power < 0.10 Hz to 0.15–0.25 Hz); and (4) time courses characterized by high dynamic range (range difference between the minimum and maximum power frequencies). These 27 ICs were then sorted into seven functional networks based on the spatial correlation values between the ICs and the template and the visual inspection results (Shirer et al., 2012). The seven functional networks were the

1 https://www.nitrc.org/projects/gretna/

auditory (AUD), basal ganglia (BG), cerebellum (CB), cognitive executive (CEN), default mode (DMN), sensorimotor (SMN), and visual (VIS) networks.

The time courses of the 27 ICs were postprocessed to remove remaining noise sources. The time courses were detrended with the 3DDESPIKE algorithm. Then, temporal bandpass filtering with a high frequency cutoff frequency of 0.15 Hz was performed (Allen et al., 2014). To obtain the static functional connectivity matrix, paired Pearson correlations were calculated and converted to z values before further analysis (Kim et al., 2017).

Dynamic functional network connectivity

We used the k-means clustering algorithm in GIFT software and a sliding window to calculate the dFNC (Allen et al., 2014; Kim et al., 2017). To examine changes in the functional connectivity matrix across time, we created a sliding window of 45 s (width of 18 TRs) with a Gaussian distribution ($\sigma = 3$ TRs) in steps of 1 TR, resulting in 212 sliding windows per patient. We selected a window length of 45 s because the window size is approximately 30–60 s, this length could optimize the balance between the temporal resolution and the quality of the functional connectivity estimates (Li et al., 2014; Si et al., 2023). The windows for each dFNC matrix were obtained using paired Pearson's correlation values between the time courses of the 27 ICs, forming a time series of FNC matrices (27×27) for the subsequent analysis. Next, all dFNC windows for each patient were classified by applying a k-means clustering method based on the Euclidean distance, which was repeated 100 times to reduce the bias of the random initialization of the centroid positions (Friedman et al., 2008). A k value of four ($k = 4$) was identified as the optimal cluster size using the elbow criterion. Furthermore, three different variables, including the fractional time, mean dwell time and number of transitions, were assessed to examine the temporal properties of the dynamic functional connectivity states. The fractional time was the percentage of time spent in one state. The mean dwell time was measured by averaging the number of consecutive windows in a specific state. The number of transitions was the number of conversions that occurred between different states.

The differences between the two groups (PD-EDS and PD-noEDS) were investigated using two-sample t tests or Mann–Whitney U tests. p values were corrected by the false discovery rate (FDR) for multiple comparisons. The threshold for statistical significance was set at $p < 0.05$.

Statistical analyses

Statistical analyses were conducted using SPSS Statistic 24.0 (Chicago, IL, United States). Two-sample t tests or Mann–Whitney U tests were applied to compare the PD-EDS and PD-noEDS groups. Chi-squared tests were used to compare categorical variables such as sex. Spearman's correlation analyses were conducted to assess the correlations between the detected temporal properties and the ESS scores (age and gender as covariates). Multiple comparison corrections were performed for dynamic functional connectivity parameters statistical analysis, and $p < 0.05$ with FDR correction was set as a threshold for statistical significance.

Results

Demographic and clinical characteristics

A total of 16 PD-EDS and 41 PD-noEDS patients were included in the analysis. There were no significant differences in demographics, disease duration and severity, cognition, anxiety, depression between groups. The ESS scores of the patients in the PD-EDS group were significantly higher than those of the patients in the PD-noEDS group ($p < 0.001$) (Table 1).

Group independent components analysis

The spatial map of all 27 ICs defined by using the group ICA is illustrated in Figure 2. These 27 ICs made up the following seven networks: auditory (AUD, IC 18), basal ganglia (BG, IC 20), cerebellum (CB, IC 16), cognitive executive (CEN, IC 32, 36, 38, 43, 44), default mode (DMN, IC 12, 19, 24, 28, 37, 49), sensorimotor (SMN, IC 1, 7, 10, 14, 31, 42, 50) and visual (VIS, IC 4, 22, 26, 35, 40, 41).

TABLE 1 Demographic and clinical characteristics of PD-EDS and PD-noEDS group.

	PD-EDS ($n = 16$)	PD-noEDS ($n = 41$)	p-value
Age	70.75 (58.93, 74.75)	62.00 (53.50, 70.60)	0.079[a]
Gender (M/F)	13/3	23/18	0.077[b]
Onset age (y)	68.45 (54.43, 72.45)	61.10 (51.70, 68.55)	0.077[a]
Disease duration (y)	2.45 (1.58, 3.83)	1.80 (1.10, 3.10)	0.324[a]
Education (y)	17.4 (14.5, 20.0)	18.0 (16.0, 20.0)	0.851[a]
H-Y staging	2 (1, 2)	2 (1, 2)	0.884[a]
UPDRS-III	24.50 (16.25, 32.50)	19.00 (14.00, 32.00)	0.374[a]
MoCA	26.5 (26.0, 29.0)	27.0 (25.5, 29.0)	0.815[a]
STAI-S	48.00 (44.25, 49.75)	47.00 (43.50, 50.00)	0.865[a]
STAI-T	45.94 ± 1.17	45.88 ± 0.56	0.957[c]
GDS	2.50 (1.00, 3.75)	1.00 (0, 2.50)	0.069[a]
RBDSQ	2.0 (1.0, 4.5)	3.0 (2.0, 4.5)	0.109[a]
ESS	12.00 (11.00,12.75)	2.00 (2.00, 3.00)	< 0.001[a]

Parametric variables are presented as mean ± SD, and non-parametric variables are presented as median (interquartile range). PD-EDS, Parkinson's disease with excessive daytime sleepiness; PD-noEDS, Parkinson's disease without excessive daytime sleepiness; M, Male; F, Female; y, Year; H-Y, Hoehn and Yahr scale; UDPRS-III, part III of the Unified Parkinson's Disease Rating Scale; MoCA, Montreal Cognitive Assessment; STAI-S, state–trait anxiety inventory-state score; STAI-T, state–trait anxiety inventory-trait score; GDS, geriatric depression scale, RBDSQ, rapid eye movement sleep behavior disorder questionnaire; ESS, Epworth Sleepiness Scale. *$p < 0.05$.
[a]Mann–Whitney U test.
[b]Chi-squared test.
[c]Two-sample t-test.

10.3389/fnagi.2023.1282962

Dynamic functional connectivity state analysis

We identified four different dynamic functional connectivity states with the k-means clustering algorithm. Combined with the visualized clustering centroids, we retained the 5% strongest functional connectivity to better illustrate the connectivity characteristics of each state. As shown in Figure 3, state IV (10%) occurred least frequently and was characterized by strong positive correlations within and between the SMN and VIS, while strong

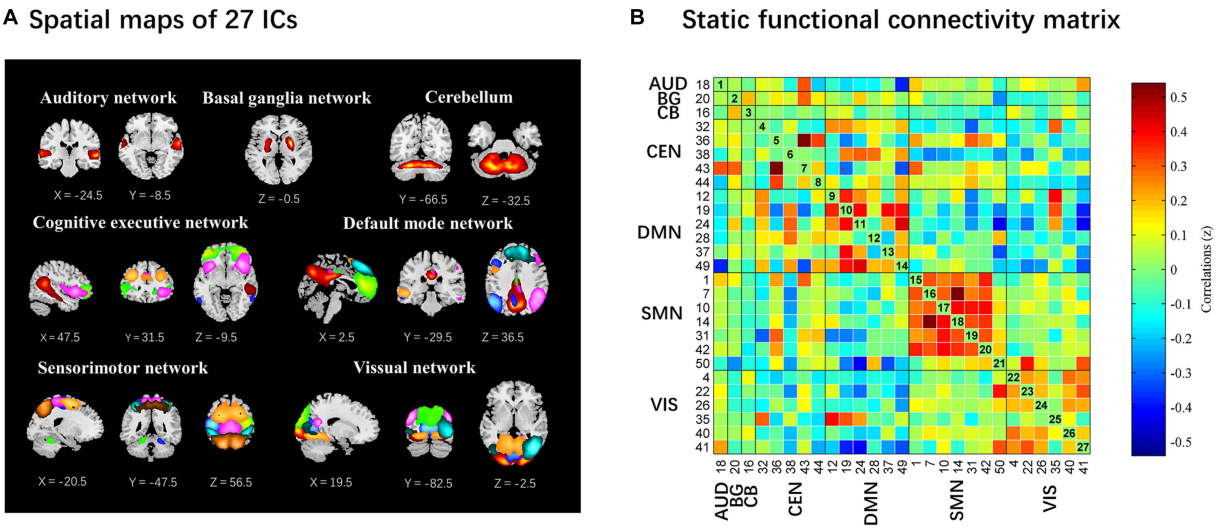

FIGURE 2
The 27 independent components identified by group independent component analysis. **(A)** Independent components spatial maps sorted into seven functional networks. **(B)** Group-averaged static functional connectivity between independent component pairs was computed using the entire resting-state data. The value in the correlation matrix represents the Fisher's z-transformed Pearson correlation coefficient. Each of the 27 independent components was rearranged by network group based on the seven functional networks. AUD, auditory network; BG, basal ganglia; CB, cerebellum; CEN, cognitive executive network; DMN, default mode network; SMN, sensorimotor network; VIS, visual network.

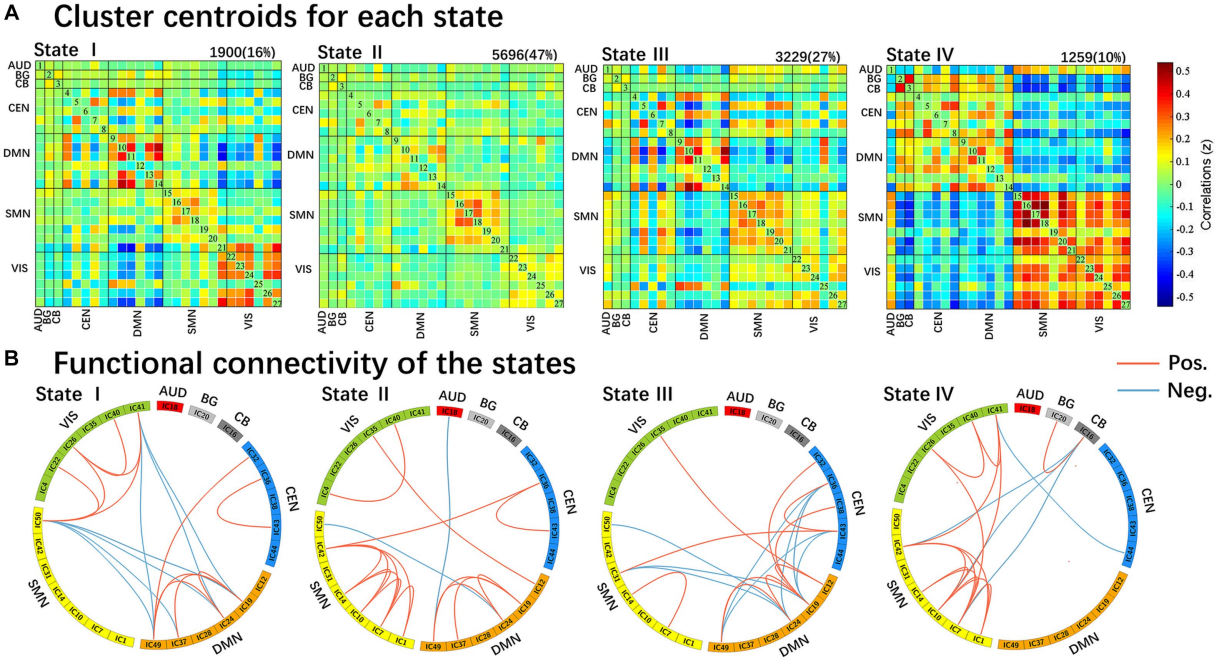

FIGURE 3
Results of the clustering analysis per state. **(A)** Resulting cluster centroids for each state. The total number of occurrences and percentage of total occurrences are listed above each cluster median. **(B)** Graphical representation of the strongest 5% functional network connectivity in each state. AUD, auditory network; BG, basal ganglia; CB, cerebellum; CEN, cognitive executive network; DMN, default mode network; SMN, sensorimotor network; VIS, visual network.

negative connectivity were observed between the SMN and VIS with other networks (DMN/CEN/BG/CB). In addition, strong positive internetwork connectivity between the BG and CB were also observed in state IV. In contrast, the other three states (state I 16%; state II 47%; and state III 27%) occurred more frequently. State II occurred most frequently and was characterized by extensive sparse weak intra/internetwork connectivity. State I was characterized by strong positive connectivity intranetwork of the DMN and VIS, while negative connectivity internetwork between the DMN and VIS. For state III, strong positive connectivity within the DMN, positive and negative connectivity between DMN and CEN, and negative connectivity between DMN with SMN and VIS.

We compared the group differences in the temporal properties of each state between the two groups ($p < 0.05$, FDR-corrected), as shown in Figure 4. We detected significant intergroup differences in the fractional time of state I and state IV and the mean dwell time of state IV. Specifically, the patients in the PD-EDS group had significantly higher fractional time and mean dwell time in state IV ($p = 0.015$, $p = 0.027$, FDR-corrected) and lower fractional time in state I ($p = 0.022$, FDR-corrected) than the patients in the PD-noEDS group. After controlling for the effects of age and gender, we found that the fractional time in state IV was slightly positively associated with ESS scores for all PD patients ($p = 0.032$, $r = 0.289$).

Strength of the dynamic functional network connectivity states

We then examined the difference in the connection strengths in each state between the two groups. The results of the two-sample t test indicated that the patients in the PD-EDS group showed stronger dynamic connectivity between the bilateral putamen and middle frontal gyrus in state II and state III than the patients in the PD-noEDS group ($p < 0.001$, FDR-corrected), as shown in Figure 5.

Discussion

In this study, dFNC analysis was used to explore the differences in dynamic functional network connectivity between the patients in the drug-naïve PD-EDS and PD-noEDS groups. Four recurrent distinct connectivity states were identified in both PD groups using a sliding time window approach. Interestingly, we observed that compared to the patients in the PD-noEDS group, the patients in the PD-EDS group showed significantly increased fractional time and mean dwell time in state IV and decreased fractional time in state I. The fractional time was positively correlated with EDS severity in state IV. Additionally, the patients in the PD-EDS group showed stronger dynamic connectivity between the bilateral putamen and bilateral middle frontal gyrus in state II and state III than the patients in the PD-noEDS group.

Temporal properties of dynamic functional connectivity states

In our study, the patients in the PD-EDS group had significantly higher fractional time and mean dwell time in state IV ($p = 0.015$, $p = 0.027$, FDR-corrected) and lower fractional time in State I ($p = 0.022$, FDR-corrected) than the patients in the PD-noEDS group. This meant that PD-EDS patients frequently moved in and out of state IV and generally stayed in state IV for a longer period of time than PD-noEDS patients. Moreover, the fractional time was positively correlated with EDS severity in state IV. These findings showed that the state may be a characteristic state of EDS. State IV was characterized by dominant patterns in the SMN and VIS. Strong positive correlations within and between the SMN and VIS were mainly exhibited in state IV, while strong negative connectivity between SMN/VIS and other networks (DMN/CEN/BG/CB) were also be found in state IV. In addition, strong positive internetwork connectivity between the BG and CB were observed in state IV.

The SMN is involved in motor, auditory and sensory processing (Yang et al., 2021). Sensory information processing occurs during sleep. Different sensory modalities encoded by particular pathways or networks may modify physiological characteristics in the waking and sleep states (Velluti, 1997). In PD patients, some regions in the sensory network are associated with the formation of PD-EDS. Wen et al. found increased regional homogeneity values in the left paracentral lobule in early PD-EDS patients compared to PD-noEDS patients by using regional homogeneity analysis (Wen et al., 2016). In our study,

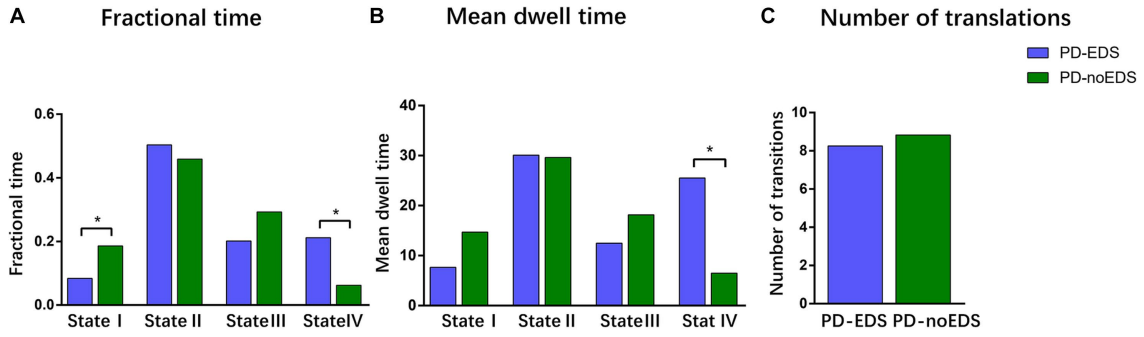

FIGURE 4
Differences in the temporal properties of the functional connectivity states between the two groups. **(A)** Fractional window spent by all subjects in each state as measured by percentage. **(B)** Mean dwell time between the two groups. **(C)** Number of transitions between the two groups. *$p < 0.05$, PD, Parkinson's disease; EDS, excessive daytime sleepiness; noEDS = without excessive daytime sleepiness.

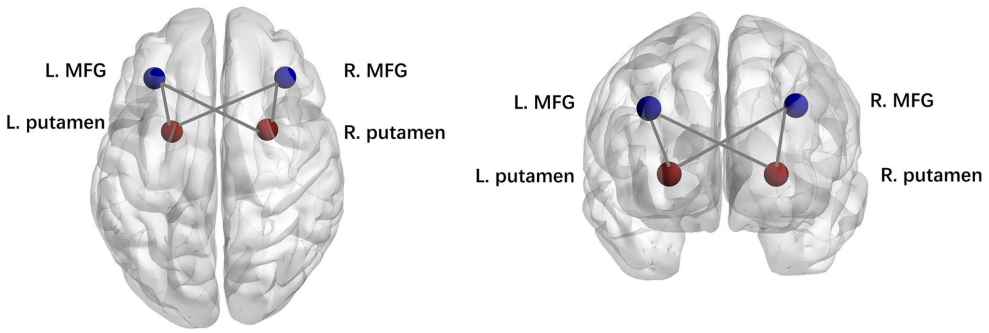

FIGURE 5
Strength of dynamic functional network connectivity (dFNC) in state II and state III. There were significant differences in state II and state III between PD-EDS and PD-noEDS groups (p<0.001, FDR-corrected) in strength of dFNC, located between the putamen and middle frontal gyrus.

we found that the patients in the PD-EDS group showed higher activity and information transmission in the SMN (high positive connectivity with the VIS and high negative connectivity with the CEN and DMN) over longer times than the patients in the PD-noEDS group, which was slightly positively correlated with EDS severity. These results suggest that the SMN increased the integration of visual processes and inhibited cognition and execution processes in patients with PD-EDS. Therefore, we concluded that patients with PD-EDS may exhibit enhanced SMN control to actively modulate sleep and wakefulness to compensate for the damage caused by EDS.

The VIS is one of the most important sensory networks. Previous neuroimaging studies have reported hypermetabolism in the visual cortex in narcolepsy patients (Dauvilliers et al., 2010; Huang et al., 2016; Dauvilliers et al., 2017) and increased functional connectivity in the visual network in adolescent narcolepsy patients (Fulong et al., 2020). These findings were similar to our results showing the strong positive connectivity within the VIS in state IV, and the fraction time in state IV was positively correlated with ESS scores. We inferred that one possibility is due to the patient's subjective efforts to resist falling asleep during the scan, and the other may be a compensatory mechanism in the early stage of the disease. Notably, because this study included only drug-naïve PD patients with mild EDS, it is possible that this compensation occurs only in drug-naïve early PD-EDS. Our findings suggest that the fractional time in state IV is a potential valuable biomarker for PD-EDS.

In addition, in contrast to the other three states, strong positive internetwork connectivity between the BG and CB were observed in state IV. As a key function of the BG, the disruption of striatal neuron signaling may facilitate the occurrence of EDS symptoms in PD patients. In early PD patients, Ooi et al. showed that BG connectivity was positively correlated with ESS scores, which suggested the existence of compensatory mechanisms in early PD patients (Ooi et al., 2019). The CB may also be associated with EDS symptoms in PD patients. Compared with the patients in the PD-noEDS group, the patients in the PD-EDS group had decreased connectivity within the CB, decreased connectivity between the CB and the insula, frontal lobe, and BG regions, and enhanced connectivity with the postcentral gyrus (Wen et al., 2016; Ashraf-Ganjouei et al., 2019; Zi et al., 2022; Zheng et al., 2023). Strong functional connectivity was observed between the CB and BG after sleep deprivation, which was thought to be a natural response to the decrease in motor alertness (Zhang et al., 2019). In our study, the dFNC analysis results demonstrated that interactions between the BG and CB were associated with the emergence of EDS in PD patients and that this strong positive connectivity may be attributed to early compensatory mechanisms.

In our study, compared to the patients in the PD-noEDS group, the patients in the PD-EDS group showed significantly decreased fractional time in state I. This meat that PD-EDS patients were more stable when they stayed in state I. State I was characterized by strong positive connectivity intranetwork of the DMN and VIS, while negative connectivity internetwork between the DMN and VIS. The DMN is a highly integrated task-negative network that is activated when people are in waking resting states and is responsible for conscious awareness and self-referential introspective states (Qin et al., 2015; Mak et al., 2017). A study focusing on early PD-EDS reported a positive correlation between the occurrence of EDS and DMN connectivity (Ooi et al., 2019), the same with our findings, suggesting the presence of compensatory mechanisms in the early stages of the disease. As mentioned above, the VIS is one of the most important sensory networks. The VIS also showed an intranetwork strong positive connectivity in state I. These findings suggested that PD-EDS patients may achieve a more stable state (state I) by strengthening the internal regulation of DMN and VIS. However, we found state I was also characterized by negative connectivity internetwork between the DMN and VIS. This may be an interesting finding. Judging from the strong negative connectivity between the DMN and VIS in state I, the DMN and VIS were functionally competitive and inhibitory networks. Therefore, we speculated that this may be due to the competition between the DMN and VIS networks for brain resource allocation when maintaining brain stability. Nevertheless, this finding needs to be further verified by future studies.

Strength of dynamic functional connectivity states

We observed that the patients in the PD-EDS group showed stronger dynamic connectivity between the putamen and middle frontal gyrus in state II and state III than the patients in the PD-noEDS group ($p < 0.001$, FDR-corrected). As mentioned above, compensatory mechanisms in the striatum may be related to EDS symptoms in PD patients (Gong et al., 2019). The putamen is one of the structures of the striatum and is an important node in various neural circuits and

neural networks. Additionally, fALFF values in the putamen and functional connectivity between the putamen and medial frontal gyrus were elevated in PD-EDS patients (Zheng et al., 2023). These findings suggested that EDS symptoms in PD patients are associated with abnormal information integration between the putamen and middle frontal gyrus. Our study supports this view from the perspective of dynamic functional connectivity analysis.

Limitations

This study has some limitations that should be considered. First, as in previous studies, head motion has an unavoidable effect on rs-fMRI data. Although we carried out several manipulations to mitigate this effect, it was still not completely ruled out. Second, in this study, the sample size of patients in the PD-EDS group was relatively small and there were differences in gender between the two groups (PD with and without EDS group). Future studies with larger sample sizes should be performed for further validation. In addition, we did not collect detailed information on patients' sleep habits or quality, which prevented us from assessing whether nocturnal sleep fragmentation or other sleep difficulties associated with PD impacted our analysis (Tandberg et al., 1998; Videnovic and Golombek, 2013). However, there was no significant difference in RBDSQ scores between the two groups, which ruled out the effect of rapid eye movement sleep behavior disorder in PD patients to some extent.

Conclusion

In summary, this study is the first to examine the dynamic functional network connectivity characteristics of PD-EDS. The dynamic functional connectivity analysis showed that PD-EDS patients preferred to be in states dominated by the SMN and VIS, with strong positive correlations within and between the SMN and VIS, while strong negative connectivity between the SMN/VIS with other networks. These findings revealed that SMN-and VIS-dominated patterns were specific network aggregation states associated with PD-EDS. Moreover, the duration of this state correlated with the severity of EDS, suggesting that SMN-and VIS-dominated patterns may compensate for EDS damage through high-intensity information output. Our research provided new insights into the neural mechanisms underlying PD-EDS, and the SMN-and VIS-dominated patterns may serve as biomarkers of the pathophysiological features of PD-EDS.

Data availability statement

The datasets presented in this study can be found in online repositories. The names of the repository/repositories and accession number (s) can be found at: https://www.ppmi-info.org/.

Ethics statement

The studies involving humans were approved by the respective ethics committees of the different data collection centers on PPMI. The studies were conducted in accordance with the local legislation and institutional requirements. Written informed consent for participation was not required from the participants or the participants' legal guardians/next of kin in accordance with the national legislation and institutional requirements. Written informed consent was obtained from the individual(s) for the publication of any potentially identifiable images or data included in this article.

Author contributions

ZT: Data curation, Formal analysis, Investigation, Methodology, Software, Writing – original draft. QZ: Data curation, Formal analysis, Investigation, Methodology, Software, Supervision, Writing – review & editing. XH: Data curation, Writing – review & editing, Visualization. DD: Data curation, Writing – review & editing. LC: Data curation, Writing – review & editing. ZL: Conceptualization, Funding acquisition, Investigation, Resources, Writing – review & editing. GC: Conceptualization, Funding acquisition, Resources, Project administration, Supervision, Writing – review & editing.

Funding

The author(s) declare financial support was received for the research, authorship, and/or publication of this article. This work was supported by the National Natural Science Foundation of China (82271944 and 82302158), Shenzhen Science and Technology Program (KCXFZ20211020163408012), and Shenzhen High-level hospital construction fund and Shenzhen Natural Science Foundation (JCYJ20190822090801701).

Acknowledgments

We are grateful to the patients who participated in the PPMI study, the researchers who contributed, and the Michael J. Fox Foundation. PPMI–a public-private partnership–is funded by the Michael J. Fox Foundation for Parkinson's Research and funding partners, including 4D Pharma, AbbVie Inc. AcureX Therapeutics, Allergan, Amathus Therapeutics, Aligning Science Across Parkinson's (ASAP), Avid Radiopharmaceuticals, Bial Biotech, Biogen, BioLegend, Bristol Myers Squibb, Calico Life Sciences LLC, Celgene Corporation, DaCapo Brainscience, Denali Therapeutics, The Edmond J. Safra Foundation, Eli Lilly and Company, GE Healthcare, GlaxoSmithKline, Golub Capital, Handl Therapeutics, Insitro, Janssen Pharmaceuticals, Lundbeck, Merck & Co., Inc., Meso Scale Diagnostics, LLC, Neurocrine Biosciences, Pfizer Inc., Piramal Imaging, Prevail Therapeutics, F. Hoffmann-La Roche Ltd., and its affiliated company Genentech Inc., Sanofi Genzyme, Servier, Takeda Pharmaceutical Company, Teva Neuroscience, Inc., UCB, Vanqua Bio, Verily Life Sciences, Voyager Therapeutics, Inc., and Yumanity Therapeutics, Inc.

Conflict of interest

The authors declare that the research was conducted in the absence of any commercial or financial relationships that could be construed as a potential conflict of interest.

Publisher's note

References

Allen, E. A., Damaraju, E., Plis, S. M., Erhardt, E. B., Eichele, T., and Calhoun, V. D. (2014). Tracking whole-brain connectivity dynamics in the resting state. *Cereb. Cortex* 24, 663–676. doi: 10.1093/cercor/bhs352

Arnone, D., Wise, T., Walker, C., Cowen, P. J., Howes, O., and Selvaraj, S. (2018). The effects of serotonin modulation on medial prefrontal connectivity strength and stability: a pharmacological fmri study with citalopram. *Prog. Neuro-Psychopharmacol. Biol. Psychiatry* 84, 152–159. doi: 10.1016/j.pnpbp.2018.01.021

Ashraf-Ganjouei, A., Kheiri, G., Masoudi, M., Mohajer, B., Mojtahed Zadeh, M., Saberi, P., et al. (2019). White matter tract alterations in drug-naive Parkinson's disease patients with excessive daytime sleepiness. *Front. Neurol.* 10:378. doi: 10.3389/fneur.2019.00378

Bloem, B. R., Okun, M. S., and Klein, C. (2021). Parkinson's disease. *Lancet* 397, 2284–2303. doi: 10.1016/s0140-6736(21)00218-x

Chan, L. G., Siang, K. S. S., Yong, T. T., Chander, R., Tan, L., and Kandiah, N. (2020). The longitudinal impact of excessive daytime somnolence on motor and nonmotor symptoms of Parkinson's disease in a southeast Asian cohort. *J. Geriatr. Psychiatry Neurol.* 33, 363–369. doi: 10.1177/0891988719892326

Dauvilliers, Y., Comte, F., Bayard, S., Carlander, B., Zanca, M., and Touchon, J. (2010). A brain pet study in patients with narcolepsy-cataplexy. *J. Neurol. Neurosurg. Psychiatry* 81, 344–348. doi: 10.1136/jnnp.2009.175786

Dauvilliers, Y., Evangelista, E., De Verbizier, D., Barateau, L., and Peigneux, P. (2017). [18F]Fludeoxyglucose-positron emission tomography evidence for cerebral Hypermetabolism in the awake state in narcolepsy and idiopathic hypersomnia. *Front. Neurol.* 8:350. doi: 10.3389/fneur.2017.00350

Fiorenzato, E., Strafella, A. P., Kim, J., Schifano, R., Weis, L., Antonini, A., et al. (2019). Dynamic functional connectivity changes associated with dementia in Parkinson's disease. *Brain* 142, 2860–2872. doi: 10.1093/brain/awz192

Friedman, J., Hastie, T., and Tibshirani, R. (2008). Sparse inverse covariance estimation with the graphical lasso. *Biostatistics* 9, 432–441. doi: 10.1093/biostatistics/kxm045

Fulong, X., Spruyt, K., Chao, L., Dianjiang, Z., Jun, Z., and Fang, H. (2020). Resting-state brain network topological properties and the correlation with neuropsychological assessment in adolescent narcolepsy. *Sleep* 43:zsaa018. doi: 10.1093/sleep/zsaa018

Gan, C., Ma, K., Wang, L., Si, Q., Wang, M., Yuan, Y., et al. (2021). Dynamic functional connectivity changes in Parkinson's disease patients with rem sleep behavior disorder. *Brain Res.* 1764:147477. doi: 10.1016/j.brainres.2021.147477

Gong, L., Li, H., Yang, D., Peng, Y., Liu, D., Zhong, M., et al. (2019). Striatum shape hypertrophy in early stage Parkinson's disease with excessive daytime sleepiness. *Front. Neurosci.* 13:1353. doi: 10.3389/fnins.2019.01353

Grover, S., Kumar Sreelatha, A. A., Pihlstrom, L., Domenighetti, C., Schulte, C., Sugier, P.-E., et al. (2022). Genome-wide association and Meta-analysis of age at onset in Parkinson disease. *Neurology* 99, e698–e710. doi: 10.1212/wnl.0000000000200699

Himberg, J., Hyvarinen, A., and Esposito, F. (2004). Validating the independent components of neuroimaging time series via clustering and visualization. *NeuroImage* 22, 1214–1222. doi: 10.1016/j.neuroimage.2004.03.027

Huang, Y. S., Liu, F. Y., Lin, C. Y., Hsiao, I. T., and Guilleminault, C. (2016). Brain imaging and cognition in young narcoleptic patients. *Sleep Med.* 24, 137–144. doi: 10.1016/j.sleep.2015.11.023

Hutchison, R. M., Womelsdorf, T., Allen, E. A., Bandettini, P. A., Calhoun, V. D., Corbetta, M., et al. (2013). Dynamic functional connectivity: promise, issues, and interpretations. *NeuroImage* 80, 360–378. doi: 10.1016/j.neuroimage.2013.05.079

Kim, J., Criaud, M., Cho, S. S., Diez-Cirarda, M., Mihaescu, A., Coakeley, S., et al. (2017). Abnormal intrinsic brain functional network dynamics in Parkinson's disease. *Brain* 140, 2955–2967. doi: 10.1093/brain/awx233

Li, X., Zhu, D., Jiang, X., Jin, C., Zhang, X., Guo, L., et al. (2014). Dynamic functional connectomics signatures for characterization and differentiation of Ptsd patients. *Hum. Brain Mapp.* 35, 1761–1778. doi: 10.1002/hbm.22290

Liu, H., Li, J., Wang, X., Huang, J., Wang, T., Lin, Z., et al. (2022). Excessive daytime sleepiness in Parkinson's disease. *Nat. Sci. Sleep* 14, 1589–1609. doi: 10.2147/Nss.S375098

Mak, L. E., Minuzzi, L., Macqueen, G., Hall, G., Kennedy, S. H., and Milev, R. (2017). The default mode network in healthy individuals: a systematic review and Meta-analysis. *Brain Connect.* 7, 25–33. doi: 10.1089/brain.2016.0438

Marek, K., Jennings, D., Lasch, S., Siderowf, A., Tanner, C., Simuni, T., et al. (2011). The Parkinson progression Marker initiative (Ppmi). *Prog. Neurobiol.* 95, 629–635. doi: 10.1016/j.pneurobio.2011.09.005

Navalpotro-Gomez, I., Kim, J., Paz-Alonso, P. M., Delgado-Alvarado, M., Quiroga-Varela, A., Jimenez-Urbieta, H., et al. (2020). Disrupted salience network dynamics in Parkinson's disease patients with impulse control disorders. *Parkinsonism Relat. Disord.* 70, 74–81. doi: 10.1016/j.parkreldis.2019.12.009

Ooi, L. Q. R., Wen, M. C., Ng, S. Y., Chia, N. S., Chew, I. H. M., Lee, W., et al. (2019). Increased activation of default mode network in early Parkinson's with excessive daytime sleepiness. *Front. Neurosci.* 13:1334. doi: 10.3389/fnins.2019.01334

Qin, P., Wu, X., Huang, Z., Duncan, N. W., Tang, W., Wolff, A., et al. (2015). How are different neural networks related to consciousness? *Ann. Neurol.* 78, 594–605. doi: 10.1002/ana.24479

Shirer, W. R., Ryali, S., Rykhlevskaia, E., Menon, V., and Greicius, M. D. (2012). Decoding subject-driven cognitive states with whole-brain connectivity patterns. *Cereb. Cortex* 22, 158–165. doi: 10.1093/cercor/bhr099

Si, Q., Gan, C., Zhang, H., Cao, X., Sun, H., Wang, M., et al. (2023). Altered dynamic functional network connectivity in levodopa-induced dyskinesia of Parkinson's disease. *CNS Neurosci. Ther.* 29, 192–201. doi: 10.1111/cns.13994

Tandberg, E., Larsen, J. P., and Karlsen, K. (1998). A community-based study of sleep disorders in patients with Parkinson's disease. *Mov. Disord.* 13, 895–899. doi: 10.1002/mds.870130606

Velluti, R. A. (1997). Interactions between sleep and sensory physiology. *J. Sleep Res.* 6, 61–77. doi: 10.1046/j.1365-2869.1997.00031.x

Videnovic, A., and Golombek, D. (2013). Circadian and sleep disorders in Parkinson's disease. *Exp. Neurol.* 243, 45–56. doi: 10.1016/j.expneurol.2012.08.018

Wang, X., Wang, M., Yuan, Y., Li, J., Shen, Y., and Zhang, K. (2020). Altered amplitude of low-frequency fluctuations and functional connectivity in excessive daytime sleepiness in Parkinson disease. *Front. Neurosci.* 14:29. doi: 10.3389/fnins.2020.00029

Wen, M. C., Ng, S. Y., Heng, H. S., Chao, Y. X., Chan, L. L., Tan, E. K., et al. (2016). Neural substrates of excessive daytime sleepiness in early drug naive Parkinson's disease: a resting state functional Mri study. *Parkinsonism Relat. Disord.* 24, 63–68. doi: 10.1016/j.parkreldis.2016.01.012

Xu, J., Yu, M., Wang, H., Li, Y., Li, L., Ren, J., et al. (2021). Altered dynamic functional connectivity in de novo Parkinson's disease patients with depression. *Front. Aging Neurosci.* 13:789785. doi: 10.3389/fnagi.2021.789785

Yang, H., Chen, X., Chen, Z.-B., Li, L., Li, X.-Y., Castellanos, F. X., et al. (2021). Disrupted intrinsic functional brain topology in patients with major depressive disorder. *Mol. Psychiatry* 26, 7363–7371. doi: 10.1038/s41380-021-01247-2

Zhang, Y., Yang, Y., Yang, Y., Li, J., Xin, W., Huang, Y., et al. (2019). Alterations in cerebellar functional connectivity are correlated with decreased psychomotor vigilance following Total sleep deprivation. *Front. Neurosci.* 13:134. doi: 10.3389/fnins.2019.00134

Zheng, J. H., Ma, J. J., Sun, W. H., Wang, Z. D., Chang, Q. Q., Dong, L. R., et al. (2023). Excessive daytime sleepiness in Parkinson's disease is related to functional abnormalities in the left angular gyrus. *Clin. Neuroradiol.* 33, 121–127. doi: 10.1007/s00062-022-01190-x

Zhu, J., Zeng, Q., Shi, Q., Li, J., Dong, S., Lai, C., et al. (2021). Altered brain functional network in subtypes of Parkinson's disease: a dynamic perspective. *Front. Aging Neurosci.* 13:710735. doi: 10.3389/fnagi.2021.710735

Zi, Y., Cai, S., Tan, C., Wang, T., Shen, Q., Liu, Q., et al. (2022). Abnormalities in the fractional amplitude of low-frequency fluctuation and functional connectivity in Parkinson's disease with excessive daytime sleepiness. *Front. Aging Neurosci.* 14:826175. doi: 10.3389/fnagi.2022.826175

Frontiers in Neurology

Explores neurological illness to improve patient care

The third most-cited clinical neurology journal explores the diagnosis, causes, treatment, and public health aspects of neurological illnesses. Its ultimate aim is to inform improvements in patient care.

Discover the latest Research Topics

See more →

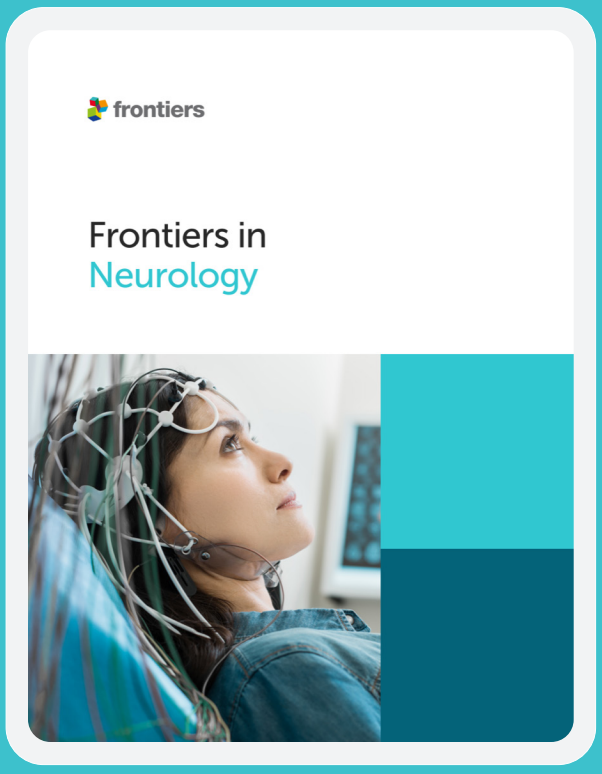

Frontiers

Avenue du Tribunal-Fédéral 34
1005 Lausanne, Switzerland
frontiersin.org

Contact us

+41 (0)21 510 17 00
frontiersin.org/about/contact